INVESTIGATING EUTECTIC MIXTURES FOR POORLY SOLUBLE COMPOUNDS

BY

Carrie Morgan

Submitted to the graduate degree program in
Pharmaceutical Chemistry and the Graduate Faculty
of the University of Kansas in partial fulfillment of the
requirements for the degree of Master of Science

_____
Chairperson

Committee Members* _____ *

_____ *

_____ *

_____ *

_____ *

Date defended: _____

The Thesis Committee for Carrie Morgan
certifies that this is the approved version of the following thesis:

Investigating Eutectic Mixtures for Poorly Soluble Compounds

_____
Chairperson Dr. John F. Stobaugh, PhD

Date approved: January 28th, 2014

Abstract

Improving the solubility and changing the dissolution rate of the poorly soluble active pharmaceutical ingredients (API's) AMG 517, glipizide, and naproxen through the preparation of eutectic mixtures was investigated. Mixtures of the API's with other small molecules were prepared to construct a phase diagram used to identify the eutectic mixture compositions. The search for a eutectic mixture in a co-crystal phase diagram was investigated by mixing AMG 517 with known co-crystal formers sorbic acid and *trans*-cinnamic acid. Glipizide was mixed with a series of amides to investigate the presence of eutectic mixtures, but the thermal instability of the API was such that chemical degradation overwhelmed any other thermal transitions. A phase diagram of naproxen and vanillin was prepared and the composition of the eutectic mixture identified. The eutectic mixture at 0.11 MF naproxen vanillin (11% naproxen/ 89% vanillin) was found to have a melting point of 75 ºC. The melt is reversible and thermally stable, as tested by multiple melts and coolings. Further studies are planned to evaluate whether the eutectic mixture may be advantageous to develop. However, expectations are modest due to the small amount of naproxen present in the eutectic mixture.

Acknowledgments

I would like to thank my family and friends, especially my parents, for their unwavering love and support during my time in the Long Distance Master's program. I also would like to thank the Pharmaceutics group at Amgen, for their insights and suggestions. I especially would like to thank Dr. Matthew L. Peterson, PhD., my supervisor and Master's program advisor at Amgen, for his patience and guidance. I would also like thank Dr. John Stobaugh, PhD. for all of his help and support as my KU advisor in the Master's Program. I have received guidance and support from many people through the classes at KU and my colleagues at Amgen. I sincerely thank them all and I extend heartfelt gratitude for this tremendous opportunity.

Table of Contents

Chapter 1. Introduction 1

Phase Diagrams of Binary Mixtures 10

Miscibility and Solubility in Phase Diagrams. 11

Free Energy of Mixing, ΔGmix. 12

The Mixture Law. 13

Construction of Phase Diagrams. 14

Types of Binary Phase Diagrams. 17

Introduction of AMG 517, Glipizide, and Naproxen. 22

Conclusions 24

References 24

Chapter 2. Background 27

Urea-Benzoic Acid: A Model Eutectic System 27

Introduction. 27

Experimental. 28

Results and Discussion 30

Conclusion 36

References 36

Chapter 3. AMG 517 Binary Systems 37

Introduction..... 37

Experimental..... 39

Results and Discussion..... 43

The AMG 517/SA System..... 43

The AMG 517 Mannitol Binary System..... 50

The AMG 517/CA system..... 50

AMG 517 Xylitol System..... 57

Conclusions..... 73

References..... 73

Chapter 4. Glipizide Binary Systems..... 75

Introduction..... 75

Experimental..... 76

Results and Discussion..... 78

Glipizide ADA Binary System..... 82

Glipizide PA Binary System..... 82

Conclusions..... 86

References..... 92

Chapter 5. Naproxen Vanillin Binary System..... 93

Experimental 95

Results and Discussion 99

Conclusions 127

References 129

Chapter 6. Conclusions and Future Considerations 132

Chapter 7. Appendix 134

Chapter 1. Introduction

Frequently Encountered Problems in Drug Development

In the early stages of drug development, one frequently encounters novel molecules, which exhibit poor physicochemical properties. For example, more than one third of the drugs listed in the U.S. Pharmacoeia fall into the poorly water-soluble or water-insoluble categories [1]. Prior to the 1980's, such situations were rarely encountered as new chemical entities (NCE's) often exhibited an aqueous solubility ≥ 10 μg/mL [2]. The emergence of large numbers of poorly soluble drug candidates has led to the necessity of developing strategies to overcome the limitations in drug product development associated with poor solubility. One of approach is the preparation of eutectic mixtures of the drug with candidate utilizing various polymers or small molecules [3]. Eutectic mixtures (from the Greek word meaning *eutēktos* [4] meaning "easily melted") are composed of a specific ratio of drug another substance, which melt at a lower temperature than either of the original components [4-8].

Eutectic mixtures have not been a widely utilized technology in drug development, chiefly due to of the difficulty in forming a eutectic mixture, the inability to predict if a eutectic exists, and the time and resources necessary to characterize the these mixtures [3]. A eutectic system is a mixture of substances that have a single composition that solidifies at a lower temperature than any component that was used to form the system [9]. A particular composition displaying such characteristics is known as the eutectic composition and the temperature at which it solidifies is known as the eutectic temperature [4]. Eutectic mixtures compromise a subcategory of solid dispersions that form the basis of a formulation strategy wherein one seeks to improve the physical properties of the API to allow for an enhanced dissolution rate and apparent solubility [2, 10]. Not every drug and compound combination are capable of forming a eutectic mixture, with current

research being focused on predicting the presence of eutectic mixtures *in silico* [3]. At the time of this writing, the criteria for forming a eutectic mixture is largely unknown, with the desired results chiefly being obtained by serendipity and/or extensive trial and error experimentation.

History of Eutectics

Over the last 60 years, solid dispersions have been utilized to increase the solubility of a drug in a multiple of ways. An advantage of a solid dispersion is to increase the surface area of the API and maximize the exposure of the drug particle to the surrounding media [11-13]. The state of the API in the solid dispersion may be crystalline or amorphous, since the dispersion mechanism may also prevent crystallization [11-14]. As a result, the intrinsic dissolution rate of a poorly soluble drug would be enhanced [11-15]. However, there are only a small number of examples where these dispersions were eutectic mixtures [10]. Eutectic mixtures are generally formed by three methods [9, 10, 12]. The fusion method is performed by melting a physical mixture of two thermally stable compounds, with subsequent cooling resulting in solidification and eutectic mixture formation [16]. The solid is then pulverized to provide a powder. The second method employs the use of solvents [9, 10, 12]. Stock solutions of two compounds of similar solubilities in a solvent are prepared. Mixtures are prepared by pipetting different proportions of the two solutions into a vial. The final method is a hybrid of the first two methods. One of the compounds is melted and the other compound is dissolved into a solution, then pipetted directly onto the melted compound, or vice versa [9]. All of the resulting mixtures are cooled, which results in solidification, followed by pulverization to prepare a homogeneous powder. Once the mixtures are prepared, a composition-temperature diagram (phase diagram) is utilized to compare the melts of the mixtures by composition [16]. Historically the phase diagram was obtained by plotting the melting temperatures of the mixtures along the y-axis that correspond to the mixture composition

along the x-axis [4-7, 11, 16]. Today, eutectic mixtures can be characterized utilizing Differential Scanning Calorimetry (DSC) [9].

The pharmaceutical industry has had little success with developing a eutectic solid dispersion of a pharmaceutical agent. Since 1961, when Sekiguchi and Obi described one of the first eutectic solid dispersions of a poorly soluble drug, there has been little progress in determining a pattern to regularly repeat the phenomenon of forming a eutectic mixture with other poorly soluble drugs [16]. Sekiguchi and Obi reported a phase diagram for the sulfathiazole-urea eutectic mixture, which was prepared by the thaw-melt method [8, 9]. They hypothesized that the two molecules were able to interact in a manner that retarded the nucleation of the mixture from a liquid to a solid [8, 9]. However, the application of this theory to predict eutectics between poorly soluble drugs has not been successful [5, 6, 16]. Eutectic mixtures have continued not make an impact in the pharmaceutical industry.

Up to the present time, eutectic mixtures have not been vigorously pursued in the pharmaceutical industry to improve physicochemical characteristics of poorly soluble active pharmaceutical ingredients (API.) In other industries, such as metallurgy and industrial construction, one frequently encountered the use of eutectic mixtures as alloys [8]. For example, eutectic alloys for soldering may be composed of tin, lead, silver, and gold. Silicon chips are bonded to gold-plated substrates through a silicon-gold eutectic by the application of ultrasonic energy to the chip by eutectic bonding [17]. Metals are frequently more thermally stable and exhibit higher melting temperatures as compared to organic compounds. Temperature plays a much different role in pharmaceutical compounds where lower melting points typically result in higher aqueous solubility. An indication of the overall stability of a molecule can be measured by the heat of fusion, which may be viewed as the energy required to remove a molecule from its

neighboring molecules in the crystalline lattice, thus the transition from the solid state to the liquid state [11]. In general, when the heat of fusion is low, the observed melting point will be low, thus the apparent solid state stability of the molecule could be considered more unstable relative to substance with a higher heat of fusion [11]. Organic compounds exhibiting low melting points may frequently be unstable with polymorphism and chemical degradation occurring with an increased frequency. In metallurgy, thermal sensitivity is not a concern due to the use of high-melting metals involved in the formation of various alloys; however, this feature is not typical in pharmaceutical applications. Therefore, despite the possible advantages of the low melting temperature of a eutectic mixture and the implications in solubility and the intrinsic dissolution rates, pharmaceutical scientists do not usually pursue the use eutectic mixtures in formulation development. This may be due to a variety of reasons, but some of the main drivers may be time and resources. One of the tools in searching for a eutectic mixture is by the preparation of a phase diagram, which is usually the result of a laborious manual process. The phase diagram also requires an amount of experimental drug that usually exceeds what may be provided in the early stages of drug development [10]. Instead, the scientists may design a solid dispersion based on the reasons previously noted and/or the percentage of drug and compound was chosen to follow the necessary protocols that govern the *in vivo/ in vitro* dosings for solid dispersions [16]. However, for some API's with physicochemical properties difficult to overcome, the investigation of a eutectic mixture may be an option.

Eutectic Mixtures and Dissolution

Eutectic mixtures are advantageous as a means of changing the physicochemical properties of a drug because the specific ratio of API and compound may improve solubility and/or the intrinsic dissolution rate when compared to the other mixtures and drug alone. This is a possibility

when the eutectic mixture forms a solid dispersion. In 1971, Chiou and Riegelman [12] defined a solid dispersion as: "A dispersion of one or more active ingredients in an inert carrier or matrix at solid state prepared by melting, solvent evaporation or melt-solvent method." Solid dispersions may be amorphous or crystalline, and the crystal morphology of the crystals, if present, can be further defined [12, 22]. As a solid dispersion, the eutectic mixture releases very small particles that maximizes the surface area of the drugs to the aqueous surroundings [12, 16]. Also, the eutectic melt is lower than the melt of API and compound, and may have a higher solubility than the drug alone. The relation between the solubility and the dissolution rate is explained by the Noyes-Whitney equation, (Equation 1) [15, 19, 20].

$$\frac{dW}{dt} = \frac{DA(C_s - C_b)}{h} \qquad \textbf{Equation 1.}$$

The dissolution rate of the drug over time (dW/dt) (mg/cm^2/mL) is described by the diffusion coefficient of the drug (D) (cm^2/sec,) the surface area of the drug (A) (cm^2,) the concentration of the drug in the bulk dissolution media (C_b) (mg/mL,) and the concentration of the drug in the dissolution layer around the surface of the drug (C_s) (mg/mL) [19, 20]. It is assumed that the drug is saturated in the dissolution layer around the mass of the solid and is the driving force of dissolution [19]. The thickness of the dissolution layer is defined by h (cm) in the equation. The diffusion coefficient, D, depends on the molecular weight of the drug and the viscosity of the dissolution media. The thickness of h is assumed to change during dissolution and be independent of particle size [15, 20]. Some intrinsic dissolution experiments enable the thickness of the saturated layer around the particle to be constant when a two-dimensional surface area is exposed with a controlled rotation rate. Further the Noyes-Whitney equation is frequently normalized per surface area to obtain equation 2 [15-20]:

$$\frac{Md}{Adt} = \frac{dQ}{dt} = \frac{D}{hC}$$ **Equation 2.**

In equation 2, the mass per area of the particle changes during time (Md/Adt) and is equal to the flux of particles during dissolution from the particle into the bulk media over time (dQ/dt). This, in turn, is equal to the diffusion coefficient (D) divided by the thickness of the dissolution layer (h) multiplied by the concentration of the dissolved particle (C). When examining equations 1 and 2, the dissolution rate is directly proportional to the equilibrium solubility of the drug in the dissolution media. This relationship is considered valid if the experimental conditions chosen to measure the solubility are the same as the parameters selected to measure the intrinsic dissolution rate. This correlation was supported by comparing the initial dissolution rate to the solubility of numerous drugs of diverse structure [15]. The data was plotted on a log scale and demonstrated a linear relationship between solubility and the initial dissolution rate that extends over five orders of magnitude and no systemic deviation (Figure 1) [15].

The manipulation of solubility and surface area has given rise to various formulation strategies. These strategies leverage the concepts described in the Noyes-Whitney equations where the dissolution rate is proportional to the surface area (equations 1 and 2.) Therefore, the formulation of a eutectic system as a solid dispersion may result in an increased dissolution rate due to the drug being dispersed as fine particles that may be amorphous or crystalline, thereby a greater drug release per unit area may occur [12, 13, 21]. It is also possible that when the eutectic mixture is released, the dissolved substances particles may become supersaturated when mixed with the local media, and then precipitates from solution as a very high surface area. For many poorly soluble drugs, the dissolution rate best reflects the bioavailability of the compound [1, 11].

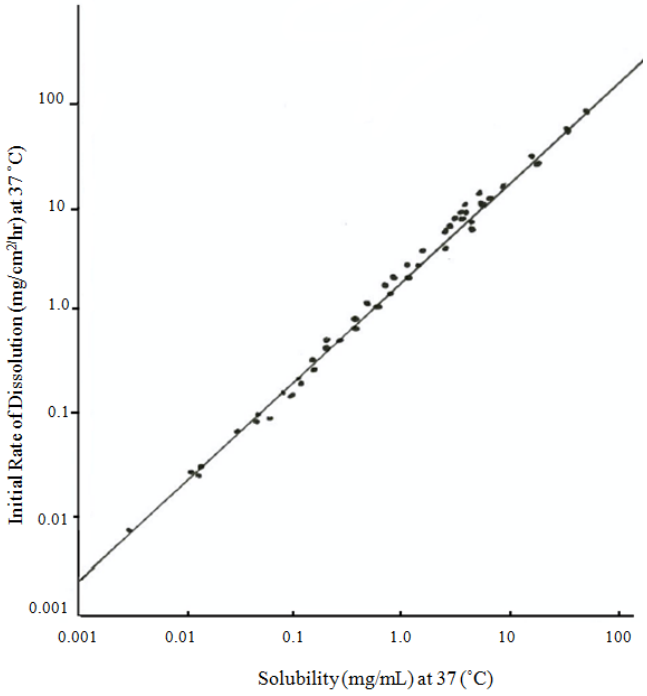

Figure 1. Data plot of the dependence of intrinsic dissolution rate on solubility as based on data of Hamlin, et al [15].

For drugs where absorption rate is limited by dissolution rate, the reduction of the particle size may increases the rate of absorption and improve bioavailability [12, 23]. Eutectic mixtures have the potential to provide for improved oral absorption for some compounds by increasing their solubility and dissolution properties [3, 9, 16]. An example of a eutectic mixture where an increased the intrinsic dissolution was achieved for a poorly soluble drug is sulfathiazole and urea [13]. As mentioned earlier, Sekiguchi and Obi wrote one of the first scientific papers to propose eutectic mixtures as an approach to reduce the particle size and increase the dissolution rate [15, 16, 22]. The sulfathiazole (mp 189 ° C) urea (mp 133 °C) eutectic mixture contained 52% sulfathiazole and 48% urea by weight and melted at 112 °C [16]. In a comparative experiment, eutectic mixture and the drug were orally administered and the resulting plasma levels compared [16.] The results indicated that after ingestion of the eutectic mixture, the drug was absorbed at a faster rate than the corresponding dose of sulfathiazole alone, which was apparently due to the release of sulfathiazole as microcrystalline particles [13, 15, 16]. The diameter of the fine particles was determined to be less than one micron. Therefore, the observed higher plasma levels of the drug was due to the increased surface area providing for an increased dissolution rate and ultimately increased bioavailability [24]. Although solubility of the eutectic mixture was not measured, numerous other solid dispersions have been characterized and found to exhibit a higher solubility as compared to the drug substance [12, 19, 25].

The relationship between melting point, solubility, and dissolution can be described in the general solubility equation (GSE) [23]. The GSE estimates the molar aqueous solubility of an organic non-electrolyte in the aqueous phase (S_w) as a function of its melting point (°C) and octanol-water partition coefficient (K_{ow}) is described by equation 3 [26].

$$\text{Log } S_w = -0.01(MP-25) - \log K_{ow} + 0.5 \qquad \textbf{Equation 3.}$$

In recent publications, the melting points were related to the Log of solubilities [26]. By utilizing the GSE, the lower melting temperature of a compound may correlate with higher solubility [23, 26]. When this concept is paired with the Noyes-Whitney equations (Equation 1 and 2), which uses factors such as solubility and surface area to describe the dissolution rate, it becomes logical that eutectic mixtures may enhance the intrinsic dissolution rate by increasing the solubility, as a result of the lower melting point, and due to an increase in the surface area of the drug. To determine which factor contributes more to the intrinsic dissolution rate, the solubility of the eutectic mixture may be compared to the drug alone. Also, the particle size of the drug in the solid dispersion can be measured by laser diffraction or microscopy.

An example of a eutectic mixture in which the intrinsic dissolution rate and solubility was measured *in vitro* was by Goldberg's study of the urea and acetaminophen (**APAP**) system. The solubility of **APAP** in water was found to linearly increase as solid urea was added up to 0.23 (g/g) urea:**APAP** [6]. The dissolution rate of the eutectic mixture was also increased due to the solubility of **APAP** in the diffusion layer and thereby increased the dissolution of the drug. It was also found that the coarser samples of the eutectic mixture also had a slower dissolution rate than the eutectic mixture with a smaller particles size [6]. Therefore, the faster intrinsic dissolution of the eutectic mixture was favored by the particle size and solubility.

Utility of Eutectic Mixtures

Eutectics may be formulated in a variety of dosage forms such as tablets, capsules, creams and suppositories [27]. Eutectics have been studied with respect to transdermal drug delivery and topical application. These formulations take advantage of the lower melting point of the drug, which results in an enhanced transdermal permeation for the eutectic mixture of prilocaine and lidocaine [9, 27].

A marketed drug that exemplifies many of these desirable physicochemical characteristics is the Eutectic Mixture of Local Anesthetics (EMLA®). EMLA® has been found to be an effective means of decreasing pain for most children subsequent to surgery [31]. The eutectic mixture of the two drugs was discovered after the construction of the phase diagram [7]. The phase diagram was composed of prilocaine and lidocaine, which displays the melt of the various mixtures of prilocaine:lidocaine [7]. The eutectic mixture consists of a 1:1 stoichiometric ratio of prilocaine:lidocaine. The eutectic point is 18 ˚C and renders the mixture a liquid at room temperature. This greatly facilitated the preparation of the 1:1 eutectic mixture of the drugs into an oil-water cream because emulsification was directly accomplished without first dissolving the drug in the oil phase [2, 7]. For both drugs, the individual solubility is less than that of the eutectic mixture. Therefore, the enhanced solubility between the two compounds was dependent on the ratio of the two drugs [7].

Phase Diagrams of Binary Mixtures

A binary phase diagram is a temperature-composition map which indicates the equilibrium phases present at a given temperature and composition [5, 12, 22, 28]. The equilibrium state can be found from the Gibbs free energy dependence on temperature and composition. A phase diagram of a binary mixture is useful to visually depict the equilibrium state of the mixture and display the phases formed at a certain temperature and composition. This knowledge can lead to the prediction of the phase the mixture may be when heated (solid or liquid) at a certain ratio of A:B and temperature. A phase is represented by a single section of the temperature-composition diagram that contains similar physical chemical characteristics [28]. The number of phases in a system is described by the Gibbs Phase Rule where the system contains the number of degrees of

freedom (F) necessary to define the energy state of a system. The Gibbs Phase Rule is described by equation 4 [11].

$$F = C - P + 2 \qquad \textbf{Equation 4.}$$

Where F is the number of degrees of freedom, C is the number of components, and P is the number of phases present at equilibrium [11]. The number of degrees of freedom is the least number of intensive variables, such as temperature, pressure, and concentration. These variables must be fixed to describe the system completely [11, 18]. The components are the smallest number of independent variables in the system. For example, it is possible to have a two phase system where two solids are immiscible in one phase and a single phase where both are miscible at a different temperature and composition. From a knowledge of the phase diagram, it is possible to calculate the composition of each component in the two conjugate phases.

Miscibility and Solubility in Phase Diagrams. Phase separation may occur due to the degree of miscibility and solubility of each component in relation to the other in a heterogeneous mixture. Solubility is a quantitative term that describes the concentration of solute in a saturated solution at a certain temperature [11]. The solvent and solute engage in a spontaneous interaction to form a homogeneous molecular dispersion [11]. In addition, the solubility of the substance also depends structural features such as the ratio of the polar to non-polar groups of the molecule [11].

Miscibility describes the ability of two molecules to form a uniform blend. Blends of polar and semi-polar solvents are miscible in all proportions. However, mixtures of polar and non-polar solvents are immiscible and will separate into discrete layers. For example, salad dressing is an emulsion of oil (non-polar) and vinegar (polar) when mixed thoroughly. However, when the liquid is at rest, the oil and vinegar equilibrates and separates into two layers of different densities. In a phase diagram, the limited miscibility between two components can be detected by the emergence

of a second phase due to the addition of one component when the solubility is exceeded in the other. From a knowledge of the phase diagram, it is possible to calculate the composition of each component in the two conjugate phases.

Free Energy of Mixing, ΔGmix. The free energy of mixing, ΔG_{mix}, determines if and to what extent two compounds mix to form a homogeneous phase [26.] ΔG_{mix} generally depends on the composition, temperature, and pressure of a system. ΔG_{mix} is the energy that is required or generated by mixing two components and is defined by equation 5 [15].

$$\Delta G_{mix} = \Delta H_{mix} - T\,\Delta S_{mix} \qquad \textbf{Equation 5.}$$

The equation combines the effects of both enthalpy and entropy into a single parameter. The terms in the equation are defined by: the enthalphy of mixing, ΔH_{mix}, (kJ/mol), the temperature, T (Kelvin), where the mixing occurs, and ΔS_{mix} (kJ/mol/K) is the entropy of mixing [15]. If the free energy of mixing is negative, then mixing occurs. If the free energy of mixing is zero, then the mixture separates into two phases. When ΔS_{mix} is positive, then the complete mixing of the two compounds is favored. When ΔS_{mix} is negative, then the system favors the two compounds remaining separate entities in a physical mixture [2]. By studying equation 4, it is apparent that ΔG_{mix} is dependent on whether the enthalpy of mixing, ΔH_{mix}, is negative or positive. The amount of mixing of the two compounds will be determined by the entropic and enthalpic factors for each compound and whether mixing is favored.[15] For example, ΔG_{mix} may be occurring when two solids are mixed by mortar and pestle or by ball milling.

The free energy of fusion, $\Delta G^{\circ}_{f,}$ is described by equation 6, which signifies the difference in free energy between the products and the reactants during melting [11].

$$\Delta G^{\circ}_{f} = \Delta H^{\circ}_{f} - T\Delta S^{\circ}_{f} \qquad \textbf{Equation 6.}$$

In the above equation, ΔH°_{f} (kJ/mol) is enthalpy of fusion, and ΔS°_{f} (kJ/mol/K) is the entropy of fusion at temperature T (Kelvin.) The ΔH°_{f} is only weakly dependent on temperature but ΔS°_{f} is strongly dependent on temperature due to the presence of T in the term. For a pure crystal, the amount of entropy in the system, $\Delta S^{\circ}_{f,}$ is practically zero. Therefore, the change in free energy of the system before and after melting is equal to the heat of fusion released during melting of a crystal as described by equation 7 [5, 12, 30].

$$\Delta G^{\circ}_{f} = \Delta H^{\circ}_{f} \qquad \textbf{Equation 7.}$$

The Mixture Law. If there is no energy associated with mixing between two compounds, then the difference between the enthalpy of fusion of the individual compounds before and after mixing should be the same. Therefore, enthalpy of fusion of the mixture, $(\Delta h^{\circ}_{f})_{mixture}$, can be calculated by the mixture law, as described by Equation 8 [4, 5, 15].

$$(\Delta h^{\circ}_{f})_{mixture} = X_A \Delta h^{\circ}_{fA} + X_B \Delta h^{\circ}_{fB} \qquad \textbf{Equation 8.}$$

In this equation, the contribution of the heat of fusion for the mixture AB, $(\Delta h^{\circ}_{f})_{mixture}$ (kJ/mol,) is the sum of the heat of fusion of A, Δh°_{fA}, multiplied by the mole fraction of A , X_{A} (moles of A,) and the heat of fusion of B, $\Delta h^{\circ}_{fB,}$ multiplied by the mole fraction of B (moles of B) in the mixture [15, 60]. The heats of fusion of the pure components determine Δh°_{fA} and $\Delta h^{\circ}_{fB.}$ In a physical mixture, the free energy of the system before and after mixing is the same and there is no free energy generated due to mixing [15].

The enthalpy of mixing of a mixture, $(\Delta h^{\circ}_{f})_{mixture}$, can be calculated by the mixture law (Equation 7) and compared to the experimental value as determined by thermal analysis [5, 15]. If the mixture is a physical mixture, and no interaction occurs during melting, the calculated and experimentally measured enthalpy of fusion, $\Delta H^{\circ}_{f,}$ will be virtually the same. However if an interaction does occur during melting, as in the solubility of a poorly soluble drug is increased by

the melt of another compound, then the difference between the values will be negative or positive. The negative and positive values will further describe the melting process as spontaneous (negative) or not spontaneous (positive) [11].

Construction of Phase Diagrams.

Differential scanning calorimetry (DSC) is a highly sensitive technique widely used to determine the melting temperature and other thermodynamic parameters of materials. The DSC provides information about thermal changes that do not involve a change in sample mass [11]. Thermocouples in the DSC measure the difference in heat flow between a "sample" and a "reference" as a function of changing temperature. Information about the sample such as the enthalpy of fusion, purity, and melting point can all be determined [32]. Eutectic mixtures are combinations of two unique compounds, so the DSC trace will reflect the eutectic mixture as a unique phase of material.

Today, a phase diagram can be constructed by interpreting the DSC traces of mixtures. Mixtures that contain two components will have respective endotherms that may be affected by the melting behavior of each component. This will result in a melting point depression. In a DSC trace, the composition of the mixture will dictate the temperature and shape of the endotherm. The DSC traces of three types of melts are described in Figure 2 [9]. The actual construction of the phase diagram relies on the transfer of thermal information recorded from the DSC curves to the phase diagram (Figures 3a and b.) When the DSC curves of the entire range of mixtures are overlaid, the pattern of the phase diagram can be seen. For example, in Figure 3a, the DSC traces of the mixtures are overlaid to coincide with the melts of the phase diagram in Figure 3b.

The phase diagram is constructed by matching the DSC curve with the two points plotted on the phase diagram that represent the solidus and liquidus curve. As can be seen in curves 2, 3,

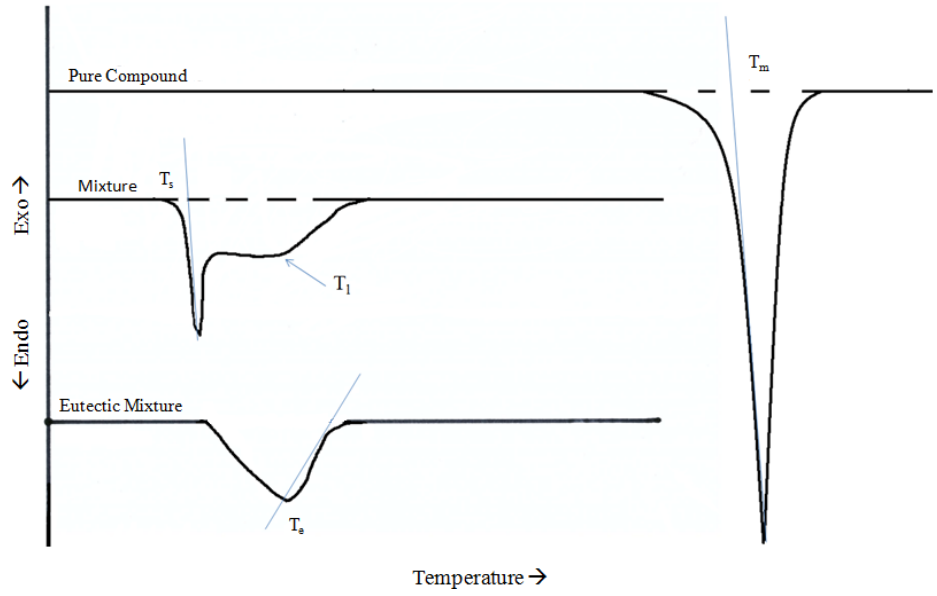

Figure 2. Three theoretical differential scanning calorimetry (DSC) traces show the determination of an onset melt of a pure compound (top, $T_{m,}$). Middle trace is a mixture with two compounds that melt at different temperatures. The initial melt of the mixture (T_s) is the melt of the lower melting compound. The temperature at which both compounds melt completely is the liquidus temperature (T_l.) The bottom trace is the melting behavior of a eutectic mixture where both components have a unified melt (T_e) and the melting temperature is determined at the bottom of the endotherm [9] as described in Figure 2 [9]. The top trace is the sharp melt indicative of a pure component (T_m.) The middle trace is the melting behavior of a mixture that has two components melting at different temperatures (T_s, T_l). The endotherm of the lower melt in the mixture, T_s, is measured at the onset of the melt of the melt of the mixture and the melt of the higher melting component, T_l, is measured from the broad endotherm at the highest temperature before it returns to baseline [9]. On the phase diagram, the solidus boundary is plotted by T_s and the liquidus boundary is plotted by T_l. The melt of the eutectic mixture, bottom trace, has a unified melt and the eutectic temperature, T_e, is measured at the lowest point of the endotherm. The eutectic melt is also plotted as a part of the solidus boundary of the phase diagram [25].

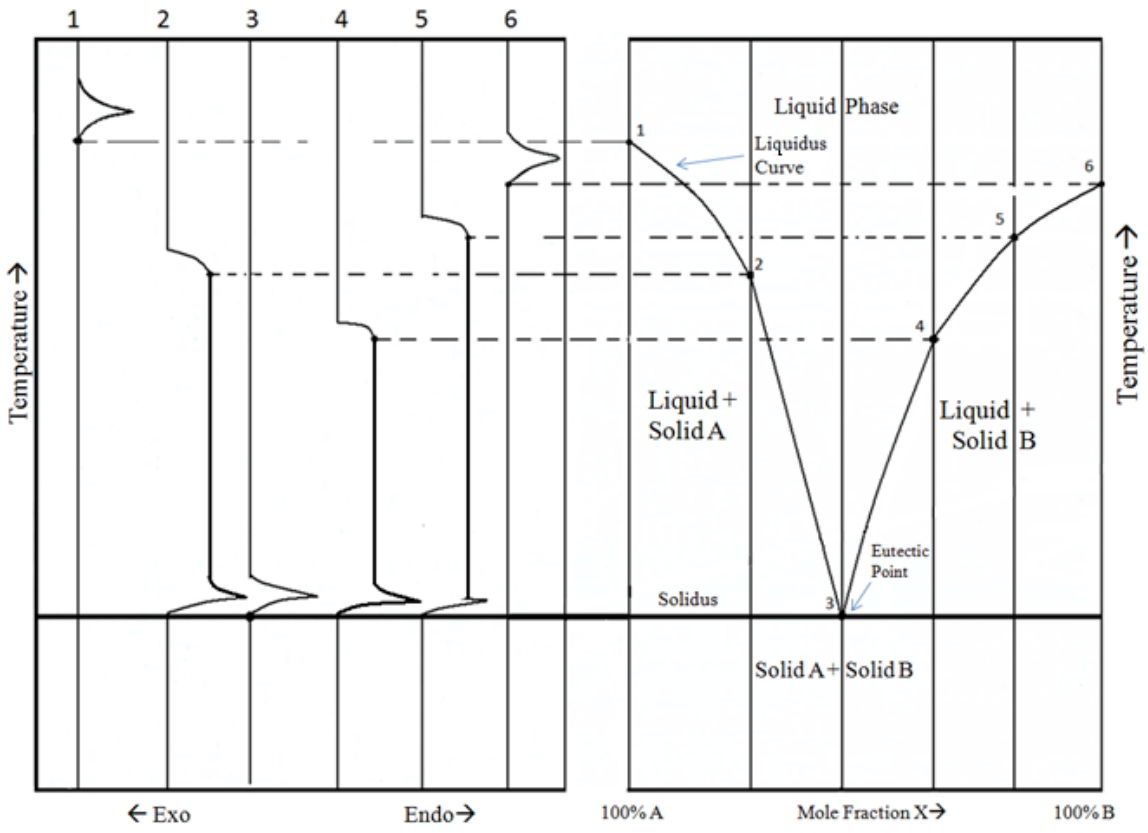

Figures 3a and b. The transfer of thermal information from a DSC curve (3a) to a phase diagram (3b) [32].

and 5, the composition ratios between pure material and the eutectic point show sharp endothermic peaks at the initial melt of the lower melting compound in the mixture.

The actual construction of the phase diagram relies on the transfer of thermal information recorded from the DSC curves to the phase diagram (Figure 3a and b.) When the DSC curves of the entire range of mixtures are overlaid, the pattern of the phase diagram can be seen. For example, in Figure 3a, the DSC traces of the mixtures are overlaid to coincide with the melts of the phase diagram in Figure 3b. The phase diagram is constructed by matching the DSC curve with the two points plotted on the phase diagram that represent the solidus and liquidus curve. As can be seen in curves 2, 3, and 5, the composition ratios between pure material and the eutectic point show sharp endothermic peaks at the initial melt of the lower melting compound in the mixture. As the temperature increases, the endotherm broadens as the entire sample liquefies and eventually returns to the baseline. A phase diagram is useful because the melt of an unknown binary mixture can be determined by using the x- and y-axis of the phase diagram [9].

Types of Binary Phase Diagrams.

There are many types of binary phase diagrams, but the discussion will only include systems that were encountered over the course of the present research. All phase diagrams imply the thermal stability of the mixtures where the temperatures of melting and resolidification are plotted. If the mixtures are not thermally labile, then an overlay of DSC curves of the mixtures can demonstrate the effect of melting the two compounds. However, in some cases, half of the phase diagram may be plotted if the mixtures that contain a majority of the higher melting temperature compound has minimal degradation.

1. Simple Eutectic Mixtures. The phase diagram of a simple eutectic mixture, where there is no solubility between the compounds in the solid state, is illustrated below (Figure 4) [9,

22]. The melting temperatures of the mixtures and pure components is plotted against mixture composition (x-axis) and temperature of the melt (y-axis.). The range of mixtures of A:B reflects the changing proportion from left (100% A/ 0%B) to right (0% B/ 100% A) of the mixtures and the pure components. There are three phases in the phase diagram. The liquid phase is one phase of melted A and B. The mixed phase, liquid + solid A, occurs at temperatures below the liquidus curve where the solid A begins to solidify and B remains a liquid as the temperature decreases. In the mirror image of this phase, liquid + solid B, liquid is present as solid B solidifies as the mixture is cooled. The solidus is the minimum temperature at which both components will solidify and represents is the boundary between the mixed phase and the solid phase of the two compounds [9, 22].

The thermal behavior of the eutectic mixture can be explained by the eutectic phase reaction where the liquid separates into two solids upon cooling below the eutectic temperature as described by equation 9 [22].

$$\text{Liquid} \rightleftarrows \text{A} + \text{B} \qquad \textbf{Equation 9.}$$

If the eutectic mixture is heated to the liquid phase and then cooled, the liquid will solidify at the eutectic temperature and all three phases will be present. The eutectic temperature is the temperature of the eutectic melt and plotted at the solidus line. The eutectic temperature is also invariant. When the eutectic mixture is cooled below the eutectic temperature, the two components will resolidify into the solid phase of A and B. The eutectic phase reaction is also a reversible reaction (Equation 8) [18]. At the eutectic point, all three phases are present simultaneously and can be seen by microscopy.

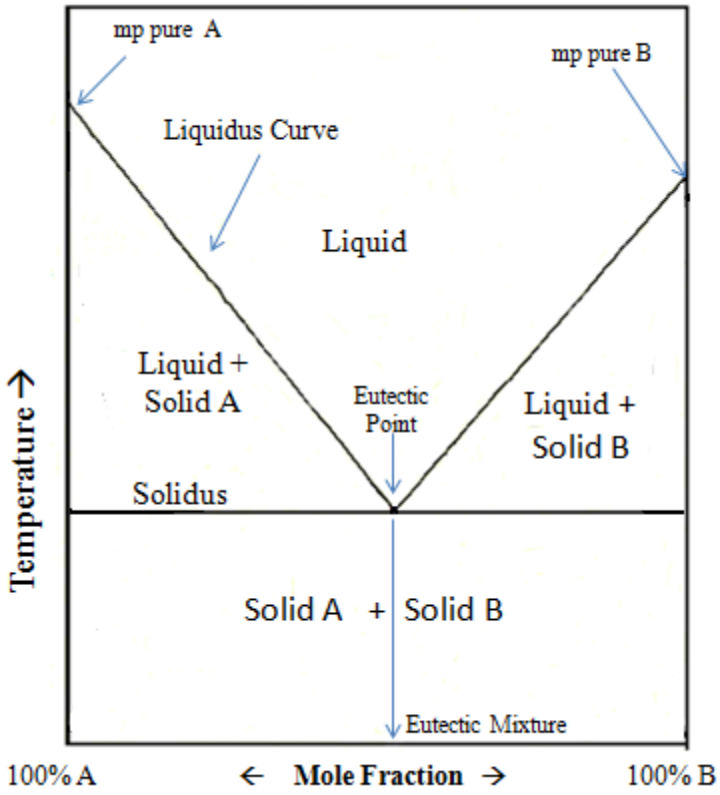

Figure 4. Phase diagram of a simple eutectic system [9, 22].

2. Co-Crystal Phase Diagrams. Pharmaceutical co-crystals are molecular complexes of API of one or more co-crystal former, which are solids at room temperature and formed mainly through hydrogen bonding [33, 35]. The co-crystal is considered a new form of the API (Active Pharmaceutical Ingredient) and may possess different physicochemical properties than the original API. The construction of co-crystals phase diagrams are necessary to find the eutectic mixtures that may present different physicochemical properties than the original co-crystal. Interest in the eutectic mixtures of co-crystals lie in the eutectic melting temperature below the original co-crystal [36].

There are few examples of binary co-crystal phase diagrams for a poorly soluble API's that have been published [33, 35]. A 1:1 co-crystal phase diagram contains two eutectic mixtures and no solid solubility between the compound and co-crystal former (Figure 5) [33]. The characteristics of a 1:1 co-crystal phase diagram are: 1.) a eutectic point, $\mathbf{E_1}$, to the left of the co-crystal melt, $\mathbf{T_{coc}}$, 2.) a second eutectic point, $\mathbf{E_2}$, to the right of $\mathbf{T_{coc}}$, and 3.) $\mathbf{T_{coc}}$ melts at a higher temperature than either eutectic point $\mathbf{E_1}$ or $\mathbf{E_2}$ [15].

The characteristics of a 1:1 co-crystal phase diagram are a eutectic point, $\mathbf{E_1}$ (to the left of the co-crystal melt, $\mathbf{T_{coc}}$), a second eutectic point, $\mathbf{E_2}$, (to the right of $\mathbf{T_{coc}}$) and $\mathbf{T_{coc}}$, which melts at a higher temperature than either eutectic point, $\mathbf{E_1}$ or $\mathbf{E_2}$ [15]. For the purposes of illustration, compound A will be the poorly soluble API and B will be the co-crystal former. The data points of the co-crystal phase diagram are plotted by the composition of the mixture (x-axis) and the melting temperature of the mixture (y-axis). Some of the phases are similar to the eutectic phase diagram discussed above with a few exceptions. For example, there are two solidus lines that are aligned with the eutectic melt of $\mathbf{E_1}$ and $\mathbf{E_2}$ that occur at slightly different temperatures. Below this line, both compounds are solids, and above this boundary one of the compounds begins to

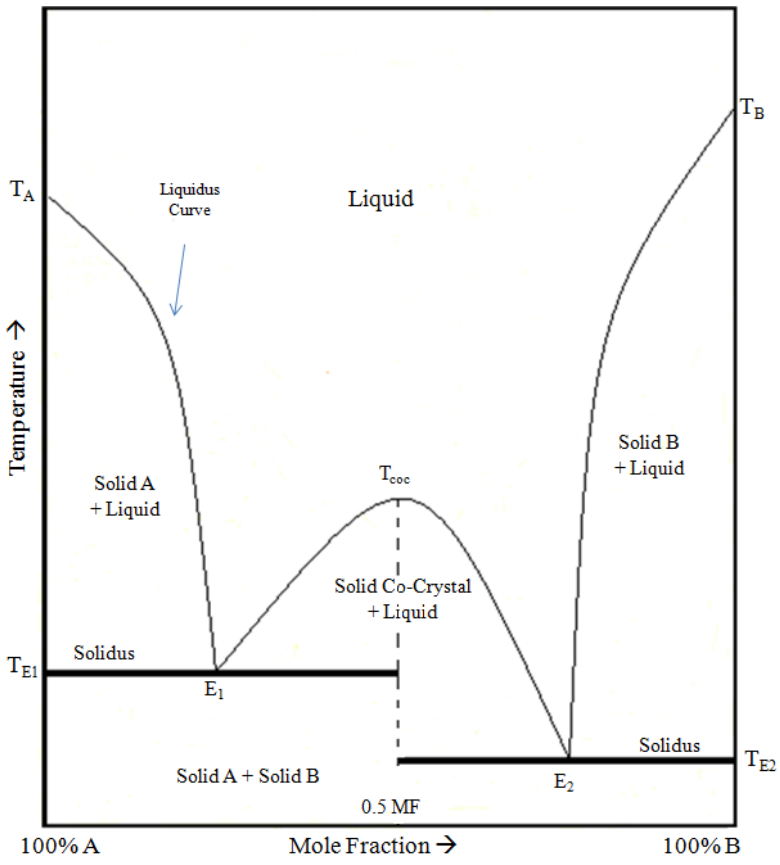

Figure 5. A typical co-crystal phase diagram for a 1:1 co-crystal. There two eutectic melts, $\mathbf{E_1}$ and $\mathbf{E_2}$, which occur at a temperature below the co-crystal melting temperature ($\mathbf{T_{coc}}$) [33, 35].

melt. The mixed phases of co-crystal and component A or B are formed above the solidus line. These phases contain melted co-crystal and solid component A or B. As the 1:1 stoichiometry of the co-crystal is approached in the mixtures, the liquidus curve is not always possible to obtain a full co-crystal phase diagram because of the thermal stability of the compounds and/or the difficulties in mixing the compounds homogeneously [33 – 35].

Introduction of AMG 517, Glipizide, and Naproxen.

The purpose of this work was to investigate eutectic mixtures in three small molecules: AMG 517, naproxen, and glipizide (Figure 6) [35, 37, 39]. All of these drugs suffer from poor solubility and a slow dissolution rate, both of which contribute to limiting bioavailability. These drugs were chosen for the investigation of eutectic mixtures because of the potential to increase solubility and, perhaps, change the intrinsic dissolution rate. AMG 517 is a potential vanilloid 1 receptor antagonist (TRPV1) that was developed by Amgen, Inc. for the treatment of chronic pain. The API was chosen because of stability at high temperatures and the ability to form co-crystals in specific conditions [35]. AMG 517 was investigated by the fusion and solvent method to form co-crystal phase diagrams and discover the possible eutectic mixture(s). Although solubility was not the issue that removed AMG 517 from the clinic, the molecule is useful to study due to its low solubility and dissolution rate [35]. Naproxen is a small molecule often employed to treat mild chronic pain as a non-steroid anti-inflammatory drug (NSAIDS). Naproxen is also thermally stable and has a lower melting point (153 ˚C), enabling it to melt at lower temperature with a complimentary compound [39]. The ability to make a eutectic mixture was investigated because naproxen is widely available, easily accessible, and exhibits low toxicity. Finally, glipizide is a small molecule that is widely prescribed for Type II diabetes [40]. It was also chosen to investigate eutectic mixtures because of low solubility in aqueous media

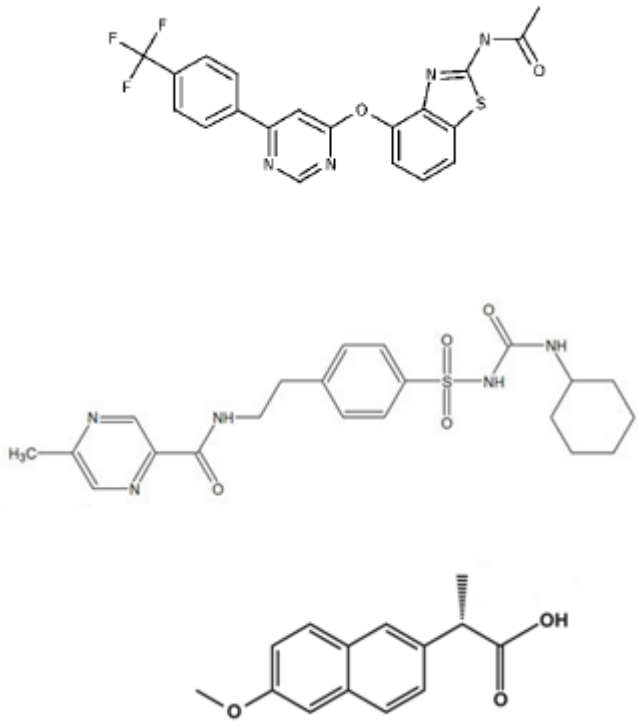

Figure 6. AMG 517 (top) [35], glipizide (middle) [39], and naproxen (bottom) [37].

and slow dissoluton rate. However,glipizide is not thermally stable, so the preparation of eutectic mixtures by the fusion method would be closely monitored for evidence of degradation.

During the experiements, if the drug displayed a depressed melt when heated with another compound or eutectic mixture was suspected to have been prepared, then the mixture was further evaluated in solubility experiments in DI water and PBS. Ultimately, if the solubility of the poorly soluble compound was increased in either media, then intrinsic dissolution experiments would be designed. If the intrinsic dissolution rate was found to be increased as well, then the pharmaceutical scientist would be able to use these parameters to select not only other forms of the drug, if possible, but to evaluate the possible bioavailability *in vivo* of the eutectic mixture as well.

Conclusions.

Eutectic mixtures have been investigated for pharmaceutical purposes since the 1960's and serve in various functionalities across industries. Interest has amplified over recent in years in the pharmaceutical industry due to advances in thermal analysis. With increased knowledge, in the future there may be sufficient information available to promote eutectic mixtures as a major strategy to overcome API physical propertery limitations.

References.

1. Chen, Y.; Qi, X.; Liu R. Chapter 3 Prediction of Solubility. In *Water-Insoluble Drug Formulation.* 2nd ed; Liu, R., Ed.; CRC Press: Boca Raton, Fl, 2008; pp 23-59.
2. Vasnthavada, M.; Tong, W.; Serajuddin, A. Chapter 18 Development of Solid Dispersion for Poorly Water-Soluble Drugs. In *Water-Insoluble Drug Formulation.* 2nd ed; Liu, R., Ed.; CRC Press: Boca Raton, Fl, 2008; pp 499-529.
3. Avula, S.; Alexander, K.; Riga, A. Predicting Eutectic Behavior of Drug Excipients by Unique Calculations. *J. Therm. Anal. Calorim.* **2010**, *99*, pp 655-658.
4. Eutectic definition. Merriam-Webster Dictionary [Online] http://www.merriam-webster.com/dictionary/eutectic

5. Rai, U. S.; Rai, R. N. Physical Chemistry of Organic Eutectics. *J. Therm. Anal. Calorim.* **1998**, *53*(3), pp 883-893.
6. Goldberg, H.; Gibaldi, M.; Kanig, L. Increasing Dissolution Rates and Gastrointestinal Absorption of Drugs via Solid Solutions and Eutectic Mixtures I - Theoretical Considerations and Discussion of the Literature. *J. Pharm. Sci.* **1965**, *54*, pp 1145-1148.
7. Brodin, A.; Nyqvist-Mayer, A.; Wadsten, T.; Forslund, B.; Brogerg, F. Phase Diagram and Aqueous Solubility of the Lidocaine-Prilocaine Binary System. *J. Pharm. Sci.* **1983**, *73*(4), pp 481-484.
8. Baker, H. (ed.) British abstracts. Chemical Engineering and Industrial Inorganic Chemistry, Including Metallurgy. London, UK: 1-29. 1945-1949.
9. Stott, P. W.; Williams, A. C.; Barry, B. W. Transdermal Delivery from Eutectic Systems: Enhanced Permeation of a Model Drug, Ibuprofen. *J. Controlled Release* **1998**, *59*, pp 297-308.
10. Vippagunta, S.; Wayne, Z.; Hornung, S.; Krill, S. Factors Affecting the Formation of Eutectic Solid Dispersions and their Dissolution Behavior. *J. Pharm. Sci.* **2007**, *96*(2), pp 294-304.
11. Martin, A. *Physical Pharmacy*, 4th ed.; Lippincot Williams & Wilkins: Baltimore, Md, 1993; pp 20–45, 62-65.
12. Chiou, W. L.; Riegelman, S.; Pharmaceutical Applications of Solid Dispersion Systems. *J. Pharm. Sci.* **1971**, *60*, pp 1281-1302.
13. Ford, J. The Current State of Solid Dispersions. *Pharm. Acta. Helv.* **1986**, *61*(3), pp 69-88.
14. Zajc, N.; Srcic, S. Binary Melting Phase Diagrams of Nifedipine-PEG4000 and Nifedipine-Mannitol Systems. *J. Therm. Anal. Calorim.* **2004**, *77*, pp 571-580.
15. Yalkowsky, S. H. *Solubility and Solubilization in Aqueous Media*, American Chemical Society: Washington, D.C. 1999; pp 2-45, 49-80, 83-90.
16. Sekiguchi, K.; Obi, N. Studies on Absorption of Eutectic Mixture. I. A Comparison of the Behavior of Euectic Mixture of Sulfathiazole and that of Ordinary Sulfathiazole in Man. *Chem. Pharm. Bull.* **1961**, 9, pp 866-872.
17. Wolffenbuttel, R. Low-Temperature Intermediate Au-Si Wafer Bonding: Eutectic or Silicide Bond. *Sens. Actuators, A* **1961**, *62*(1), pp 680-686.
18. Dhirendra, K.; Lewis, S.; Udupa, N.; Atin, K. Solid Dispersions: A Review. *Pak J. Pharm. Sci*. **2009**, *22*(2), pp 234-246.
19. Jansenns, S.; Van den Mooter, G. Review: Physical Chemistry of Solid Dispersions. *J. Pharm. Pharmacol.* **2009**16:1571-1586.
20. Carstenson, J. T.; Patel, M. Non-Sink Dissolution Rate Equations. *J. Pharm. Sci.* **1975,** *64*(10), pp 1651-1656.
21. Kawakami, K. Modification of Physicochemical Characteristics of Active Pharmaceutical Ingredients and Application of Supersaturable Dosage Forms for Improving Bioavailability of Poorly Absorbed Drugs. *Adv. Drug Delivery Rev.* **2012**, *64*, pp 480-495.
22. Pilling J. *Phase Diagrams and Microstructure: A Computer-Aided Learning Guide.* The Institute of Materials: London, UK, 1992; pp 28-85
23. Ran, Y; Jain, N; Yalkowsky, S.H. Prediction of Aqueous Solubility of Organic Compounds by the General Solubility Equation (GSE.) *J. Chem. Info Comp. Sci.* **2001**, *41*, pp 1208-1217.

24. Serajuddin, A. T. M. Solid Dispersions of Poorly Water-Soluble Drugs: Early Promises, Subsequent Problems, and Recent Breakthroughs. *J. Pharm. Sci*. **1999**, *88*(10), pp 1058–1066.
25. Bak, A.; Gore, A.; Yanez, E.; Stanton, M.; Tufekcic, S.; Syed, R.; Akrami, A.; Rose, M.; Surapaneni, S.; Bostick, T.; King, A.; Neervannan, S.; Ostovic, D.; Koparkar, A. The Co-Crystal Approach to Improve the Exposure of a Water-Insoluble Compound: AMG 517 Sorbic Acid Co-Crystal Characterization and Pharmacokinetics. *J. Pharm. Sci.* **2008**, *97*(9), pp 3942-3956
26. Jain, N.; Yalkowsky, S. H. Estimation of the Aqueous Solubility I: Application to Organic Nonelectrolytes. *J. Pharm. Sci.* **2001,** *90*, pp 234-252.
27. Oberoi, L. M.; Alexander, K. S.; Riga, A. T. Evaluation of an Index Based on Van't Hoff Equation to Predict PEG-Drug Eutectic Composition. *J. Therm. Anal. Calorim.* **2004**, *78*, pp 83-89.
28. Predel, B.; Hoch, M.; Pool, M. *Phase Diagrams and Heterogenerous Equilibria: A Practical Introduction.* Springer: Berlin, Germany, 2004: p 58.
29. Liu, R. *Chapter 1: Introduction.* In Water-Insoluble Drug Formulation 2nd ed; Liu, R., Ed.; CRC Press: Boca Raton, Fl, 2008; pp 1-20.
30. Rai U. S; Pandi, P. Solidification Behavior of Binary Organic Eutectics and Monotectics; 1,2,4,5-tetrachlorobenzene-*m*-aniophenol System. *Materials Letters* **1998**, *39*, pp 166-172.
31. Pesaturo, K. A.; Matthews, M. Topical Anesthesia Use in Children: Eutectic Mixtures of Local Anesthetics. http://www.medscape.com/viewarticle/704761_2
32. Component Analysis of Minute Amounts of Solder in IC Chip. Application brief. TA No.29 SII NanoTechnology, Inc. **1986**, pp 1-3.
33. Yamashita, H.; Hirakura, Y.; Teramura, T.; Terada, K. Detection of Cocrystal Formation Based on Binary Phase Diagrams Using Thermal Analysis. *Pharm Res* **2013**, *30*, pp 70-80.
34. Stanton, M.; Kelly, R.; Colletti, A.; Kiang, Y-H.; Langley, M.; Munson, E.; Peterson, M.; Roberts, J.; Wells, M. Improved Pharmacokinetics of AMG 517 through Co-Crystallization Part 1: Comparison of Two Acids with Corresponding Amide Co-Crystals. *J. Pharm. Sci*. **2010**, *99*(9), pp 3769-3778.
35. Sangster, J. Phase Diagrams and Thermodynamic Properties of Binary Organic Systems Based on 1,2-, 1,3-, 1,4-diaminobenzene or benzidine. *J. Phys. Chem.* **1994**, *23*, pp 295-338
36. Gavva, N. R.; Treanor J. J. S.; Garami, A.; Fang, L.; Surapaneni, S.; Akrami, A.; Alvarez, F.; Bak, A.; Darling, M.; Gore, A.; Jang, G.; Kesslak, J. P.; Ni, L.; Norman, M. H.; Palluconi, G.; Rose, M. J.; Salfi, M.; Tan, E.; Romanovsky, A. A.; Banfield, C.; Davar, G. Pharmacological Blockade of the Vanilloid Receptor TRPV1 Elicits Marked Hyperthermia in Humans. *Pain* **2008**, *136*, pp 202-210.
37. Naproxen, Material Safety Data Sheet obtained by Sigma Aldrich, Co. 2013
38. Glipizide, Material Safety Data Sheet obtained by Alexis Biochemicals. 2010.
39. Mura, P.; Faucci, M. T.; Manerioli, A.; Bramanti, G.; Parrini, P. Thermal Behavior and Dissolution Properties of Naproxen from Binary and Ternary Solid Dispersions. *Drug Dev. Ind. Pharm.* **1999**, *25*(3), pp 257-764.
40. Vankateswarlu, K.; Shanthi, A. Formulation and Evaluation of Sustained Release glipizide Matrix. *J. Pharm. Bio. Sci*. **2012**, *2*(5), pp 17-22.

Chapter 2. Background

Urea-Benzoic Acid: A Model Eutectic System

Introduction. A simple model eutectic binary system comprised of urea (**U**) and benzoic acid (**BA**) has previously been established (Figure 1) [1]. **U** and **BA** mixtures have no solid solubility at room temperature and one eutectic point [1 – 3]. The purpose of this work was to compare the preparation of the **U:BA** phase diagram using DSC analysis and ball-milling to the thaw-melt (or fusion) method as previously published [1, 5].

Some methods of preparing eutectic mixtures are well-established: the fusion method, the solvent method, and the hybrid fusion-solvent method. All of these methods rely on the ability to form a homogeneous mixture of two compounds. Ball milling is another method that can be used to form homogeneous mixtures of two, or more, compounds. In this work, ball milling was investigated as a method to prepare homogeneous mixtures of **U:BA** used in the preparation of the 2-component phase diagram.

The 2-component phase diagram of **U:BA** mixtures have been previously published by Rai, et al [1]. They used the fusion method to construct the phase diagram [1, 5, 6] with the experiments being performed by filling capillary tubes with physical mixtures of **U** and **BA** in different proportions, followed by repeated melting and freezing. The temperatures at which the mixtures would thaw and melt were visually observed and recorded. On heating the solidus temperature was noted when the mixture first began to melt. The liquidus temperature was marked when the mixture completed melted. During cooling, the liquidus temperature was recorded when the liquid first began to solidify and the solidus temperature was marked again when the mixture completed solidified. This cycle was repeated as needed. The eutectic mixture was identified as the mixture composition where the solidus and liquid curves met. The **U:BA** system was chosen

because it was known and the difference in temperature between the eutectic and liquidus melts was large (> 50°C), which should aid detection, and the compounds were readily available making it a good system to use to develop the experimental techniques that would be used throughout this research project.

Experimental.

Materials. Urea (**U**) was purchased by Fluka (lot1328820) and used as received. **BA** was purchased by Spectrum (lot VC116) and used as received.

Preparation of eutectic mixtures. U and **BA,** 25 mg combined, were weighed into tared aluminum weigh boats and transferred into 1.5 mL Retsch ball jars. A 5 mm stainless steel ball was added to each ball jar, and then placed into the Retsch ball mill (Retsch, Inc. Newton, PA.) The ball jars were agitated for 2 minutes at 30 Htz. The mixtures were then removed from the ball jar and analyzed. The mole fractions (MF) of **BA** were calculated by adding the total number of moles in the mixture, and then dividing the total by the number of moles of **BA** [6]. The mixture attains equilibrium at different phases in the phase diagram. When the eutectic mixture solidifies, it forms a microstructure that can be detected by microscopy [6].

Differential Scanning Calorimetry (DSC.) Physical mixtures prepared for the phase diagram were analyzed by DSC on a TA Instruments Q100 calorimeter. The melting temperature of the mixtures were determined by one DSC sample per mixture. The weights of the DSC samples and the standard deviation between the DSC weights was recorded (1.17 ± 0.12 mg.) The samples were equilibrated at 25 °C, and then ramped to 275 °C at 10°C/min in aluminum hermetically sealed DSC pans. The enthalpies of fusion were determined by integrating the endotherm of the onset melt of the mixture.

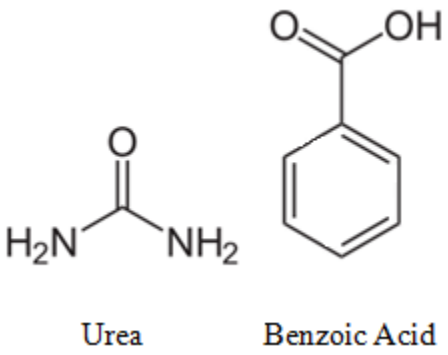

Figure 1. Chemical structures of **U** and **BA** [2, 3].

Further analysis involving the 0.2 MF mixture, 0.6 MF mixture, 0.442 MF eutectic mixture, and 0.8 MF mixtures were analyzed in a heating/cooling cycling experiment. Sample sizes of 3.25 ± 0.25 mg were weighed into a hermetically sealed DSC pan and equilibrated to 25 °C. The sample was then heated to 125 °C at 5 °C/min and cooled to 25 °C. Each sample was heated and cooled in three cycles, except for the 0.6 MF mixture which was heated and cooled to the same temperature range twice. The data obtained for the 0.2, 0.6, and 0.8 MF mixtures are included in the Appendix.

X-Ray Powder Diffraction (XRPD). The XRPD data were obtained for **U**, **BA**, and the 0.442 MF **U:BA** mixture. The data were obtained on a PANalytical X'Pert PRO X-ray diffraction system with RTMS detector. Samples were scanned in continuous mode from 5-45 ° (2θ) with step size of 0.0334 ° at 45 kV and 40 mA with CuKα radiation (1.54 Å). The incident beam path was equipped with a 0.02 rad soller slit, 15 mm mask, 4 ° fixed anti-scatter slit and a programmable divergence slit. The diffracted beam was equipped with a 0.02 rad soller slit, programmable anti-scatter slit and a 0.02 mm nickel filter. Samples were prepared on a low background sample holder and placed on a spinning stage with a rotation time of 2 s.

Results and Discussion

Phase Diagram. The DSC curves from the experiment (Figure 2) were overlaid to construct the **U:BA** phase diagram below (Figure 3). In both figures, the melting temperature of **U** decreases with the addition of **BA** as it reaches the eutectic temperature at the eutectic point. At this point, the system is invariant [6, 7]. When the eutectic mixture is heated above the eutectic temperature, the mixture melts into liquid. The eutectic temperature becomes the solidus boundary [1, 6, 7]. The experimental eutectic point is located at 0.442 MF mixture, which is the same eutectic mixture composition as previously reported [1].

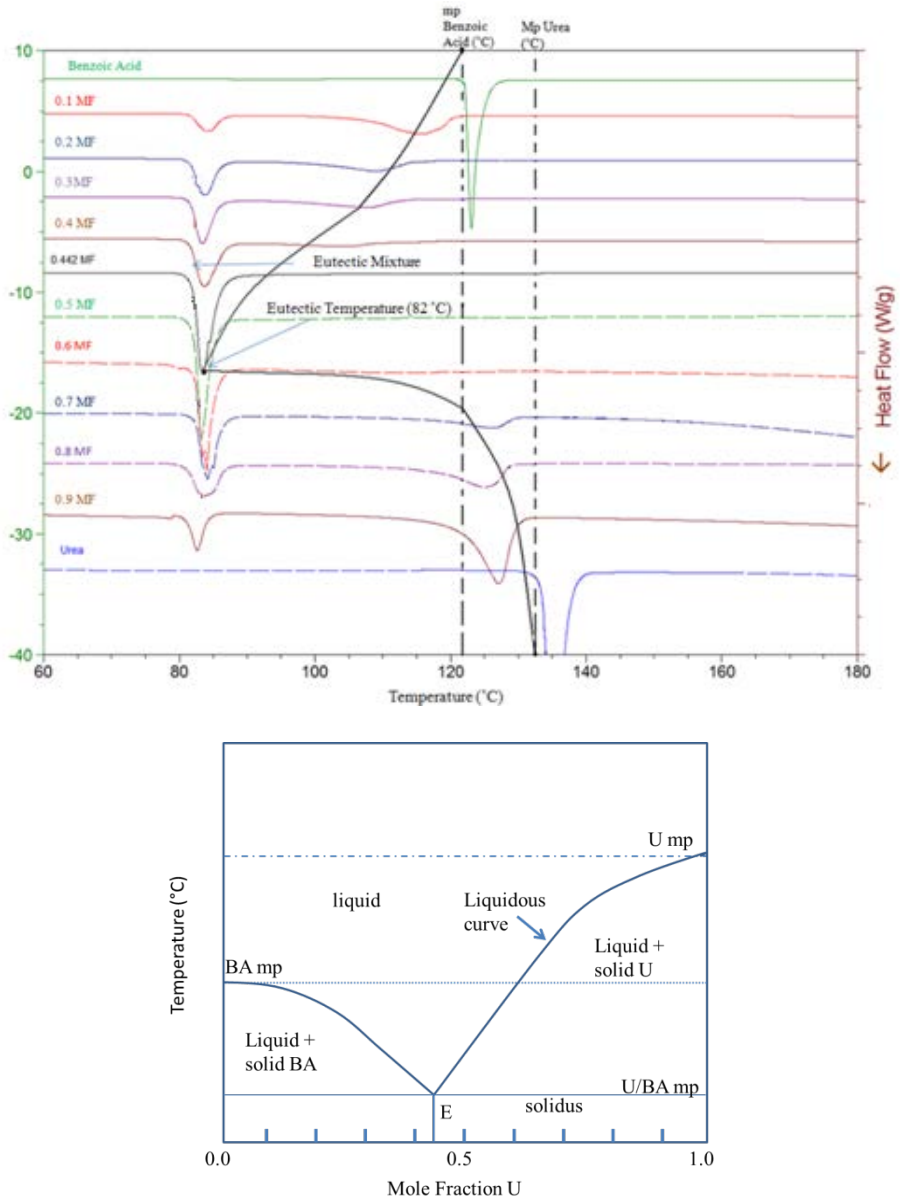

Figure 2. (Top) DSC curves of ball milled mixtures of **U** and **BA.** Mixtures are arranged with **BA** at the top and then mixtures of increasing amounts of **U** being added to the system progressively move downward. (Bottom) **U:BA** phase diagram. The melting temperatures of **BA** and **U** are indicated with solid (BA) and dashed (U) lines across the phase diagram. A solid black line follows the depressed endotherms from pure **U** (right) down to pure **BA** (left).

As more **BA** is added to the system past the eutectic point, the melting point of the mixture increases until the melting temperature of pure benzoic acid is obtained. The eutectic point is at 0.442 MF (E).The experiment resulted in an observed melting temperature of the eutectic mixture at 83.6 °C versus 87.5 °C from literature [1]. The thaw-melt method that was followed in the literature heated and cooled the mixtures at a different rate as compared to the rate used in the present work. The heating rate for the mixtures in the present DSC experiment (10 ˚C/min) was faster than the original published experiment and may play a factor in the discrepancy between the melting and cooling temperature of the mixtures when compared, although faster heating rates are often associated with a shift to higher temperatures. The most important aspects from the comparison of the experimental and literature techniques for analysis are: the shape of the phases in the diagrams are similar, the eutectic mixtures occur at similar temperatures and the same mixture composition, and the other **U:BA** mixtures displayed similar thermal behaviors as the published experiments [1].

XRPD Analysis. The detection of an unknown form of an Active Pharmaceutical Ingredient (API) can be determined by the presence of unknown melts when a mixture is heated and analyzed by DSC. The confirmation of the new form can be aided by the observation of a unique XRPD pattern. To determine whether or not a new form was discovered during the ball milling process to prepare the mixtures, the XRPD patterns of the original compounds and the 0.442 MF eutectic mixture were compared. The peaks of the original compounds (top and bottom traces) are also are present in the 0.442 MF **U:BA** eutectic mixture (middle trace). These results confirms a physical mixture and not the presence of a new form (Figure 3).

DSC cycling experiments. DSC heating/cooling cycling experiments were conducted to verify the reversible phase formation of various mixture compositions of **U** and **BA**. This DSC

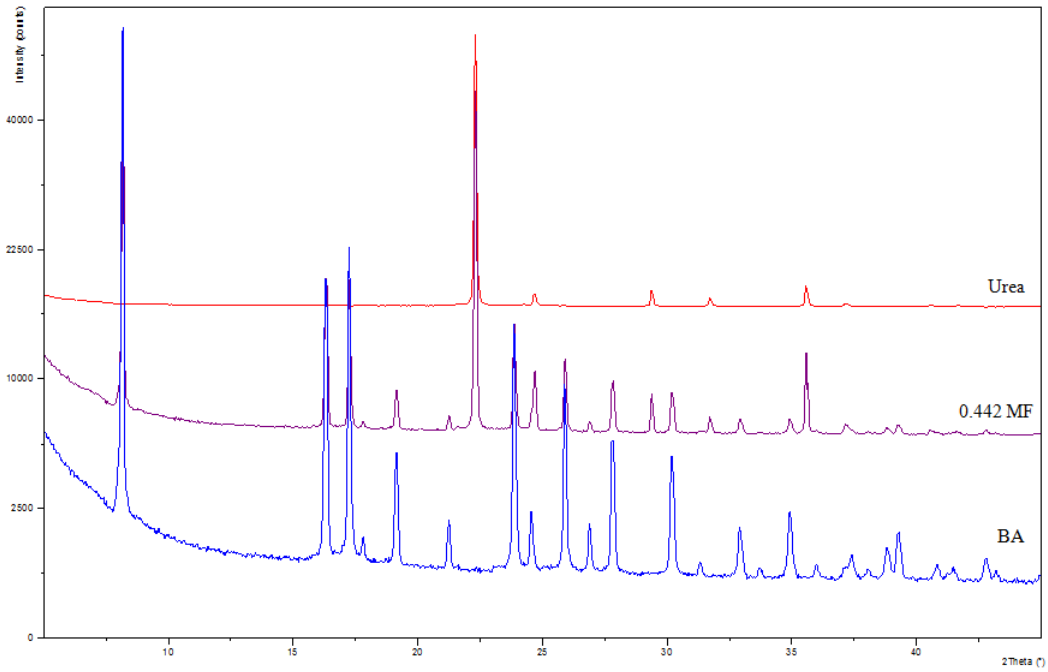

Figure 3. Overlay of XRPD traces of **U** (top red trace), the 0.442 MF **U:BA** mixture (middle trace), and **BA** (**BA**, bottom blue trace.)

method would be similar to the thaw-melt method published previously [1]. The heating/cooling cycle will be useful to analyze the melting behavior of mixtures because the data provides a solidus and a liquidus temperature that can be plotted on a phase diagram. The resulting melting endotherms will refer to the melt of the mixture and the exotherms correspond to the melt re-solidifying into the original components. If a mixture does not exhibit this reversible phase transition, then it cannot be classified as a eutectic.

The mixtures chosen for heating and cooling all displayed the ability to melt and reform to the original components. The only difference between the other mixtures and the eutectic composition was that at the eutectic composition a lower melting temperature was observed. The DSC trace of the 0.442 MF mixture, the eutectic composition identified from heating/cooling experiments, is shown in Figure 4. The sample was heated and cooled in three consecutive cycles that ranged from room temperature (25 ˚C) to the melting temperature of benzoic acid. The onset melting temperature of the mixture occurred at 77 ˚C (± 2 °C), slightly below the reported eutectic melting temperature and ~ 7 °C below the eutectic melting point from the first freeze-thaw cycle. The exotherms that correspond to re-solidification of the original compounds upon cooling were fairly consistent (44 ˚C ± 4 ˚C.) All of the mixtures were thermally stable and did not show evidence of degradation. The lack of degradation and the consistent onset melting temperature and resolidification of the mixtures are characteristic of the eutectic phase transition [1, 6, 7]. The heating and cooling cycling technique can therefore be used to test future mixtures for evidence of eutectic formation.

Thermochemistry. The enthalpies of fusion of the pure components and eutectics are significant to determine the mechanism of solidification/crystallization as the eutectic mixture cools [1, 4, 7]. The specific mechanism of solidification of the eutectic mixture of **U** and **BA** is

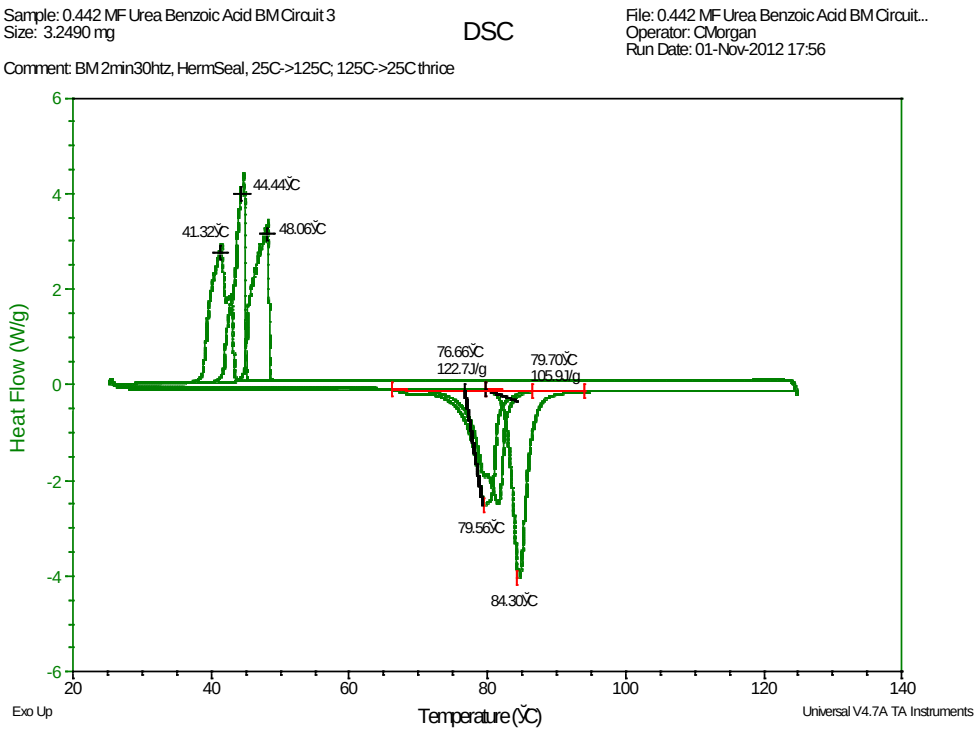

Figure 4. DSC overlay of three cycles the 0.442 MF eutectic mixture heated and cooled during the DSC cycling experiment. The melting of urea and **BA** is a reversible reaction, which can be seen by the melt at 77°C - 80 °C and the accompanying recrystallization which occurs between 41 °C - 48°C.

beyond the scope of this work, but the enthalpy of fusion, enthalpy of mixing, and melting point can be determined [1, 5, 7].

Conclusion

The **U:BA** system is a useful system to determine a new method to prepare and analyze eutectic mixtures. The phase diagram of mixtures of **U: BA** was prepared and the eutectic mixture was identified. The experimental results were very similar to the data previously published in literature.

References

1. Rai, U. S.; Rai, R. N. Physical chemistry of organic eutectics. *J. Therm. Anal.* **1998**, *53*, pp 883-893.
2. Urea, MSDS, Fluka.
3. Benzoic Acid, MSDS, Spectrum.
4. Rai, U. S.; George, S. Physicochemical Studies on Eutectics and the 1:1 Addition Compound: benzidine-α-naphthol System. *J. Mater. Sci*. **1992**, *27*, pp 711-718.
5. Singh, N. P.; Shukla, B. M; Singh, N.; Singh, N. B. Structures of Melts in Binary Organic Eutectics and Molecular Complexes: phenanthrene-picric acid and anthracene-picric acid Systems. *J. Chem. Eng. Data*, **1985**, *30*, p 49.
6. Pilling, J. *Phase Diagrams and Microstructure: A Computer-Aided Learning Guide.* Institute of Materials: London, UK, 1992; pp 30-40.
7. Yalkowsky, S. H. *Solubility and Solubilization in Aqueous Media*, American Chemical Society: Washington, D.C. 1999; pp 20-35.

Chapter 3. AMG 517 Binary Systems

Introduction. The goal of this work was to utilize a novel underutilized strategy to enhance the solubility and may change the intrinsic dissolution rate of AMG 517. This was in binary AMG 517 systems known to form small molecule co-crystals. Few eutectic mixtures have been pursued vigorously in the pharmaceutical industry for a variety of reasons (Chapter 1). Eutectic mixtures, however, might present one part of the solution to evaluate or develop compounds exhibiting dissolution limited bioavailability.

AMG 517, a vanilloid 1 receptor antagonist (TRPV1) being developed for the treatment of chronic pain, is an anhydrous freebase small molecule that encountered challenges in development due to various physicochemical characteristics, such as poor solubility in water and buffers at physiological pH (Figure 1) [1]. Salt formation was unsuccessful in overcoming the solubility limitation to *in vivo* exposure due to rapid disproportionation and precipitation of the insoluble freebase hydrate in aqueous media The other existing forms of **AMG 517** also have low solubility in aqueous media resulting in these forms being unsuitable for development [1, 2]. The drug is also thermally stable and melts at 226 - 230 ˚C, which presented **AMG 517** as a candidate to form eutectic mixtures by the fusion method [3, 4]. Due to the thermal stability of the API, and the exhistence of several co-crystals, **AMG 517** was utilized in this study in a search to find a eutectic mixture [3, 4, 7].

In this work, the two component phase diagrams for **AMG 517** and another compound, for example the co-crystal former sorbic acid (**SA**), were prepared and evaluated. The preparation of the mixtures necessary to construct the phase diagrams of **AMG 517** and the small molecules was accomplished by ball milling or solvent evaporation [3, 4]. Phase diagrams were prepared for **AMG 517** with the following small molecules: the **SA**, *trans*-cinnamic acid **(CA)**, xylitol **(XYL)**,

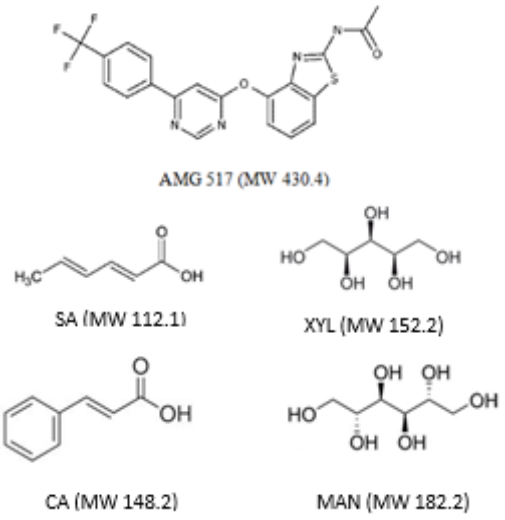

Figure 1. Chemical structures of **AMG 517**, **SA**, **CA**, **XYL**, **MAN** [2, 12].

and mannitol (**MAN)** (Figure 1) [8– 10]. The co-crystal phase diagrams of **AMG 517** and **SA** and **AMG 517** and **CA** were also investigated. Differential scanning calorimetry (DSC) is a common method to discover eutectic mixtures by comparing the melting points across a series of mixtures [3, 4, 7, 8 -11].

Experimental

Materials: AMG 517, the **AMG 517 SA** co-crystal **(AMG 517/SA)**, the **AMG 51**7 **CA** co-crystal (**AMG 517/CA)**, and **AMG 517** hydrate (**AMG 517·H_2O**) were synthesized by Amgen medicinal chemistry [1, 13]. **SA, CA**, **MAN,** tetrohydrofuran (THF**)**, and **XYL** were purchased from Sigma Aldrich and used as received. Methyl ethyl ketone (MEK)**,** diethyl ether, acetone were all purchased from JT Baker. Ethanol (EtOH) was purchased from Pharmco. All compounds were stored on the bench top, except for **AMG 517**, **AMG 517/SA**, **AMG 517/CA**, and the **AMG 517·H_2O** which were stored in room temperature desiccators.

X-Ray Powder Diffraction (XRPD). XRPD patterns were obtained on a PANalytical X'Pert PRO X-ray diffraction system (Almelo, the Netherlands). Samples were scanned in continuous mode from 5-45 º (2θ) with step size of 0.0334 º on a spinning stage at 45 kV and 40 mA with CuKα radiation (1.54 Å). The incident beam path was equipped with a 0.02 rad soller slit, 15mm mask, 4 º fixed anti-scatter slit and a programmable divergence slit. The diffracted beam was equipped with a 0.02 rad soller slit, programmable anti-scatter slit and a 0.02 mm nickel filter. Samples were prepared on a low background sample holder and placed on a spinning stage with a rotation time of 2 sec. Detection was accomplished with an RTMS detector (X'Celerator). Data analysis was conducted with PANalytical X'Pert Data Viewer software.

Thermal Analysis Methods. DSC was performed on a TA Instruments Q100 calorimeter (New Castle, DE) at 10 ºC/min from 25 to 275-300 ºC. The melts of each mixture in the phase

diagram was determined by one DSC sample as analyzed in hermetically sealed pans, except for the **AMG 517** and **SA** mixtures (**AMG 517:SA**) and the **AMG 517/SA** mixtures, which were analyzed by open DSC pans.

AMG 517:**SA** mixtures were weighed into DSC pans in triplicate (2.81 ± 0.27 mg) and analyzed in open and hermetically sealed DSC pans, but only data obtained by open DSC pans were ultimately used to compare the melts of the mixtures prepared for the phase diagram. One of the melts of the mixtures analyzed in triplicate was chosen as representative of all three and overlaid in Figure 3.

Some, such as the **AMG 517:XYL** mixtures, were also analyzed by thermal gravimetric analysis (TGA). This analysis was performed on a TA instruments Q500 analyzer at 10 °C/min from 25 – 275 °C in a platinum pan under dry nitrogen at 90 mL/min. Data analysis was collected by TA Instruments Universal Analysis 2000 software v4.4A.

Ball milling Experiments.

Binary Mixtures of AMG 517 with SA, XYL, and MAN. Physical mixtures of **AMG 517**:**SA**, **AMG 517:XYL**, and **AMG 517:MAN** were prepared by weighing the two starting materials in different proportions to cover the range of mole fractions needed to prepare the phase diagram in 25 – 40 mg sample sizes. The mixtures were transferred to a 1.5 mL Retsch ball jar and a 5 mm steel ball was added to each jar. The ball jars were placed into the Retsch ball mill (Retsch Inc., Newton, PA.) The **AMG 517:SA** and **AMG 517:XYL** mixtures were ball milled for 2 minutes at 15 Htz. The **AMG 517:MAN** mixtures were ball milled for 5 minutes at 30 Htz. The samples were then removed and analyzed by XRPD and DSC for analysis. The **AMG 517:XYL** mixtures analyzed similarly, but TGA analysis was included.

The AMG 517/SA Mixtures. Mixtures were prepared for the **AMG 517/SA** phase diagram by adding **AMG 517** or **SA** to **AMG 517/SA**. The compounds were weighed into tared aluminum weigh boats and transferred to a 1.5 mL Retsch ball jars and a 5 mm stainless steel ball was added before milling (Table 1). The **AMG 517/SA** mixtures were ball milled for 2 minutes at 15 Htz. The total mole fraction of **AMG 517** in the resulting mixture was calculated as follows (Equation 1):

$$\text{Mole Fraction} = \frac{\text{mmoles AMG 517}}{\text{mmoles AMG 517} + \text{mmoles of SA}} \qquad \textbf{Equation 1}.$$

Organic Solvents Solubility Screen

The solubility of **AMG 517** was visually estimated in several organic solvents. **AMG 517** was weighed (5.5 – 5.7 mg) and transferred into 2.5 mL Eppendorf tubes. Ether, EtOH, acetone, THF, and MEK were pipetted (500 uL) into each tube. **CA** (5.5 mg) was weighed and added to a 2.5 mL Eppendorf tube containing **AMG 517** and then 500 µL MEK was added. All of the samples were labeled and vortexed briefly. The samples that contained **AMG 517** in EtOH and ether and ether were cloudy suspensions. The samples that contained THF, MEK, and acetone were solutions. The sample that contained **CA** and **AMG 517** was also in solution. The samples were then placed on a shaker for 24 hours at 25 ˚C. The next day, the samples did not change in appearance of solubility. The caps were opened and left on the benchtop to allow solvent to evaporate. However, the sample that contained **AMG 517** and ether did not contain any recoverable solids. The remaining solids were analyzed by XRPD.

Solvent Evaporation Experiments.

AMG 517 CA in MEK. Stock solutions of **AMG 517** and **CA** were prepared in **MEK** at 10 mg/mL. Nine mixtures and two starting material samples were prepared by pipetting different volumes of stock solutions into 4 mL vials. Each sample was vortexed briefly. All samples,

	AMG 517/SA					SA Addition		
	AMG 517/SA (mg)	**SA** (mg) (21%)	**AMG 517** (mg) (79%)	**SA** (mmols)	**AMG 517** (mmols)	(mg)	(mmol)	Mole Fraction of **AMG 517**
Sample 1	25	5.25	19.75	0.047	0.046	20.66	0.184	0.17
Sample 2	25	5.25	19.75	0.047	0.046	7.7	0.069	0.28
Sample 3	50	10.5	39.5	0.094	0.092	6.9	0.062	0.37
Sample 4	50	10.5	39.5	0.094	0.092	8.27	0.074	0.35
						AMG 517 Addition		
Sample 5	10	2.1	7.9	0.019	0.018	31.73	0.074	0.83
Sample 6	25	5.25	19.75	0.047	0.046	29.75	0.069	0.71
Sample 7	25	5.25	19.75	0.047	0.046	13.22	0.031	0.62
Sample 8	40	8.4	31.6	0.075	0.073	7.93	0.018	0.55

Table 1. This table summarizes the preparation of **AMG 517/SA** mixtures for the phase diagram. For each sample (Samples 1 – 8) the mole fraction of **AMG 517** was determined in two steps. First, the number of mmoles of **AMG 517** and **SA** were calculated from the weighed amount of **AMG 517/SA** in the sample, as seen in the left hand side of the table. Second, **SA** (top column on right) or **AMG 517** (bottom column on right) was added to the corresponding amounts of **AMG 517/SA** in each sample. The additions of **AMG 517** and **SA** were converted from mg (column third from right) to mmols (second column to right). Once the total mmoles of each component was determined, the mole fraction of **AMG 517** for each sample was determined by Equation 1 and tabulated in the far right column, including the end points, precipitated and were placed on bench top stir plates to mix overnight at room temperature. When the solvent evaporated, the remaining precipitate was analyzed by DSC, TGA, and XRPD.

AMG 517:XYL in EtOAc. Mixtures of **AMG 517** and **XYL** were prepared by weighing both compounds (0 - 25 mg) into tared aluminum weigh pans on an analytical balance. The compounds were transferred to eleven 4 mL amber vials with screw-top caps. The vials were labeled from 0.0 MF (100% **CA)** – 1.0 MF (100% **AMG 517**) to cover the range of compositions needed to construct the phase diagram. **EtOAc** (3 mL) was pipetted into each sample, the vials capped, and vortexed briefly (20 sec). All of the samples, including 100% **XYL** and 100% **AMG 517**, were suspensions. The samples were left mixing at 100 rpms. After 3 days, there was no change in the appearance of the samples; all remained suspensions. The caps were removed and the vials were placed in the hood to allow the solvent to evaporate. The precipitates were analyzed by XRPD, DSC, and TGA.

Results and Discussion

The AMG 517/SA System.

The goal of this experiment was to prepare the **AMG 517:SA** phase diagram by using **AMG 517** and **SA** as starting materials and by adding **AMG 517** and **SA** to **AMG 517/SA**. The mixtures would then be analyzed to determine the eutectic mixtures in the system. A typical 1:1 co-crystal phase diagram may contain up to two eutectic mixtures, $\mathbf{E_1}$ and $\mathbf{E_2}$ (Figure 2) [3, 4, 6]. The eutectic mixtures in the system would be identified by the lowest melt of the mixtures that occur below the original melts of the starting materials.

The **AMG 517:SA** mixtures were analyzed by XRPD, DSC, and TGA to determine the results of mixing the two compounds and then heating the resulting mixtures. The purpose of the XRPD analysis was to detect form changes due to milling. The mixtures contained **AMG 517** and **SA** and no other forms were present (Figure 3). The mixtures prepared for the phase diagram were

then analyzed by DSC to compare the melts of the mixtures and to determine if a eutectic mixture was present (Figure 4.) The characteristic melt of **SA** by DSC analysis indicates that **SA** melts at 134 ˚C and TGA shows that it degrades with simultaneous weight loss of 100% (Figure 5). This degradation makes it impractical to determine the two component phase diagram for this system. **AMG 517/SA** may be present in all of the phase diagram mixtures between 0.1 - 0.9 MF, as indicated by the broad and shallow endotherm between 168 – 190 ˚C (Figure 3), but the melting point of **AMG 517/SA** has been reported to be 159 °C [1]. The 0.1 – 0.4 MF mixtures contain proportionally more **SA** to **AMG 517**, which is reflected in the very slight melt depression of **SA**.

The **AMG 517/SA** system was also studied by a separate method in which the mixtures were prepared by adding **SA** or **AMG 517** directly to **AMG 517/SA**. The resulting **AMG517/SA** mixtures were analyzed by XRPD and no new forms were found (Figure 6). All of the mixtures contained **AMG 517**, **SA**, and **AMG 517/SA** as contained in the starting materials. When the mixtures were subsequently analyzed by DSC, hermetically sealed pans were chosen initially to limit chemical degradation products of **SA.** However, the characteristic melt and resulting endotherms of **AMG 517/SA** was not reproduced in hermetically sealed pans, and so open DSC pans were used (Figure 7). The following change in melting temperature of the resulting broad shallow endotherm of the **SAC** melt at 159 °C was used to determine the effect of the addition of **AMG 517** and **SA** to **AMG517/SA** mixtures (Figure 7). In this example, using **AMG 517/SA** as a starting material was critical in the preparation of the phase diagram. Only after adding **SA** and **AMG 517** to **AMG 517/SA** were the eutectic mixtures (E1 and E2, Figure 8) were observed and the liquidus lines revealed. Even with subsequent degradation, clear eutectics can be observed in this case (**E_1** and **E_2**, Figure 8**).** The liquidus line **SA** and **AMG 517**, respectively. This indicates a melting point depression of ~ 60 °C for **E_1** relative to the melting point of **AMG 517**. **E_2** melts

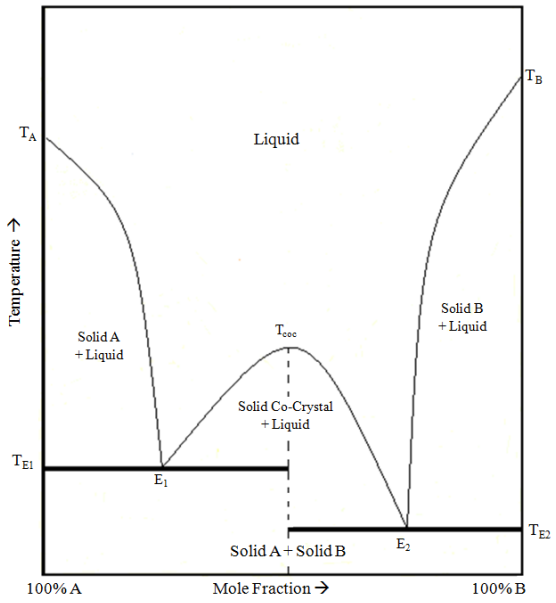

Figure 2. An idealized 1:1 co-crystal phase diagram, where the vertical dotted line delineates the diagram at the 0.5 MF co-crystal mixture and the melting temperature of the co-crystal ($\mathbf{T_{coc.}}$). The x-axis is plotted by the composition of **A:B** mixtures with increasing amounts of compound **B** to compound **A** from left to right of the diagram. The y-axis is the temperature of the mixtures, with increasing heat up the axis. $\mathbf{T_A}$ and $\mathbf{T_B}$ is the melting temperature of pure **A** and **B**, respectively. $\mathbf{T_{E1}}$ and $\mathbf{T_{E2}}$ is the melting temperature for each eutectic mixture and becomes the solidus boundary for the corresponding side of the diagram. $\mathbf{E_1}$ and $\mathbf{E_2}$ indicate the composition of the eutectic mixture at the eutectic temperature. The solidus boundary is the minimum temperature of the mixtures melting. Beneath the solidus, compounds **A** and **B** are solid. Above the solidus temperature, one of the compounds begins to melt. The liquidus curve is the boundary between both compounds melted (above the curve) and one compound melted and the other is solid (below the curve). The liquid phase contains both components melted. **Solid A/B + Liquid** is a mixed phase of solid **A/B** and melted **A/B**, depending on which side of the co-crystal the mixture composition is located on the x-axis [4, 6, 7].

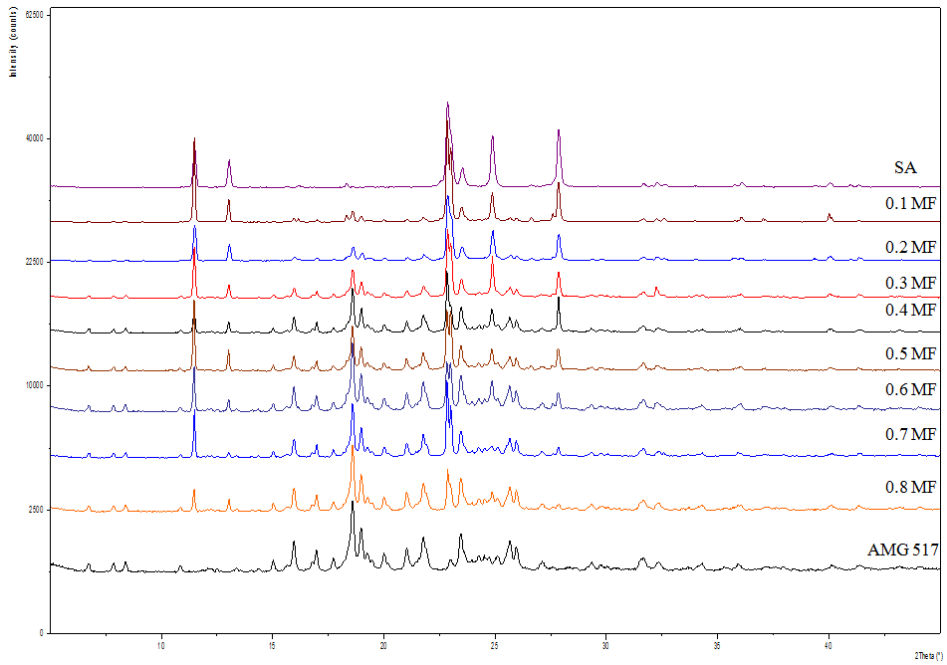

Figure 3. Physical mixtures of **AMG 517** and **SA** prepared to determine the phase diagram were analyzed by XRPD. The intensities of the peaks are relative to the mixtures and not to scale. All of the mixtures of **AMG 517** and **SA** (0.1 – 0.8 MF, trace second to the top to trace second to the bottom) contain all of the peaks of each compound, therefore there are no new forms. The 0.5 MF mixture does not contain any peaks unique to **AMG 517/SA** and is a physical mixtures containing peaks of **AMG 517** and **SA.**

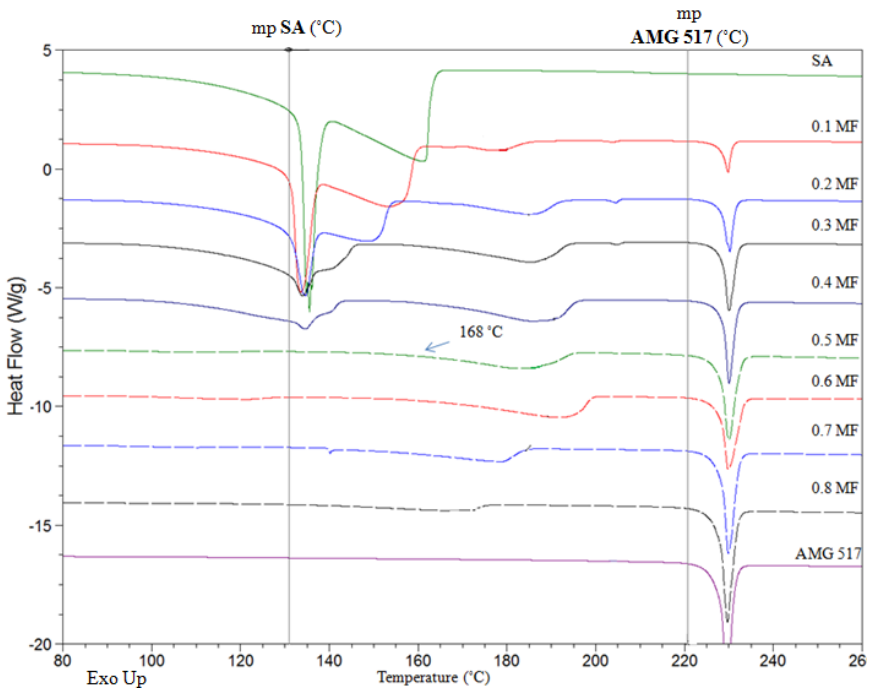

Figure 4. Thermogram of a DSC overlay of the **AMG 517:SA** mixtures prepared for the phase diagram as analyzed in open DSC pans. The 0.1 – 0.4 MF mixtures (traces second to the top – fifth from the top) show degradation after the melt of **SA** (130 – 160 ˚C), followed by the melt of **AMG 517/SA** (160- 180 ˚C), and the melt of **AMG 517** (onset melt at 223 ˚C). The 0.4 MF mixtures contain proportionally more **SA** to **AMG 517**, which is reflected in the very slight melt depression of **SA**. The 0.5 MF mixture contains **AMG 517/SA** and the melt is shifted to a higher temperature due to some **AMG 517** in the mixture did not convert to the co-crystal. The 0.6 – 0.8 MF mixtures include the **AMG 517/SA** melt (160- 190 ˚C) and the melt of **AMG 517** (223 ˚C).

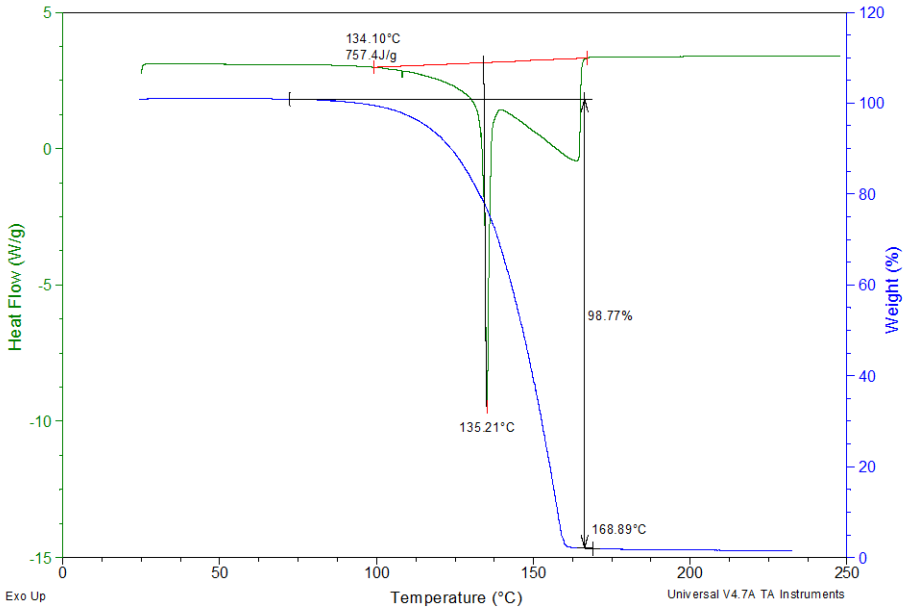

Figure 5. The onset melt of **SA** is analyzed by DSC (green trace, top) and the weight loss evaluated by TGA (blue trace, bottom) at 10 °C/min. It has an onset melt of 134 °C and experiences 99% weight loss before 170 °C.

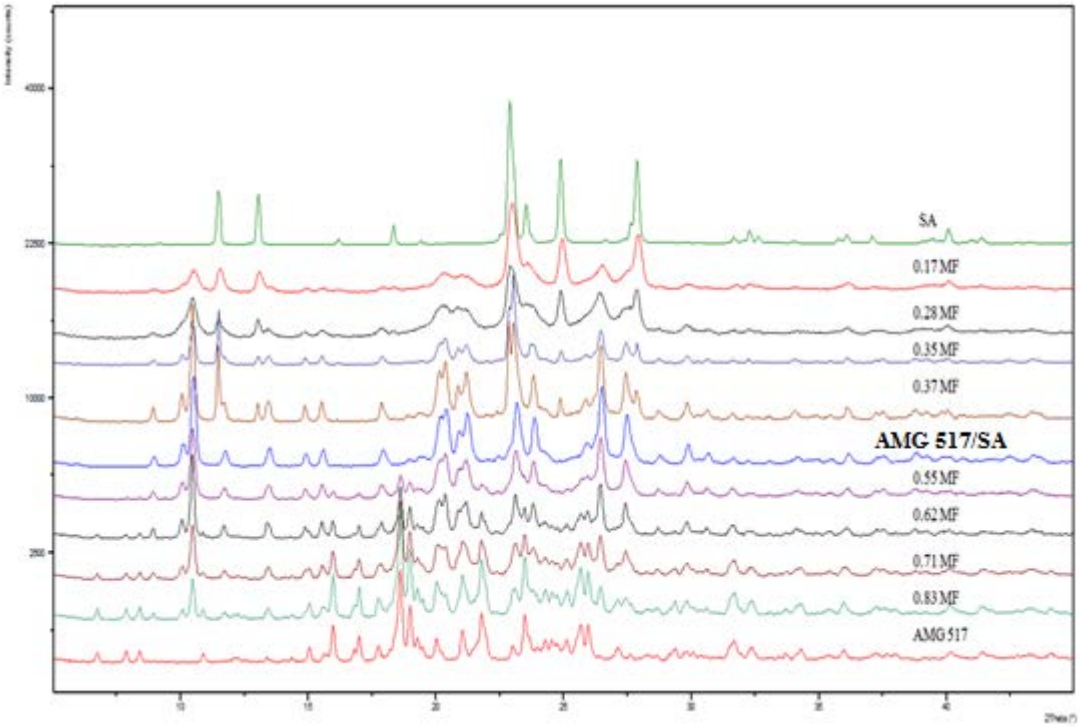

Figure 6. XRPD overlay of **AMG 517** (red trace on bottom,) **AMG 517/SA** (middle blue trace,) and **SA** (top green trace) with mixtures of **AMG 517/SA** (middle blue trace) with added **AMG 517** and **SA**. The graph is structured with increasing amounts of **AMG 517** added to the mixtures moving down y-axis. The intensities of the peaks are relative to each other and are not to scale.

slightly above the onset melt of **AMG517/SA** at 175°C, and may not be a eutectic of **AMG 517/SA**, but rather a eutectic melt of **AMG 517** (original onset melt 223 – 228 °C).

The AMG 517 Mannitol Binary System

When the mixtures of **AMG 517**:**MAN** were heated and analyzed by DSC, it was apparent that there was very little mixing between the two compounds (Figure 9). The physical mixtures did not exhibit a melt depression of either compound when heated. The melt of **MAN** is shown at the top of the thermogram (top green DSC trace,) and the mixtures proportionally increase in **AMG 517** and reduce in **MAN** until pure **AMG 517** is indicated at the bottom of the figure (bottom blue DSC trace, Figure 9.) All of the mixtures contain two melts, indicative of each compound, that occur at different ends of the temperature range. The original melts of the compounds changed very little with the presence of either compound in the mixture.

The AMG 517/CA system

AMG 517/CA is a known co-crystal and expansion of the phase diagram was attempted by the solvent evaporation method. An organic solubility screen of **AMG 517** and **CA** was designed to determine a suitable solvent for the mixing experiment. The organic solubility of **AMG 517** and **CA** were visually determined in several solvents. Then, when a solvent was descends from the **AMG 517/SA** up to each eutectic and is traced back to the melting point of decided upon, a series of mixtures were prepared to construct the phase diagram. XRPD analysis was utilized to characterize the solids resulting from the preparations.

Organic Solubility Screen. The purpose of the organic solubility screen was to identify a solvent where the solubilities of **AMG 517** and **CA** were similar and which gave the stable polymorph of each of the compounds. The solubilities of **AMG 517** were estimated in ether, EtOH, acetone, THF, and MEK. The solubility of **CA** was only estimated in MEK (Table 2). Several of

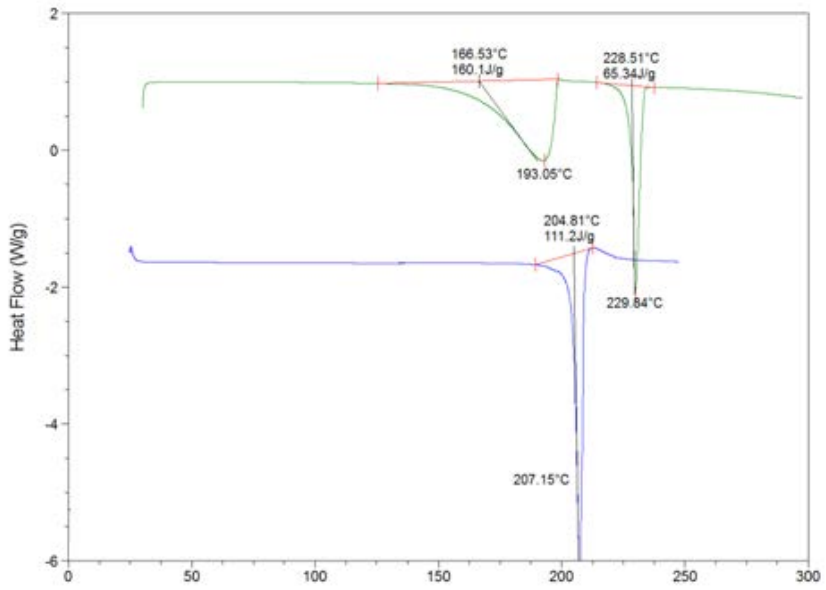

Figure 7. Comparison of DSC analysis of **AMG 517/SA** in open DSC pans (green trace, top) and hermetically sealed DSC pans (blue trace, bottom.)

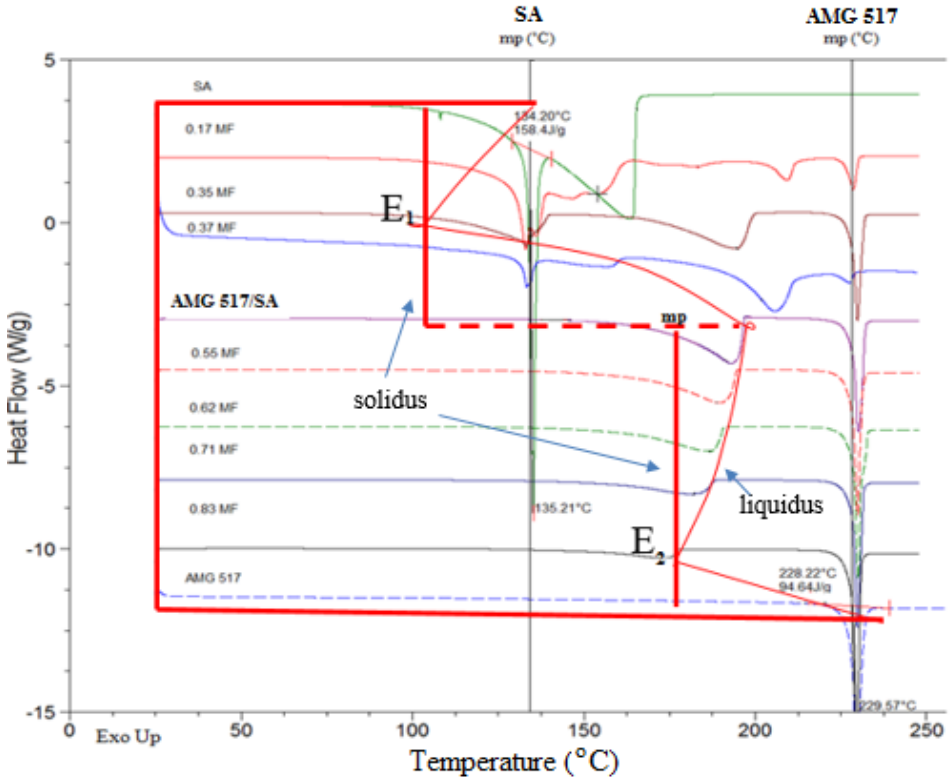

Figure 8. The DSC thermograms of the mixtures of **AMG 517**, **SA**, and **AMG 517/SA** are shown with increasing amounts of **AMG 517** from top to bottom of the thermogram. The 0.17 – 0.37 MF mixtures may contain degradation products of **SA**, and **AMG 517/SA**, and **AMG 517**. The 0.55 - 0.83 MF mixtures melt contain **AMG 517/SA** melting at temperatures above the onset melt of **AMG 517/SA**. **E_1** and **E_2** are identified as the eutectic mixtures in the **AMG 517/SA** system due to the depressed melt.

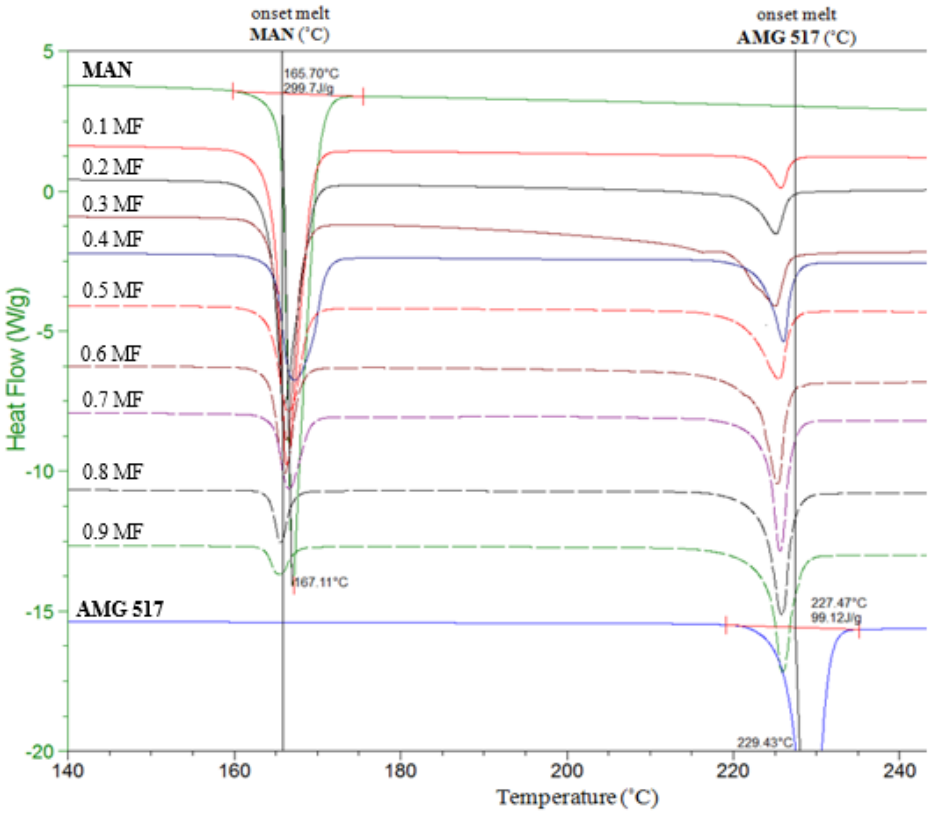

Figure 9. DSC traces of physical mixtures of **AMG 517** and **MAN** analyzed in hermetically sealed DSC pans. There is very little change in the onset melt of either component.

the XRPD patterns of the solids remaining after the organic solubility screen indicate the presence of new form are shown in Figure 10. **AMG 517** appears to form a solvate in THF (second from bottom, Figure 10). The precipitates of both **AMG 517** and **CA** from MEK match their respective starting forms. MEK was chosen as the solvent for subsequent solvent evaporation work.

Solvent Evaporation Experiment. Mixtures used to prepare the phase diagram were analyzed by DSC (Figure 11). As more **AMG 517** is added the **CA** melt is depressed from 134 to 130 °C (Figure 11). Also, the **AMG 517/CA** melt is not identified due to the degradation of **CA**. The 0.5 MF mixture, which is composed of a 1:1 stoichiometric mole ratio **AMG 517**:**CA**, melts at onset temperature associated with **AMG 517/CA.** The 0.5 MF mixture, which is composed of a 1:1 stoichiometric mole ratio **AMG 517**:**CA**, melts at onset temperature associated with **AMG 517/CA.** As more **AMG 517** was added the resulting melts are actually shifted to a higher temperature, possibly indicating a peritectic system [4, 6, 7]. A eutectic mixture with a slightly lower melting point than **CA** may be present in the **CA** rich mixtures, but precise determination of its composition was not possible.

Further investigations were conducted to determine if other forms are present in the precipitates after the mixing of the two compounds during the solvent evaporation experiment. The mixtures prepared for the phase diagram from the **AMG 517 CA** solvent evaporation experiment were also analyzed by XRPD before DSC analysis (Figure 12). All of the mixtures contained multiple forms, such as the solvate of **AMG 517** in MEK **(AMG 517** MEK), **CA,** and **AMG 517/CA**. The **AMG 517** MEK XRPD pattern was not present in the organic solubility screen (Figure 10), which indicates that the solvate may not always form. However, the pattern was present in some of the resulting mixtures. The presence of **AMG 517/CA** was detected in most mixtures that contained a peak at 20.2˚ 2θ, such as the 0.4 MF mixture (arrow, fifth trace

Estimated solubilities of **AMG 517** and **CA** in organic solvents					
Compound	Ether	EtOH	acetone	THF	MEK
AMG 517	no precipitate	< 11 mg/mL	> 11 mg/mL	> 11 mg/mL	> 11 mg/mL
CA	n/a	n/a	n/a	n/a	> 11 mg/mL

Table 2. Solubilities of AMG 517 in several solvents were estimated by the visual appearance of the sample (suspension/solution). The solubility of **CA** was only estimated in MEK.

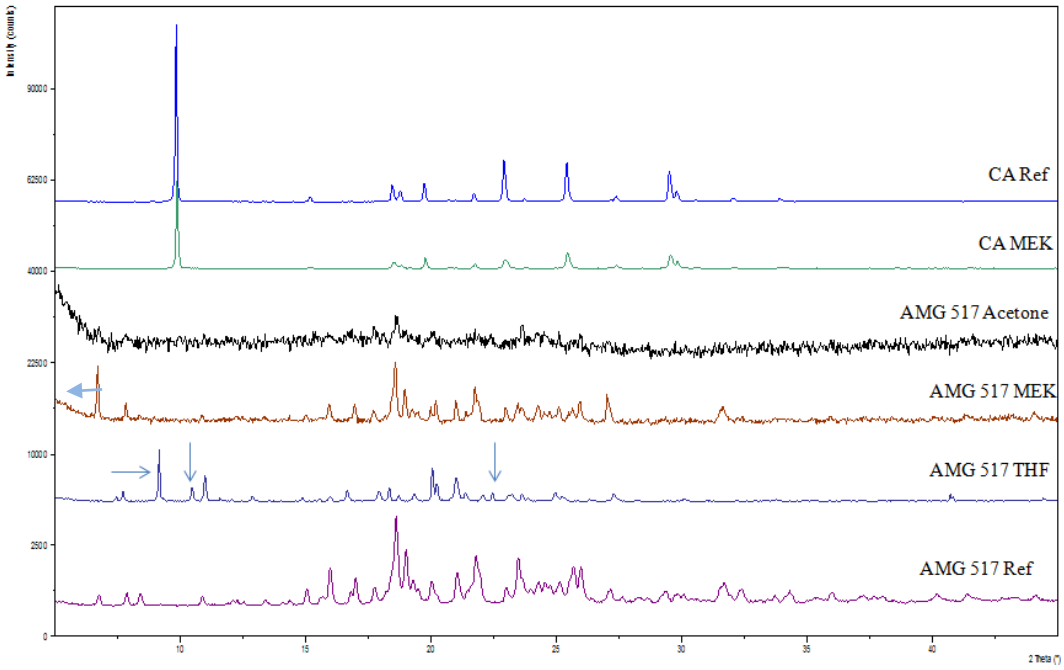

Figure 10. Overlay of XRPD patterns from the isolated materials during the organic solubility screen with **AMG 517** in **MEK**, Acetone, and **THF**. The isolated material of **CA** evaporated from **MEK** is also compared to **CA (**CA Ref, top trace). New peaks, as indicated by the arrows, were found in the **AMG 517 THF** precipitate and the **AMG 517 MEK precipitate** (trace second from bottom.) **AMG 517** in acetone (middle trace) had an insufficient amount of sample to obtain a clear scan of the precipitate.

from the top, Figure 12). The XRPD powder patterns of the α- and β- polymorphs of **CA** (**α-CA** and **β-CA**) and **AMG 517/CA** were also compared to the resulting precipitates of the physical mixtures to identify the forms contained in the mixtures [14 – 16]. These unknown forms were not compared to the **CA** γ-polymorph because a crystallized pattern was not available for comparison in the Cambridge Structural Database (CSD) [17] nor in a literature search.

The 0.4 MF, 0.5MF, and 0.8 MF mixtures were analyzed more closely to identify the forms present in the mixtures. The 0.4 MF mixture was expected to contain **CA** and **AMG 517** as determined by DSC analysis. The XRPD diffractogram of the 0.4 MF mixture contained **AMG 517**, **AMG517/CA**, **α-CA,** and **CA** MEK (Figure 13). The 0.5 MF mixture was expected to form **AMG 517/CA.** However, the XRPD data showed the presence of **AMG 517** MEK, **AMG517/CA**, and **α-CA** present (Figure 14). The 0.8 MF mixture was expected to contain the depressed melt of **AMG 517/CA** due to prior DSC analysis (Figure 15). However, the XRPD analysis showed the mixture contained **AMG 517** MEK, **α-CA**, and **AMG 517/CA**. In conclusion, there may be a eutectic mixtures found in the **AMG 517/CA** system, but XRPD analysis showed multiple forms present in the mixture.

AMG 517 Xylitol System

Mixtures of **AMG 517** and **XYL** were prepared by ball milling and solvent evaporation and analyzed by XRPD and DSC (Figures 16 and 17).

Ball Milling Experiment. **XYL** was ball milled with **AMG 517** because of the low melting temperature of **XYL** (onset melt at 92 ˚C), and the thermal stability of the compound when melted to higher temperatures [12]. The melt of **XYL** is characterized by a sharp melt and weight loss occurs at temperatures > 200 ˚C (35 % weight loss by 275 ˚C) (Figure 18). Therefore, **XYL** should not degrade at or below the melting temperatures of **AMG 517** (onset melt at > 220 ˚C.)

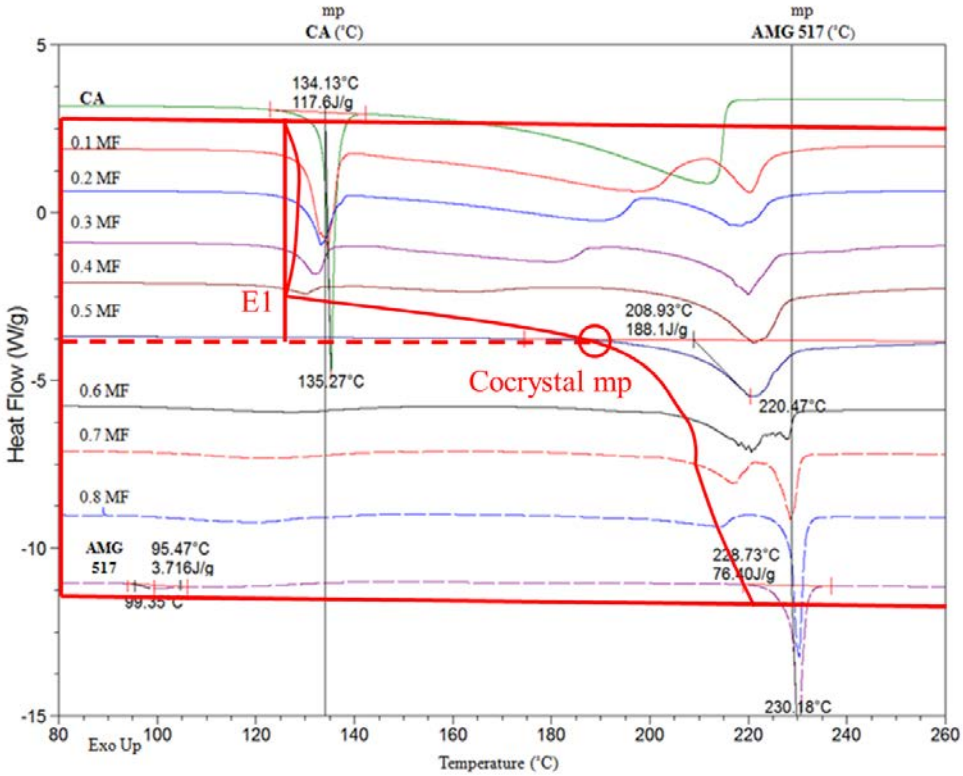

Figure 11. Overlay of DSC traces for **AMG 517:CA** solvent evaporation experiment in MEK. The melting temperature of **CA** and **AMG 517** are indicated by vertical lines. The mixtures composition is indicated on th left. The 0.1 – 0.4 MF mixtures show the **CA** melt and subsequent degradation products may be present. The 0.5 MF mixture has an onset melt at 209 °C as expected for **AMG 517/CA**. The phase diagram is outlined in red. E1 is the possible eutectic composition in the **CA** rich portion of the phase diagram.

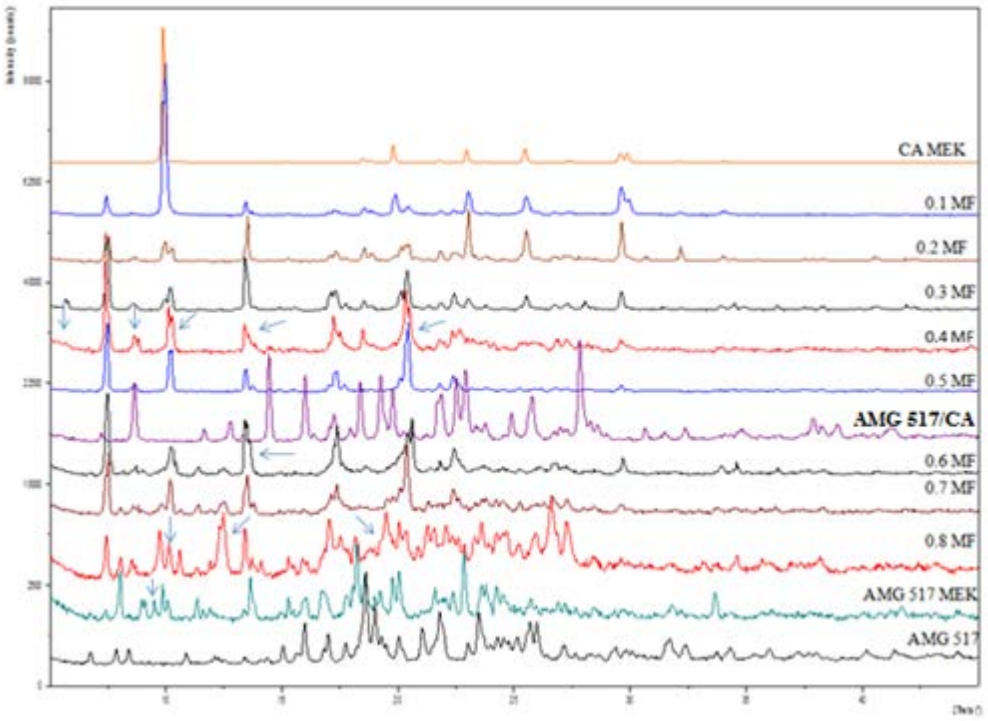

Figure 12. XRPD patterns of the mixtures prepared for the **AMG 517/CA** phase diagram with increasing amounts of **AMG 517** added to the mixture moving down the figure. Some of these peaks also match the XRPD diffractogram of **AMG 517 MEK** precipitate (green trace, second from bottom), which is indicative of the presence of a solvate. Multiple forms have been idenitifed in most of the mixtures that include **AMG 517, CA, α-CA, AMG 517/CA**, and **AMG 517** MEK.

The physical mixtures of **AMG 517:XYL** show two melts that correspond to the original compounds and no eutectics (Figure 19). No indication of degradation after **XYL** melting was observed. The XRPD diffractograms of the mixtures indicate only the presence of **AMG 517** and **XYL** (Figure 20). Solvent evaporation experiments were designed to increase mixing between the compounds.

Solvent evaporation in EtOAc. The DSC overlay of the **AMG 517**:**XYL** samples indicate a melting depression of **XYL** as more **AMG 517** is added, resulting in a depressed melt of **XYL** in the 0.5 MF mixture at 88 ˚C (Figure 21.) The 0.5 MF mixture also contains the most depressed melt of **XYL** at 88 ˚C, but is not considered a eutectic mixture. This is due to the definition of a eutectic mixture, which contains only one melt, and the 0.5 MF mixture contains a separate melts for both compounds [4, 5]. This is in contrast to a co-crystal phase diagram where two eutectic melts can be observed [5, 6]. In between the 0.8 – 0.9 MF mixtures, the melt of **XYL** is not detected by the DSC and the melt of **AMG 517** is not depressed. The melts of the mixtures were also compared to the onset melts of **AMG 517/XYL** from a HTS screen and was not comparable (onset melts at 98.2 ˚C and 213 ˚C) (Figure 17). The 0.5 MF mixture was analyzed by DSC and TGA in order to more fully characterize the mixture (Figure 22). At 80 ˚C, **XYL** melts and solvent is boiled away as signified by the simultaneous weight loss of 3.6 %. The depressed melt of **AMG 517** occurs at 200 ˚C with a simultaneous weight loss of 22%.

The XRPD patterns of the mixtures contain multiple forms (Figure 23) do not show gradual increase of **AMG 517** across the samples, nor do they indicate that **AMG 517/XYL** is present in the samples. In some specific diffractograms, 0.5 MF for example (Figure 24), the corresponding peaks do not match any known forms of **AMG 517**, **AMG 517/XYL**, or **XYL**. This apparent phase heterogeneity and the observed lack of eutectic mixture formation justified no further work

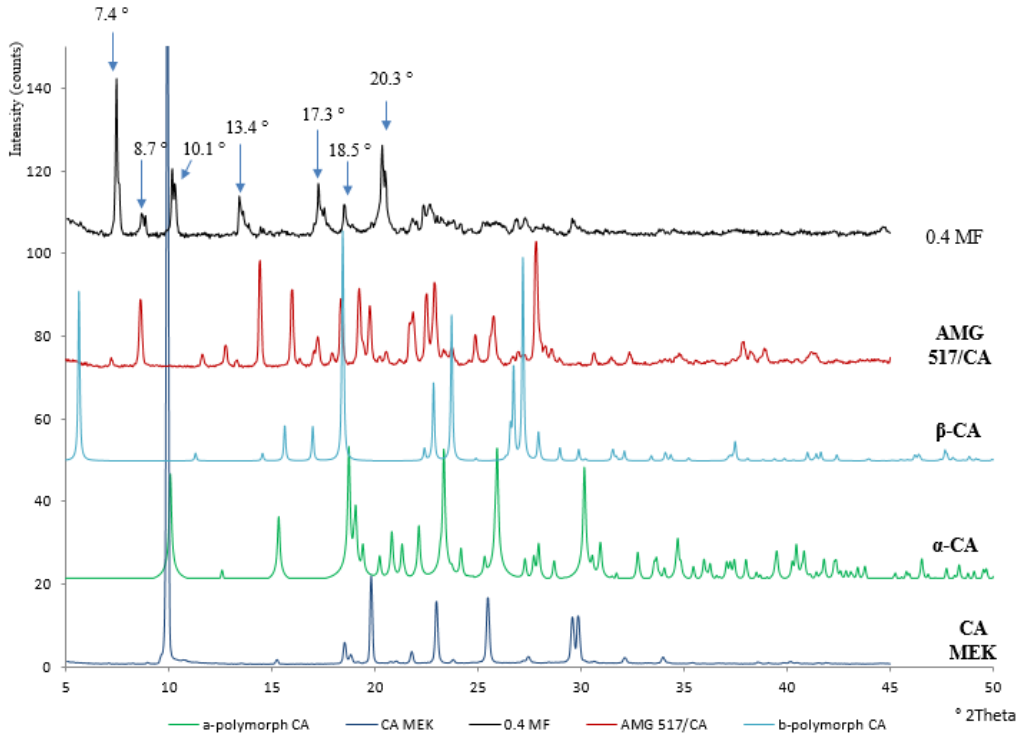

Figure 13. The 0.4 MF mixture contained multiple forms. The mixture (0.4 MF, top trace) is compared to **AMG 517/CA** (second from top), **β-CA** (middle), **α-CA** (second from bottom), and **CA** MEK (bottom trace). The mixture contains multiple forms as indicated by the peaks that are labeled by diffractography angle 2θ. None of the peaks matched **β-CA.**

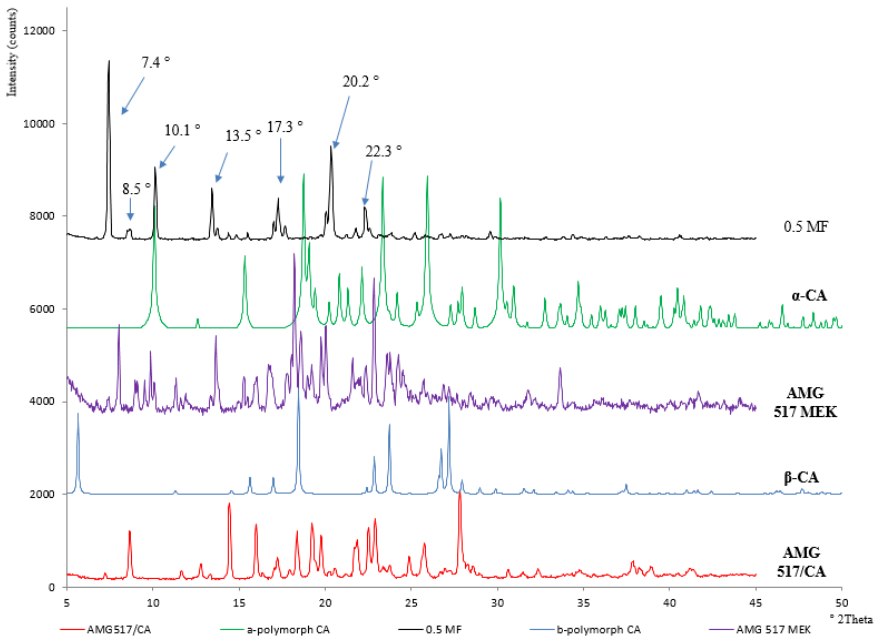

Figure 14. The 0.5 MF mixture (top trace) was compared to **AMG 517/CA** (bottom trace,) **β-CA** (second from bottom), **AMG 517** MEK (middle), and **α-CA** (second from top.) The 0.5 MF mixture contained multiple forms including **AMG 517/CA**, **α-CA**, and **AMG 517**.

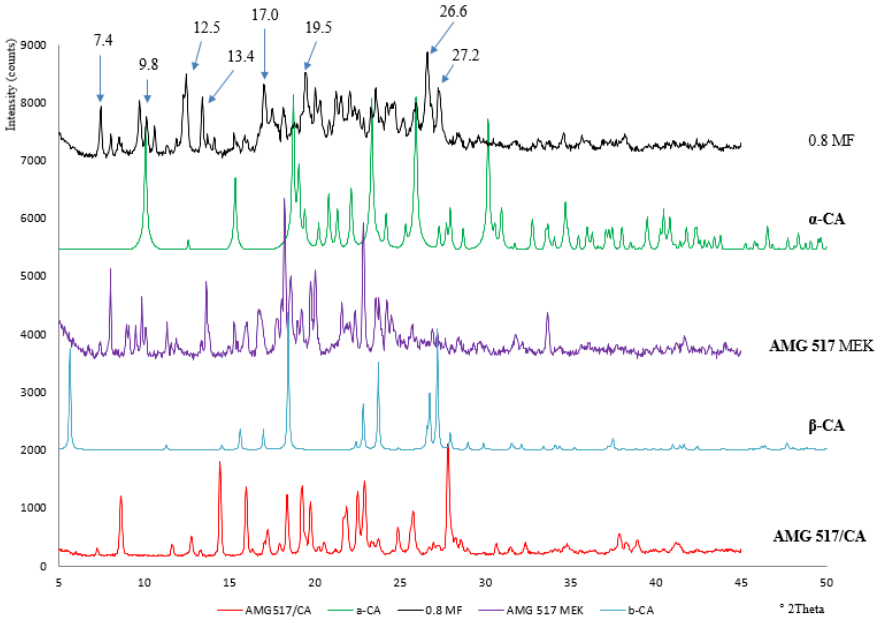

Figure 15. The XRPD patterns of the 0.8 MF mixture (top) is compared to **α-CA** (second from top), **AMG 517** MEK (middle), **β-CA** (second from bottom), and **AMG 517/CA** (bottom.) The mixture contained multiple forms.

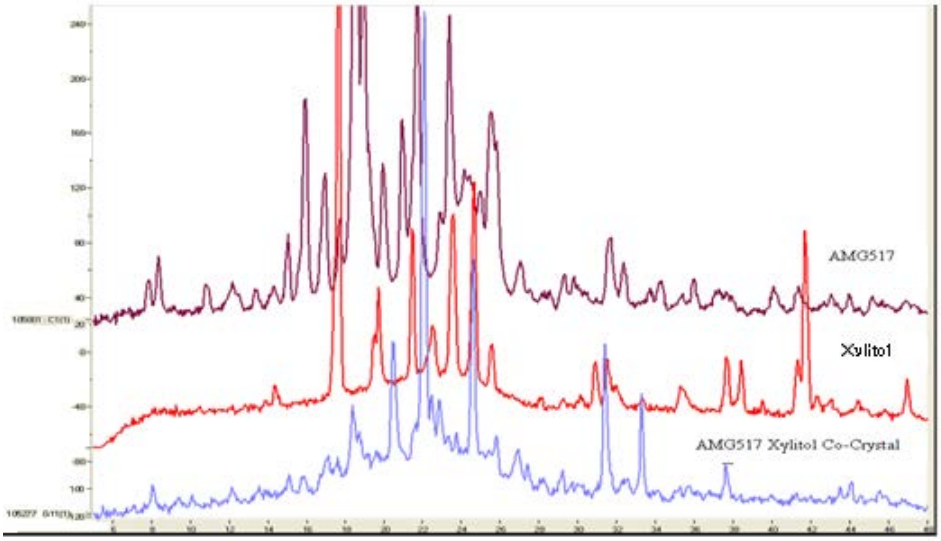

Figure 16. XRPD overlay of **AMG 517** (top purple trace,) **XYL** (middle red trace), and **AMG 517/XYL** (bottom blue trace.)

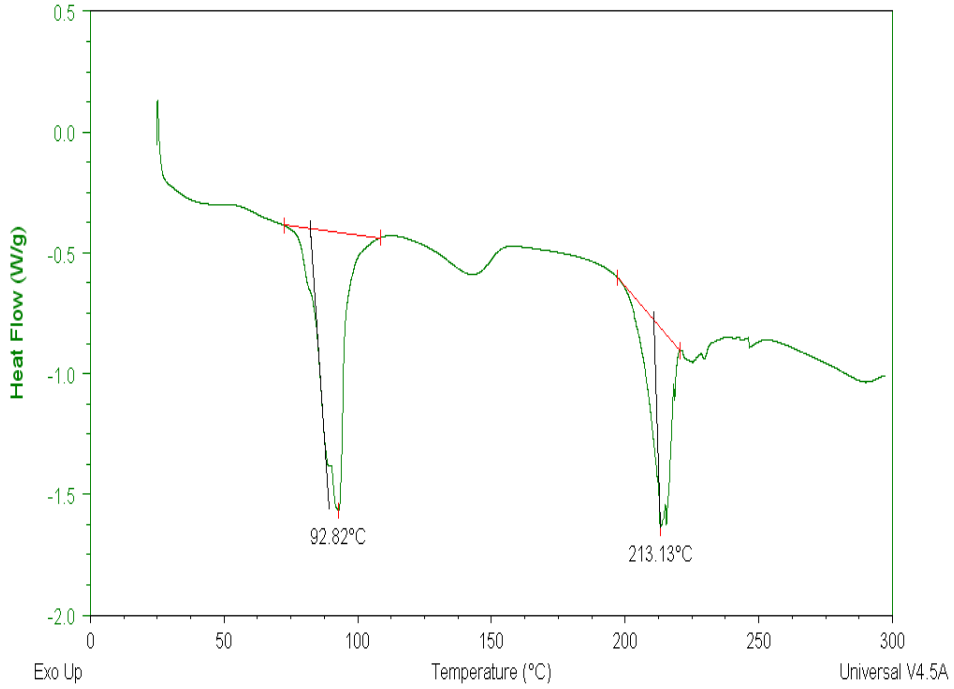

Figure 17. DSC trace of **AMG 517/ XYL** obtained from HTS.

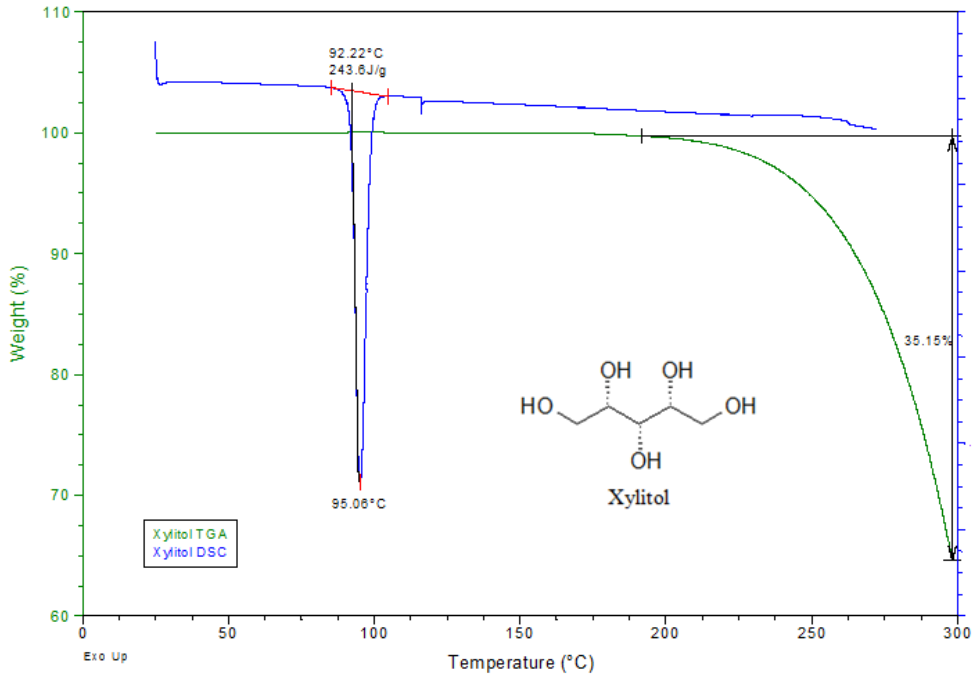

Figure 18. DSC (top, blue trace) and TGA (bottom, green trace) of **XYL**.

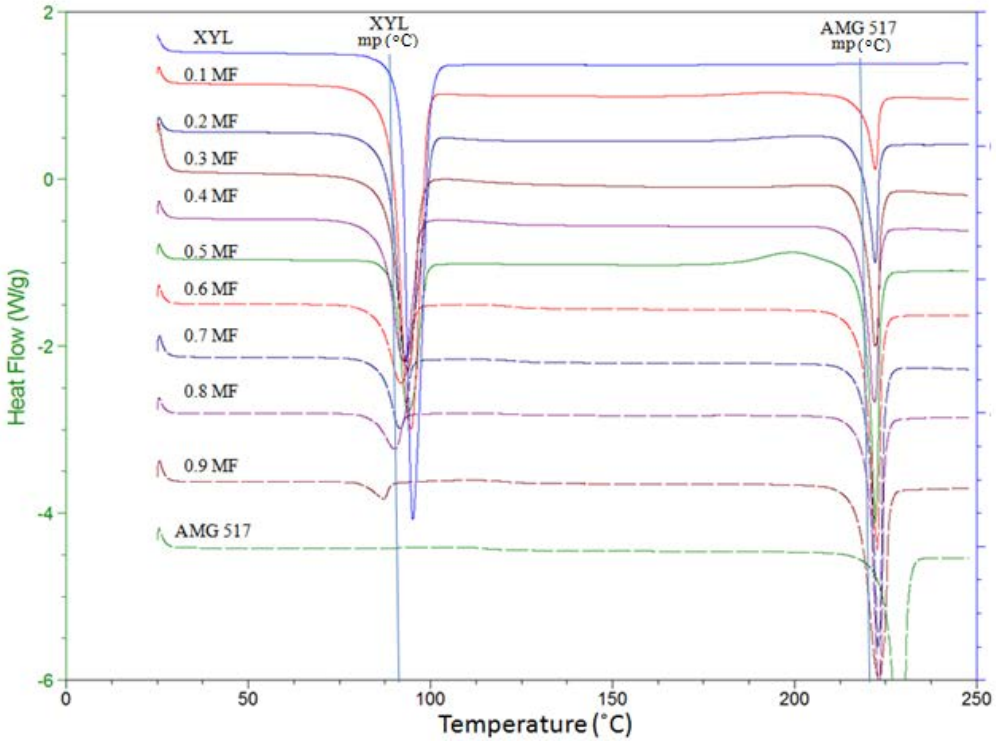

Figure 19. Physical mixtures of **AMG 517:XYL** prepared by ball milling. Very little shifting in melting temperature of the mixtures was attributed to added compounds in the mixture.

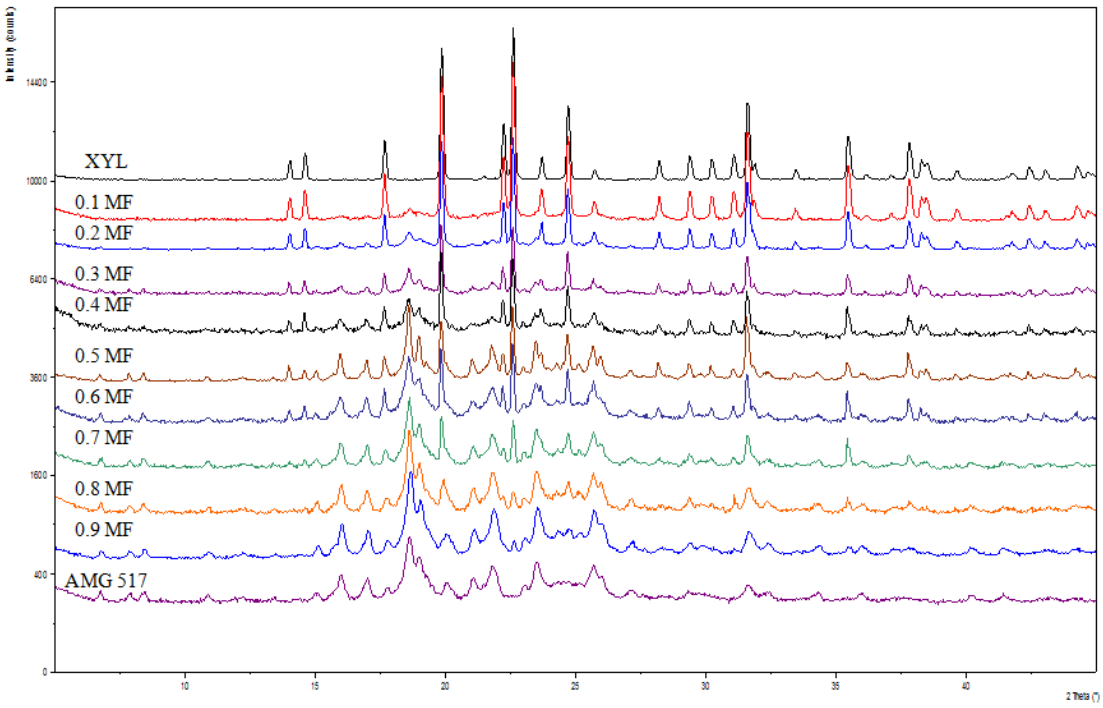

Figure 20. Ball milled mixtures of **AMG 517** and **XYL** did not show the presence of any unknown forms after XRPD analysis.

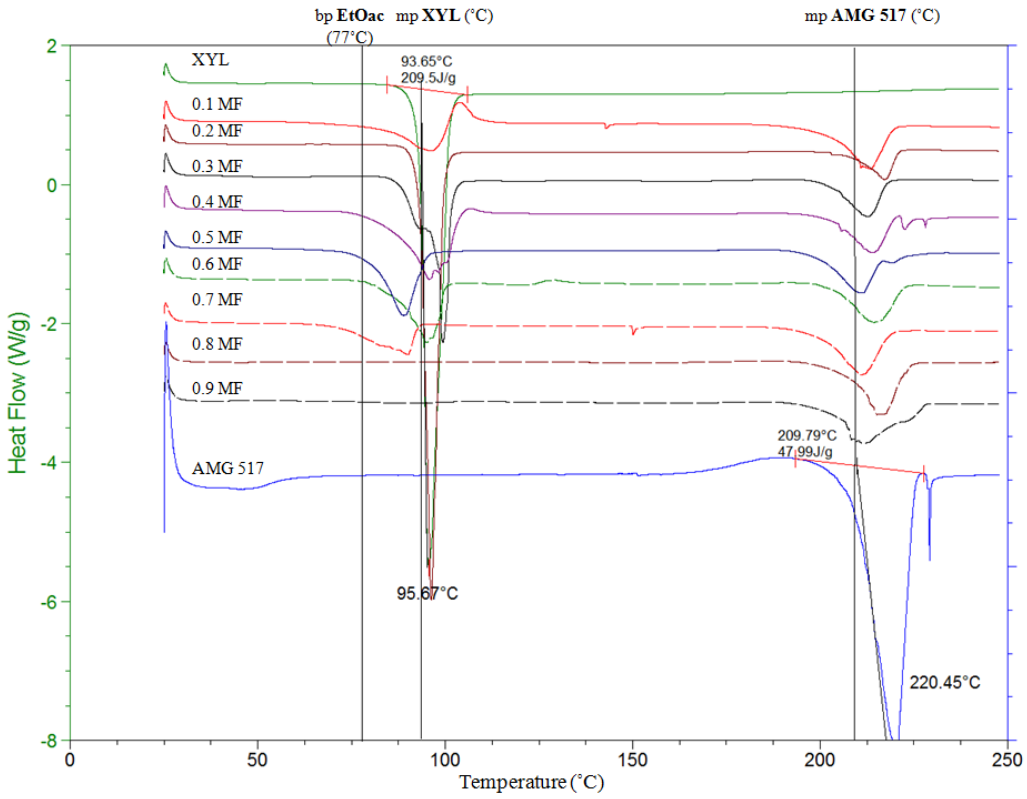

Figure 21. **AMG 517** and **XYL** mixed in **EtOAc** are analyzed by DSC in hermetically sealed DSC pans. As more **AMG 517** is added to the mixture, the corresponding endotherm (220 – 223 °C) becomes deeper.

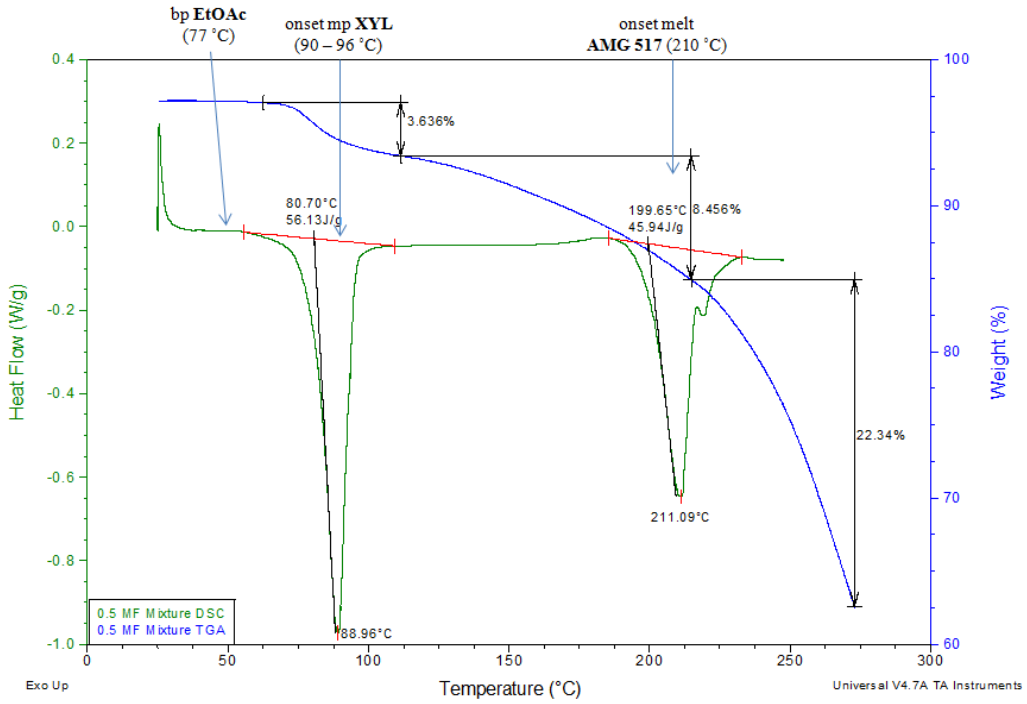

Figure 22. The DSC/TGA overlay of the 0.5 MF mixture contains the depressed melt and weight loss of **XYL** (90˚C) and **AMG 517** (200 ˚C). The TGA shows a simultaneous weight loss of 3.6 % which is not the expected weight loss of **XYL** at 81 ˚C, and so the form may be a solvate of **EtOAc**. The 8.4% weight loss between 100 – 200 °C that may be due to degradation of **XYL**. The melt of **AMG 517** at 200 ˚C is accompanied by a weight loss indicative of chemical degradation.

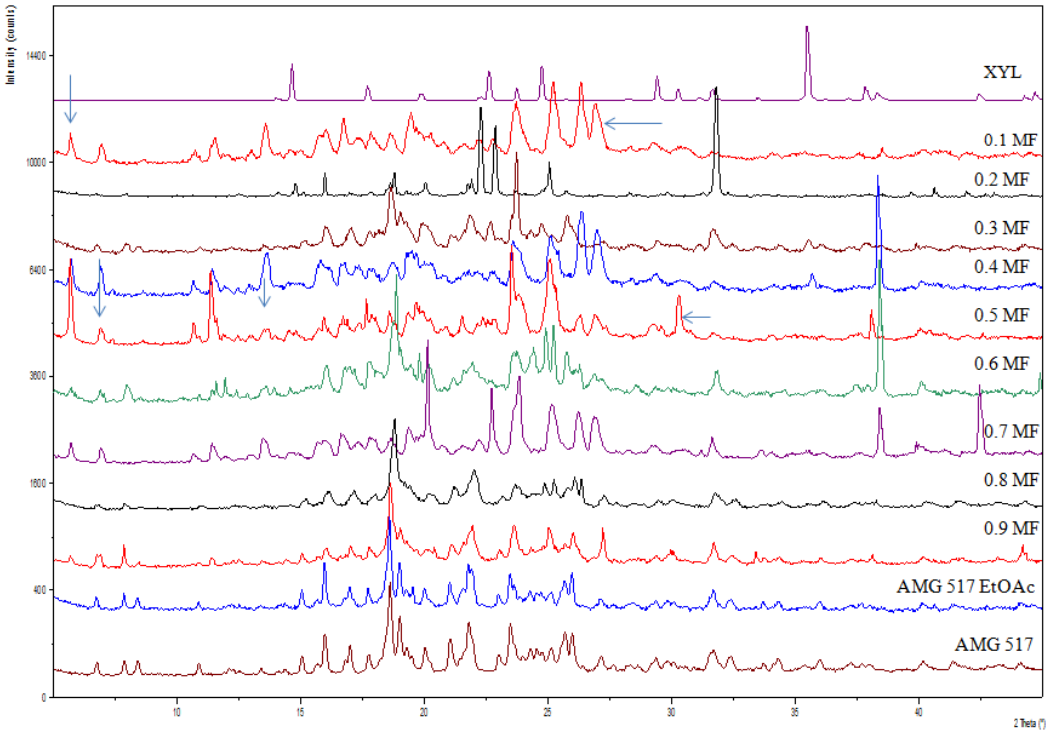

Figure 23. XRPD traces of all of the **AMG 517 XYL** mixtures in **EtOAc**. As more **AMG 517** is being added to the mixtures, the peaks of **AMG 517** become more pronounced. The arrows in 0.1 MF and 0.5 MF mixtures (second from top trace and sixth from top trace, respectively) highlight peaks of a new form that that also appear in some of the other mixtures.

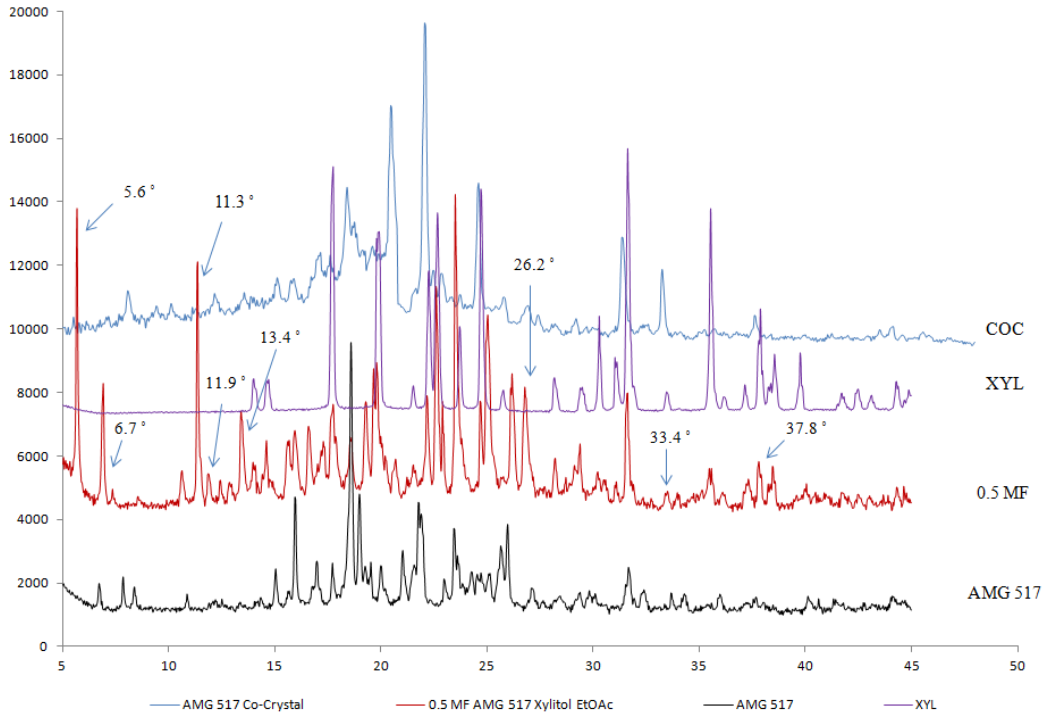

Figure 24. XRPD patterns of the **AMG 517 XYL COC** (COC, top) compared to **XYL** (XYL, second from top), 0.5 MF mixture (red, second from bottom), and **AMG 517** (AMG 517, bottom.) The 0.5 MF mixture contains **AMG 517** (arrow at matching peak at 6.7 ˚), unknown peaks at 11.3˚, 11.9˚, and 26.2˚, and **XYL** (arrows of matching peaks at 33.4˚, and 37.8˚ 2θ).

on this system.

Conclusions.

The purpose of this work was to use DSC analysis of AMG 517 mixtures to prepare binary phase diagrams and investigate the presence of a eutectic mixture. Only when **AMG 517/SA** was used as a starting material for the **AMG 517:SA** phase diagram were potential eutectic mixtures observed. It is doubtful, however, that the presence of degradation would still be able to consider these eutectic mixtures as true eutectics, since degradation should not be detected. Also, it is important to consider that chemical degradation upon heating confounds interpretation of the data to some extent.

References

1. Bak, A.; Gore, A.; Yanez, E.; Stanton, M.; Tufekcic, S.; Syed, R.; Akrami, A.; Rose, M.; Surapaneni, S.; Bostick, T.; King, A.; Neervannan, S.; Ostovic, D.; Koparker, A. The Co-Crystal Approach to Improve the Exposure of a Water-Insoluble compound: AMG 517 sorbic acid Characterization and Pharmacokinetics. *J. Pharm. Sci.* **2008**, *97*(9), pp 3942-3956.
2. Stanton, M. K.; Bak, A. Physicochemical Properties of Pharmaceutical Co-Crystals. *Crys Growth Des* **2008**, *8*(10), pp 3856-3862.
3 Vippagunta S. R.; Wang, Z.; Hornung, S.; Krill, S. Factors Affecting the Formation of Eutectic Solid Dispersions and their Dissolution Behavior. *J. Pharm. Sci.* **2007**, *96*(2), pp 294-304.
4. Stott, P. W.; Williams, A. C.; Barry, B. W. Transdermal Delivery from Eutectic Systems: Enhanced Permeation of a Model Drug, ibuprofen. *J. Controlled Release* **1998**, *59*, pp 297-308.
5 Doherty E. M.; Fotsch, C.; Bannon, A. W.; Bo, Y.; Chen, N.; Dominguez, C.; Falsey, J.; Gavva, N. R.; Katon, J.; Nixey, T.; Ognyanov, V. I.; Pettus, L.; Rzasa, R.; Stec, M.; Surapaneni, S.; Tamir, R.; Zhu, J.; Treanor, J. J. S.; Norman, M. H. Novel Vanilloid Receptor-1 Antagonists: 2. Structure-Activity Relationships of 4-oxopyrimidines Leading to the Selection of a Clinical Candidate. *J. Med. Chem.* **2007**, *50*(15), pp 3515-3527.
6. Sangster, J. Phase Diagrams and Thermodynamic Properties of Binary Organic Systems Based on 1-,2-, 1,3-, 1,4-diaminobenzene or benzidine. *J. Phys. Chem.* **1994**, *23*, pp 295-338.
7. Yamashita, H.; Hirakura, Y.; Yuda M.; Teramura, T.; Terada, K. Detection of Cocrystal Formation based on Binary Phase Diagrams Using Thermal Analysis. *Pharm. Res.* **2013**, *30*, pp 70-80.
8. Jain, N.; Yalkowsky, S. Prediction of Aqueous Solubility I; Application to Organic Nonelectrolytes. *J. Pharm. Sci*. **2001**, *90*, pp 234-252.

9. Ran, Y.; Jain, N.; Yalkowsky, S. Prediction of Aqueous Solubility of Organic Compounds by the General Solubility Equation (GSE). *J. Chem. Inf. Comp. Sci*. **2001**, *41*, pp 1208-1217.
10. Yalkowsky, S. H. *Solubility and Solubilization in Aqueous Media*. American Chemical Society: Washington, D.C. 1999; pp 2-45.
11. Amidon, G. L.; Lennernas, H; Shah, V. P.; Crimson, J. A Theoretical Basis for Biopharmaceutic Drug Classification: the Correlation of *in-vitro* Drug Product Dissolution and *in-viv*o Bioavailability. *Pharm Res* **1995**, *12*, pp 43-420.
12. Rowe, R. S., Sheskey, P. J., Cook, W. G., Fenton, M. E., Eds. *Handbook of Pharmaceutical Excipients.* 7th ed.; Pharmaceutical Press: Philadelphia, PA.
13. Doherty E. M.; Bannon, A. W.; Bo, Y.; Chen, N.; Dominguez, C.; Falsey, J.; Fotsch, C.; Gavva, N. R.; Katon, J.; Nixey, T.; Ognyanov, V. I.; Pettus, L.; Rzasa, R.; Stec, M.; Surapaneni, S.; Tamir, R.; Zhu, J.; Treanor, J. J. S.; Norman, M. H. Novel Vanilloid Receptor-1 Antagonists: Structure-Activity Relationships in the "A-Region" and the Selection of a Clinical Candidate, AMG 517. *J. Med. Chem.* **2007**, *50*, pp 3515-3527.
14. α- and β- polymorphs of trans-cinnamic acid XRPD patterns obtained from the Cambridge Structural Database.
15. Fonseca, I.; Hayes, S. E.; Blumich, B.; Bertmer, M. Temperature Stability and Photodimerization Kinetics of β-cinnamic acid and Comparison to its α-polymorph as Studied by Solid-State NMR Spectroscopy Techniques and DFT Calculations. *Phys Chem Chemical Physics*. **2008**, *10*, pp 5898-5907.
16. Stanton, M. K.; Bak, A. Physicochemical Properties of Pharmaceutical Co-Crystals: A Case Study of Ten AMG 517 Co-Crystals. *Cryst Growth Design* **2008**, *8*(10), pp 3856-3862.
17. Mercury, Cambridge Structural Database 3.1 Development (Build RC5.) Copyright CCDC 2001 – 2012. http://www.ccdc.cam.ac.uk/mercury/

Chapter 4. Glipizide Binary Systems

Introduction. Glipizide is a popular second generation sulfonylurea drug used extensively to complement other treatment and manage the disease Type II diabetes [1, 2]. The small moleclue is a weak acid (pKa = 5.9), which is practically insoluble in water (1.4 μg/mL) and in acidic environments (Figure 1) [2, 3]. Glipizide is categorized by the Biopharmaceutical Classification System (BCS) as a class II drug with high permeability and low soubility, resulting in dissolution rate limited bioavailability [2 – 4]. The pH-solubility profile displays a sharp rise in aqueous solubility above the pKa [5]. A eutectic mixture may be able to address low aqueous solubility and a slow dissolution rate in acidic aqueous environments [5, 10]. In this work, glipizide and other small molecules were ball milled to prepare physical mixtures that were studied by DSC. The melts of the mixtures were plotted to construct phase diagrams and find the eutectic mixtures [6 – 8, 10, 12].

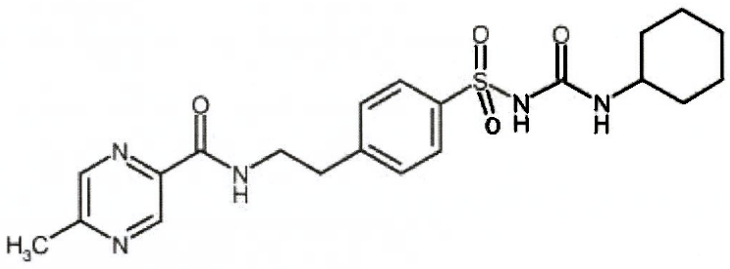

Figure 1. Chemical structure of glipizide (445.5 MW) [13].

Experimental

Materials. Glipizide (**G**) was purchased from Alexis Biochemicals [13]. 2-Chloroacetamide (**2CA**) was purchased from Fluka [14]. Propionamide (**PA**), benzamide (**BAD**), succinamide (**SU**), and adipamide (**ADA**) were obtained from Sigma Aldrich [15 – 18]. D-glucamide (**GA**), n-capronamide (**n-CAP**), and crotonamide (**CRT**) was purchased from TCI [19 – 21]. Anhydrous citric acid (**ACA**) was purchased from JT Baker [22]. Methanol (MeOH) was purchased from JT Baker. All compounds were used as received.

Ball milling Experiments.

Mixtures containing **G** and **ADA**, **2-CA**, **GA**, **SU**, **BAD**, **n-CAP**, **CRT**, **PA**, or **ACA** were weighed and transferred to 1.5 mL Retsch ball jars (Table 1.) Mixtures prepared for the phase diagrams were prepared as mole fractions (MF) of **G** to the amide [23]. The ball jars were assembled, tightened, and placed onto the Retsch ball mill. The ball jars were agitated for 2 minutes at 30 Htz. The ball jars were removed from the mill, and the samples were recovered and analyzed by PXRD and DSC.

Thermal Analysis Methods

Differential Scanning Calorimetry (DSC) measurements were performed on a TA Instruments Q100 calorimeter (New Castle, DE). All mixtures were weighted into hermetic pans and the pans were sealed prior to being placed in the DSC. Samples were equilibrated at 25 °C then ramped to 300 °C at 10 °C/min.

Thermal gravimetric analysis (TGA) was performed on a TA Instruments Q500 analyzer at 10 ºC/min from 25 ˚C to 275 ºC in a platinum pan under dry nitrogen at 90 mL/min. Data analysis was accomplished with TA Instruments Universal Analysis 2000 software v4.4A.

Compounds	Onset melt (˚C)
Glipizide	213-5
ADA	227
2-CA	115
GA	126
SU	207
BAD	125
n-CAP	101
CRT	159
PA	80
ACA	153

Table 1. Experimentally determined onset melts of amides determined during the **G** amide screen. Amides were weighed into hermetically sealed DSC pans and heated at 10 °C/min.

X-Ray Powder Diffractometry Method

X-ray diffraction patterns (XRPD) were obtained on a PANalytical X'Pert PRO X-ray diffraction system (Almelo, the Netherlands). Samples were scanned in continuous mode from 5-45 º (2θ) with step size of 0.0334 º on a spinning stage at 45 kV and 40 mA with CuKα radiation (1.54 Å). The incident beam path was equipped with a 0.02 rad soller slit, 15mm mask, 4 º fixed anti-scatter slit and a programmable divergence slit. The diffracted beam was equipped with a 0.02 rad soller slit, programmable anti-scatter slit and a 0.02 mm nickel filter. Detection was accomplished with an RTMS detector (X'Celerator).

Results and Discussion.

Glipizide-Amide Screen. The purpose of the screen was to determine which **G-**amide mixture, prepared in a 1:1 stoichiometric ratio, would have the greatest melting depression for **G**; degradation on melting was also noted. (Table 2) [10, 11]. The melt of the mixtures were compared to that of **G** which melts at 215 °C with degradation and limited degradation would be carried forward for full expansion of the phase diagram.

In most of the mixtures, the melt and subsequent degradation of the samples obscured the melt of **G** by DSC analysis (Figure 3). For example, **G:n-CAP** (dashed green trace, third from bottom) and the **G:CRT** mixture (red dash trace, second from bottom) (Figure 3) both degrade starting around 175 °C. In the **G:ADA** mixtures, the presence of **ADA** depressed the melt of **G** to around 200 ˚C, which is 14 ˚C below the original melt of **G** (Figure 3, second from top trace.) As mentioned previously, **ADA** melts at a higher temperatures than **G**. Therefore, more **G:ADA** mixtures were prepared in order to construct the phase diagram. Degradation is minimal in the **G:ADA** mixtures and the **G:PA** mixtures. **PA** was also chosen to prepare mixtures to develop a

1:1 Glipizide Amide Screen Results				
Components	Original melt (˚C)	1:1 Glipizide Amide Mixture onset melt (˚C)	Degradation after melt? (Y/N)	Chemical Structure
Glipizide [12]	213.1	N/A	Y	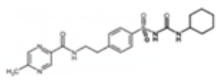
ADA [17]	226.8	199.7	N	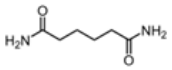
2-CA [21]	114.8	no glipizide melt*	Y	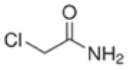
GA [18]	125.6	no glipizide melt*	Y	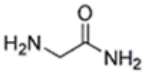
SU [16]	206.6	no glipizide melt*	Y	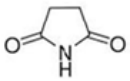
BAD [15]	124.3	199.2	Y	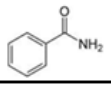
n-CAP [19]	100.5	100	Y	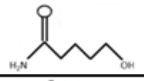
CRT [20]	158.8	no glipizide melt*	Y	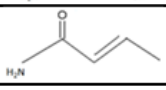
PA [14]	80.3	199.5	N	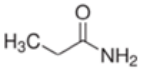

* The **G** melt was indiscernible due to degradation.

Table 2. The results of the 1:1 glipizide amide screen. Most of the mixtures had degradation, which obscured the **G** melt in the DSC analysis [13, 22]. The **G**:**ADA** mixture did not seem to indicate degradation by DSC analysis.

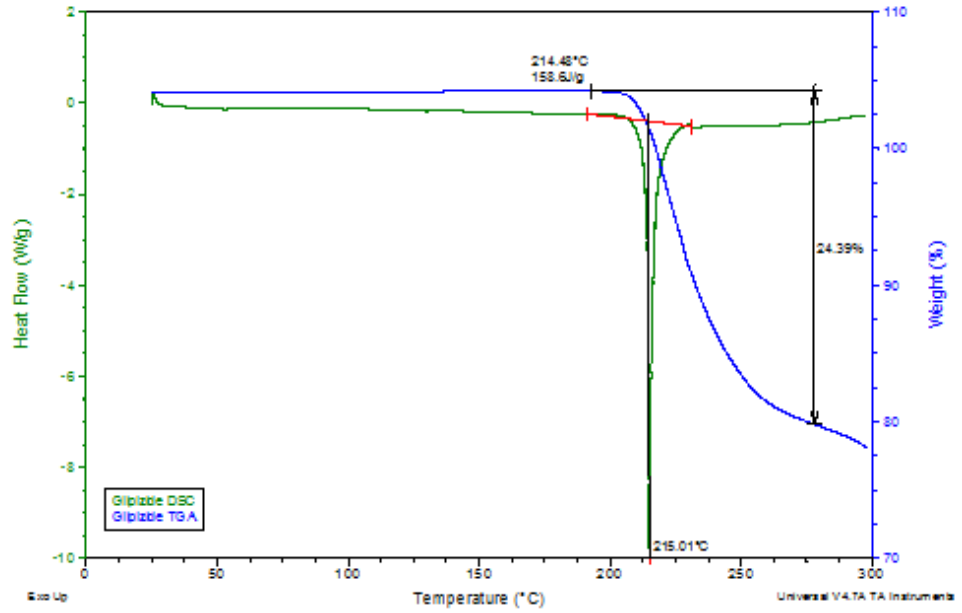

Figure 2. DSC (bottom) and TGA (top) overlay of **G** that was ball milled for 2 minutes at 30 Htz, and analyzed in a hermetically sealed DSC pan. **G** has an onset melt at 215 °C where it loses 24 % of its weight.

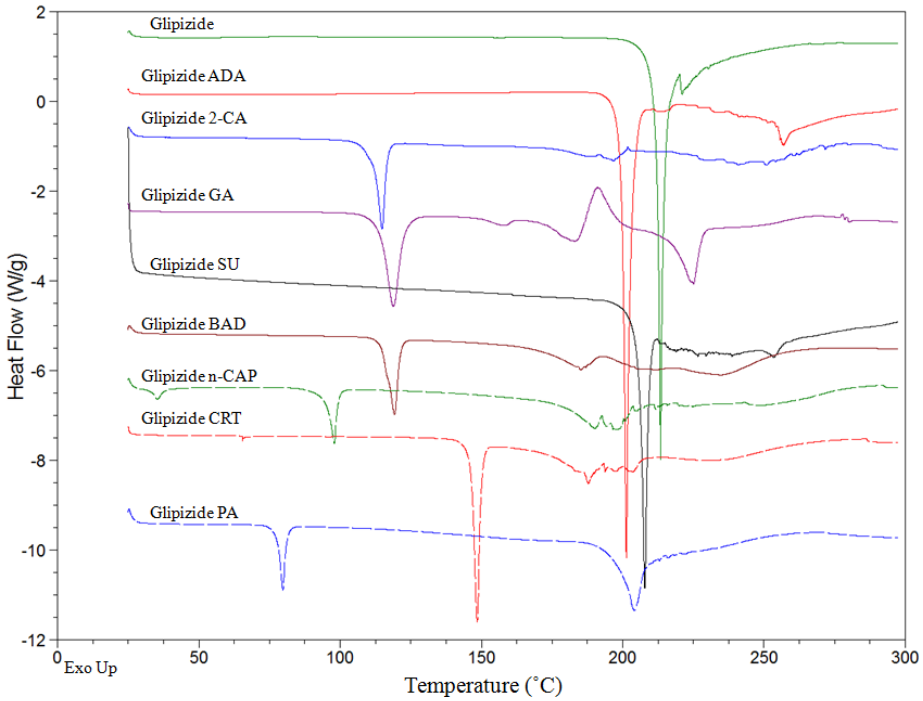

Figure 3. The DSC thermogram of 1:1 physical mixtures of **G** (top trace) and amides as analyzed in hermetically sealed DSC pans. Degradation is apparent in most of the mixtures.

phase diagram because the mixture (Figure 1, bottom dashed trace) also results in a melt depression of **G** (~10 °C to 200 ˚C) and a minimal amount of degradation.

Glipizide ADA Binary System

Mixtures were prepared to construct a phase diagram for **G:ADA** with a goal to identify the eutectic mixture which would have the lowest melting point. DSC/TGA analysis of the starting materials show that **ADA** melts 15 °C above **G**. Both compounds melt and degrade simultaneously (Figure 4). The **G:ADA** mixtures were analyzed by XRPD and the resulting data verified that the forms of **G** and **ADA** were unchanged after the ball milling process (Figure 5).

The physical mixtures were then analyzed by DSC to determine the melts needed to prepare a composition-temperature phase diagram (Figure 6). As more **G** is added to the mixture, the melt of **G** is depressed and shifts below 200 °C (curved, Figure 6). The 0.65 MF **G:ADA** mixture has a single symmetrical melt that occurs at the lowest melting temperature. Therefore, this mixture may be considered a eutectic mixture. The mixtures between 0.1 – 0.55 MF have the characteristic melt of a physical mixture signified by the resulting asymmetrical double peaks. The double peaks signify the mixture contains a MF mixture (green trace, third from bottom) begins to degrade and experience weight loss at lower temperatures than the 0.55 MF mixture (blue trace.) Also, the 0.45 MF and 0.55 MF mixtures experience melting and weight loss simultaneously. In either case, the mixtures are not thermally stable and there is degradation in both mixtures.

Glipizide PA Binary System

The presence of a **G:PA** eutectic mixture was investigated. The physical mixtures of **G** and **PA** were prepared by ball milling. The melting behavior of these mixtures were consistent with a monotectic system. **G:PA** mixtures were analyzed by XRPD and DSC. The XRPD analysis indicated that the mixtures contained the original compounds and no other forms (Figure 8). The

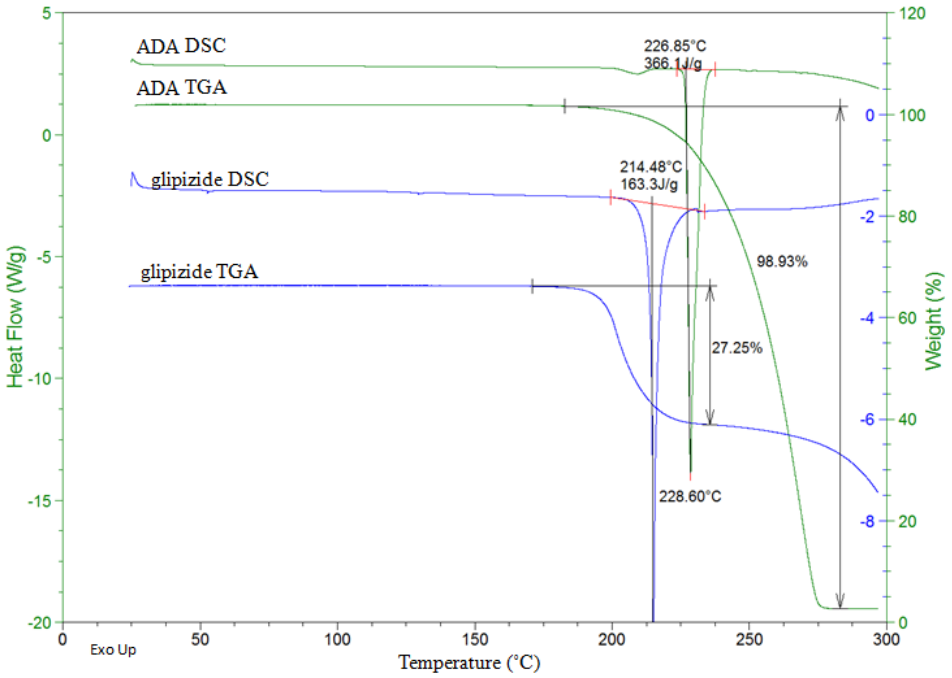

Figure 4. Overlay of DSC and TGA of **ADA** (top pair, green trace) and **G** (bottom pair, blue trace.) DSC samples were analyzed in hermetically sealed pans at 10°C/min for both components.

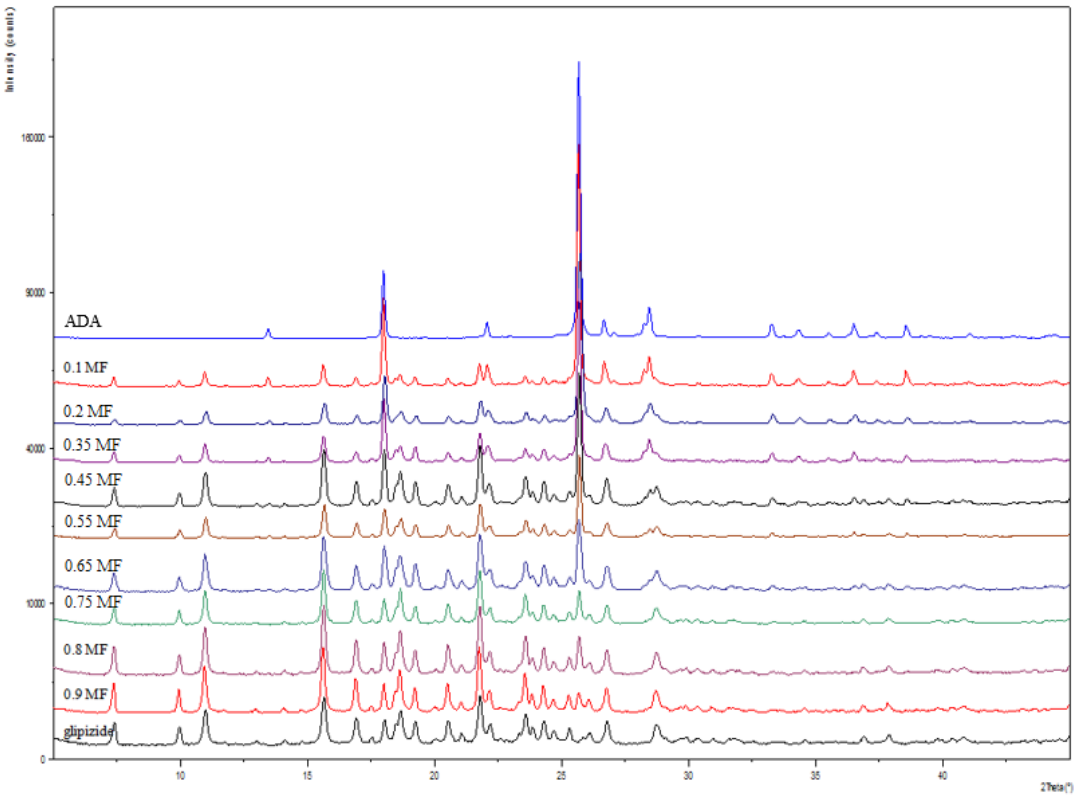

Figure 5. The physical mixtures of **G** (bottom trace) and **ADA** (top trace) contain the two original compounds and no new forms. The amount of **G** increases in the mixtures from the top (100% **ADA**) to the bottom (100% **G**) in the XRPD diffractograms.

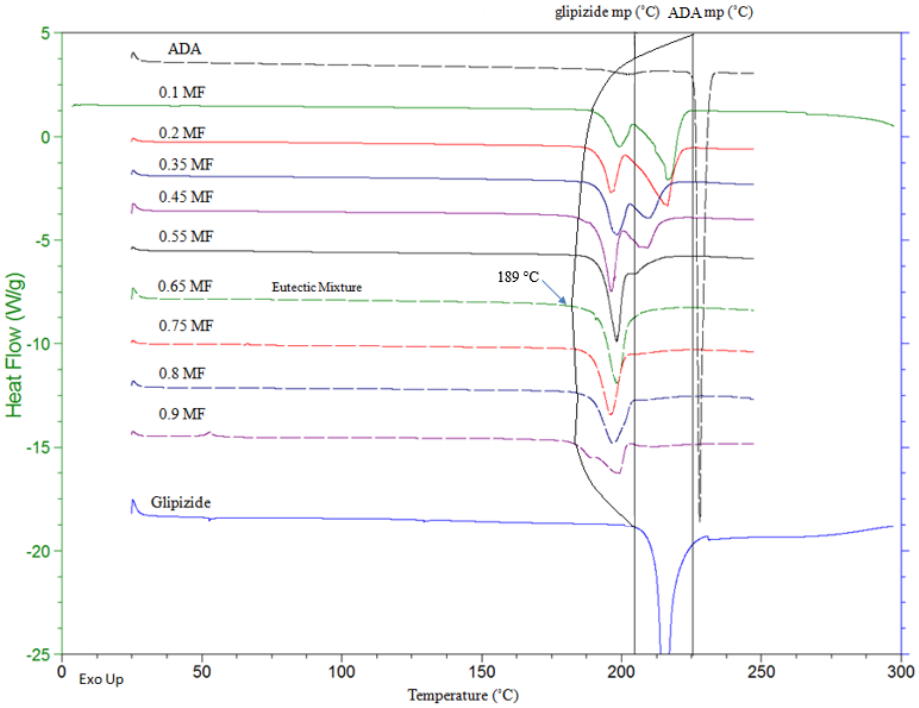

Figure 6. DSC traces for **G:ADA** mixtures show the gradual effect of proportionally added **G:ADA** on the melting temperature of the mixture. As more **G** is added to the mixtures, moving down the thermogram, the eutectic melt is formed at 189 ˚C in the 0.65 MF mixture.

DSC data shows that the melting point of G drops with addition of PA. The mixtures in the monotectic system are characterized by melting point depression for the higher melting compound, **G**, and unchanged melting point for the lower melting compound, **PA** [9]. In all of the mixtures, the melting point of **PA** is minimally affected by the increasing amount of **G** in the mixture, but **G** is depressed by the large amount of **PA** in the mixture (Figure 9).

As seen in the other amide mixtures that include **G**, degradation is a concern when preparing eutectic mixtures by the fusion method. The 0.5 MF **G:PA** mixture was analyzed by DSC and TGA in a closed DSC pan (Figure 10) to determine if degradation was occurring. The 0.5 MF mixture has an initial onset melt of 70˚ C and a simultaneous weight loss of 13%, corresponding to the loss of **PA**. The mixture then melts again at 163 ˚C with a subsequent weight loss of 29%. Because weight loss is occurring during melting, the composition of the mixture is changing during the melt, either by sublimation or degradation, therefore no further investigation was pursued.

Conclusions

The depressed melts of **G** was only observed in a few systems (Table 4). The depressed melts of **G** were lowest in the 0.65 MF **G**:**ADA** mixtures, and may be considered a eutectic mixture. The thermal degradation of **G** was observed in all systems evaluated and the production of degradants from the API and/or the amide confounded data interpretation.

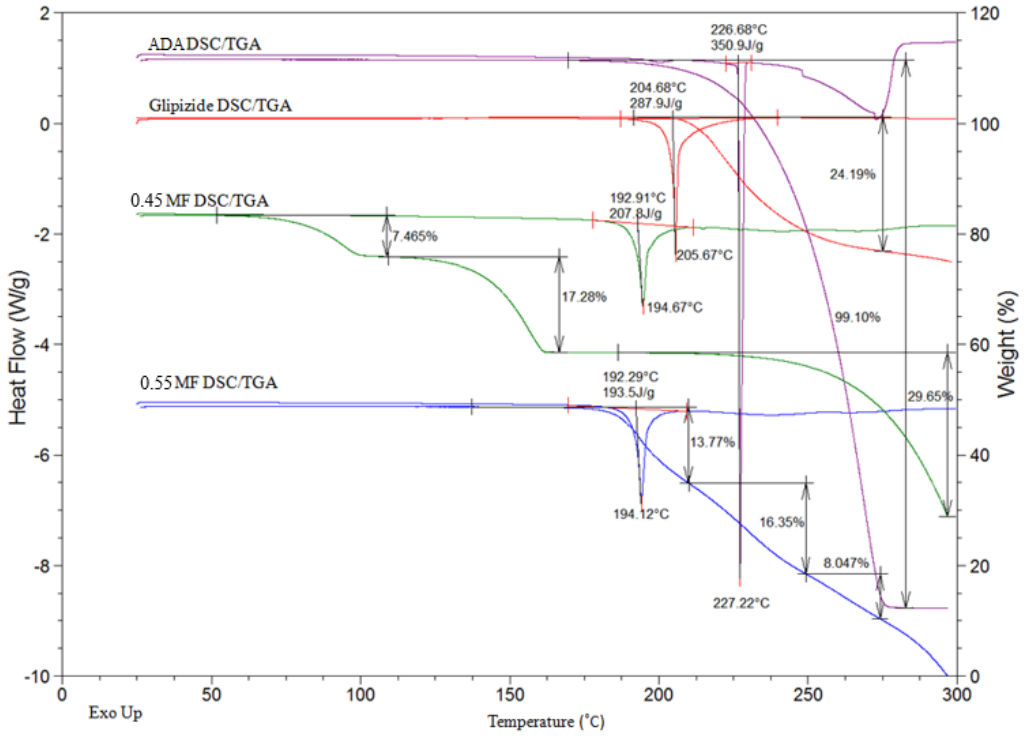

Figure 7. The 0.45 MF and 0.55 MF **G**:**ADA** mixtures were analyzed by DSC (open pans) and TGA. The multiple weight loss is due to **ADA** and **G** melting and forming separate degradants.

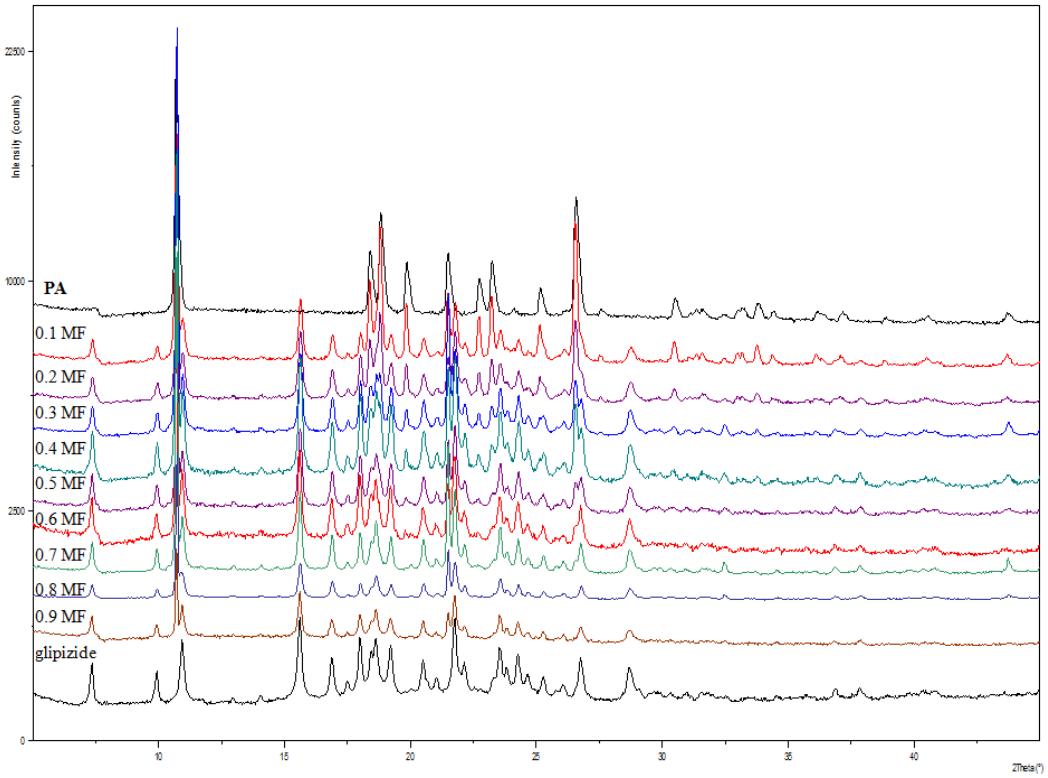

Figure 8. The physical mixtures of **G:PA** prepared by ball milling. All of the mixtures contained the original compounds and no other forms.

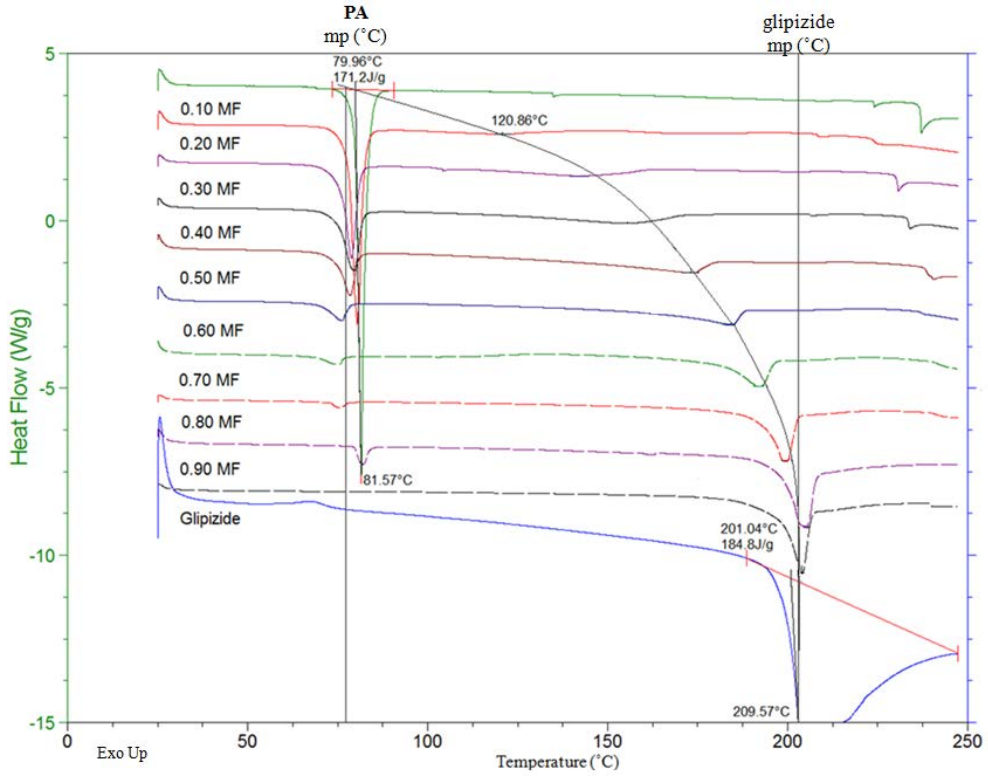

Figure 9. DSC overlay of ball milled mixtures of **G:PA**. Top trace (green) and bottom trace (black) are propionamide and glipizide, respectively, starting materials. The DSC traces are relative to each other with samples with the most propionamide at the top of the graph least amount at the bottom.

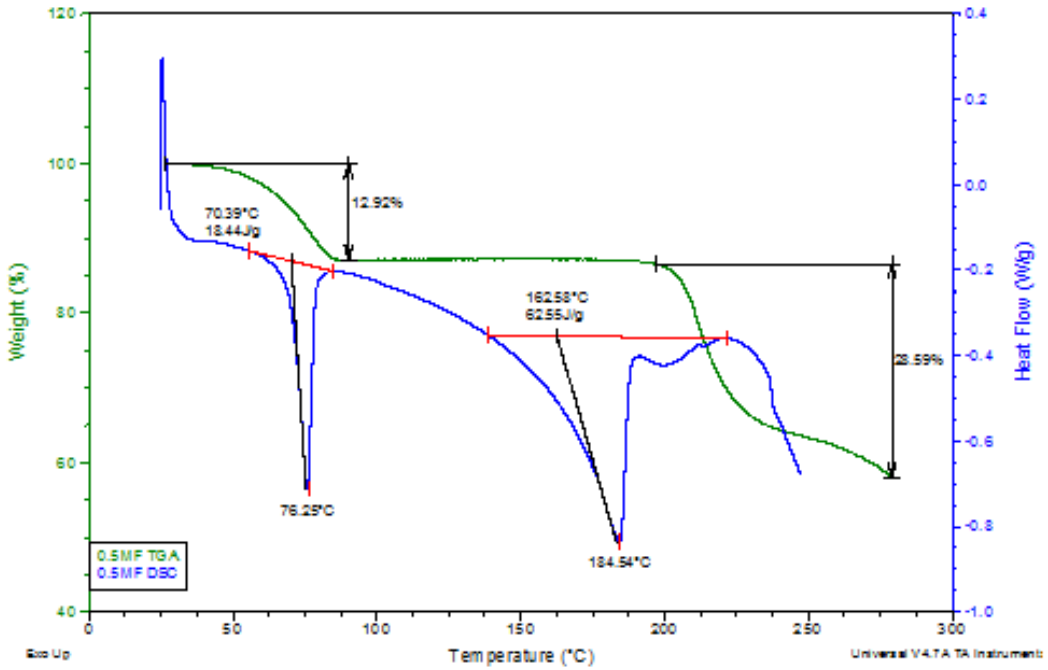

Figure 10. The 0.5 MF **G:PA** mixture was analyzed by DSC (blue trace, bottom) and TGA (green trace, top). Weight loss occurs simultaneously during melting, producing degradation products as indicated in the figure.

System	COC?	Eutectic Mixture	Melt (˚C)	Further Analysis?	Future Plans
Glipizide **ADA**	No	0.65 MF Mixture	189	No, Degradation Present	Solvent Evap, Hybrid Method
Glipizide **PA**	No	No	N/A	No, Degradation Present	Solvent Evap, Hybrid Method

Table 4. Mixtures prepared for the phase diagrams of the glipizide systems are summarized. A eutectic in the **G:ADA** mixtures was found, and but then the mixture degraded with increasing temperature.

References

1. Shuman, C. Glipizide: An Overview. *Am. J. Med.* **1983,** Nov *30*, pp 55-59.
2. Shukla. M.; Rathore, P.; Jain, A.; Nayak, S. Enhanced Solubility Study of Glipizide Using Different Solubilization Techniques. *Int. J. Pharm. Sci*. **2010**, *2*(2), pp 46–48.
3. Venkateswarlu, K.; Shanthi, Formulation and Evaluation of Sustained Release Glipizide Matrix. *J. Pharm. Bio. Sci.* **2012**, *2*(5), pp 17-23. www.iosrjournals.org
4. Yalkowsky, S. H. *Solubility and Solubilization in Aqueous Media*. American Chemical Society: Washington, D.C. 1999, pp 1-55.
5. Jamzaad, S. S.; Fassihi, R. Role of Surfactant and pH on Dissolution Properties of fenofibrate and glipizide – a technical note. *AAPS PharmSciTech* **2006**, *7*(2), pp E1-E6.
6. Chiou, W. L.; Niazi, S. Phase Diagrams and Dissolution Rate Studies on sulfathiazole-urea Solid Dispersions. *J. Pharm. Sci.* **1971**, *60*(9), pp 1333-1337.
7. Janssens, S.; Van den Mooter, G. Review: Physical Chemistry of Solid Dispersions. *J. Pharm. Pharmacol*. **2009**, *61*, pp 1571–1585.
8. Ford, J. L. The Current Status of Solid Dispersions. *Pharm. Acta. Helv*. **1986** *61* (3), pp 69-88.
9. Craig, D. Q. W. Review: The Mechanisms of Drug Release from Solid Dispersions in Water Soluble Polymers. *Int J. Pharm.* **2002**, *231*, pp 131-144.
10. Pilling J 1992. Phase Diagrams and Microstructure: A computer-aided learning guide. The Institute of Materials: London, UK, pp 25 – 58.
11. Stott PW, Williams AC, Barry BW 1998. Thermal delivery from eutectic systems: enhanced permeation of a model drug, ibuprofen. J Controlled Release 50:297-308.
12. Glipizide. MSDS sheet. Alexis Biopharmaceuticals.
13. 2-Chloroacetamide, MSDS from Sigma Aldrich.
14. Propionamide, MSDS, Sigma Aldrich.Benzamide, MSDS, Sigma Aldrich.
15. Succinamide, MSDS from Sigma Aldrich.
16. Adipamide, MSDS, Sigma Aldrich.
17. d-Glucamide, MSDS, TCI Chemicals.
18. n-Capronamide, MSDS, TCI Chemicals.
19. Crotonamide, MSDS, TCI Chemicals.
20. Anhydrous Citric Acid, MSDS, JT Baker.
21. Nic M, Jirat J, Kosata B., eds. (2006–). "amount fraction". IUPAC Compendium of Chemical Terminology (Online ed.). doi:10.1351/goldbook.A00296. ISBN 0-9678550-9-8. http://goldbook.iupac.org/A00296.html.

Chapter 5. Naproxen Vanillin Binary System

Introduction. Utilizing a eutectic mixture as a crystalline solid dispersion is a strategy to improve the solubility or change the intrinsic dissolution rate of a drug [1 -7]. The poorly soluble compound naproxen (**NAP**) and the highly aqueous soluble compound vanillin (**VAN**) were prepared in mixtures of varying proportions to form a phase diagram. The molecular structure of **NAP** and **VAN**, and some physicochemical properties, are listed in Table 1.

NAP is an example of a BCS class II drug that has poor solubility and high permeability [8]. The drug is a non-steroidal anti-inflammatory drug (NSAID) characterized by poor wettability and low aqueous solubility [11]. The mechanism of action of **NAP** is through the inhibition of the enzyme cycloxygenase (COX) in the inflammation pathway [12 – 13]. **NAP** is a weak acid (pKa of 4.2) [14], has poorly aqueous solubility (27 mg/L at 25 ˚C) [15], and a melting point of 153 - 156 °C [10]. A eutectic mixture of **NAP** and **VAN** was investigated as a strategy to increase solubility [6, 15].

VAN was selected because previous studies have shown that the compound forms a eutectic mixture with other compounds, such as *p*-anisidine [16]. **VAN** was also a practical choice because the compound is a member of the Everything Added to Food in the United States (EAFUS) by the U.S. Food and Drug Administration [17]. **VAN** is safe to handle and freely water soluble (10 mg/mL) [18]. **VAN** is weakly basic with a pKa of 7.8, and melts between 81 - 83 °C [18 – 20]. Samples were prepared to determine the phase diagram for **NAP** and **VAN** by the fusion method [4, 15, 20 – 22]. The mixtures were analyzed by DSC, and then the melts recorded on the phase diagram. The eutectic mixture is identified as the mixture that exhibited the lowest melt [4, 5, 20 – 22].

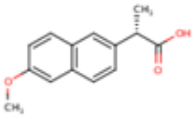	**Naproxen** Water solubility = 15 mg/L MW = 230.26 mp = 155 °C pKa = 4.2
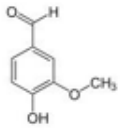	**Vanillin** Water solubility = 10 mg/mL MW = 152.1 mp = 81-83 °C pka = 7.8

Table 1. Some physicochemical properties and molecular structures of **NAP** and **VAN** [10, 18].

Experimental

Materials. **NAP** (Sigma Aldrich) and **VAN** (Alfa Aesar) were used as received. 1-Methyl-2-pyrrolidone (NMP) (Sigma Aldrich), dimethyl sulfoxide (DMSO) (Sigma Aldrich), ethanol (EtOH) (Pharmco), acetonitrile (MeCN) (Sigma Aldrich), ethyl acetate (EtOAc) (Burdick & Jackson), methanol (MeOH) (Sigma Aldrich), toluene (Burdick & Jackson), and n-heptane (Burdick & Jackson) were obtained from Fischer Scientific. Dulbecco's Phosphate Buffered Saline (PBS) was obtained from Sigma Aldrich and stored on bench top. **VAN** was stored at refrigerated temperatures and **NAP** was stored on the bench top.

Organic Solubility Screen. The solubilities of **NAP** and **VAN** were determined in several organic solvents. A series of Eppendorf tubes (2.5 mL) were labeled by organic solvent and whether the tube contained of **NAP** or **VAN**. **NAP** and **VAN** were weighed (1.5 – 2.5 mg) and transferred to Eppendorf tubes. NMP, DMSO, EtOH, MeCN, EtOAc, MeOH, toluene, and n-heptane were pipetted (250 μL) into each tube. Vials were capped and placed into a shaker at 25 °C for 24 hours to allow the samples to equilibrate. The next day, the **NAP** samples were solutions and the **VAN** samples were suspensions. The samples were removed from the shaker, and then transfer pipets were used to add 0.2 mL of each sample into the labeled 0.2 μm PTFE filter insert attached to an Eppendorf tube. The caps were closed, the samples were centrifuged and spun at 25000 rpm for five minutes. The solubility of the filtrates were analyzed by HPLC-UV.

Ball Milling Experiment. **NAP:VAN** mixtures were prepared for a phase diagram by weighing the compounds in different proportions and then transferring into 1.5 mL Retsch Ball jars. A 5 mm stainless steel ball was added, and the jars were assembled and placed in the Retsch ball mill (Retsch, Inc. Newton, PA). The mixtures were milled for 2 minutes at 15 Htz, and then

analyzed on DSC, TGA, and XRPD. For the phase diagram, the melts were determined by a single mixture by DSC analysis.

Aqueous solubility experiment of naproxen and 0.11 MF NAP:VAN mixture. The solubilities of the eutectic mixture and the original drug were compared in DI Water and PBS at 25 ºC and 37 ºC. **NAP** was weighed into 20 mL scintillation vials for DI Water (8.5 mg) and PBS (34 mg) for 25 ºC and 37 ºC. The 0.11 MF **NAP VAN** (11% **NAP**/ 89% **VAN**) eutectic mixture was prepared by the fusion method. The eutectic mixture was prepared in duplicate for DI Water solubility testing by weighing **NAP** (8.5 mg) and **VAN** (45 mg) into two 1.5 mL Retsch ball jars. The mixtures prepared for PBS solubility measurements were prepared by weighing **NAP** (17 mg) and **VAN** (90 mg) into 4 Retsch ball jars. The jars were combined to form mixtures of 34 mg **NAP** and 180 mg **VAN**. All of the samples were agitated for 2 minutes at 15 Htz. The mixtures prepared for DI Water and PBS solubility measurements were transferred to 20 mL scintillation vials labelled by **NAP**, eutectic mixture (EM), and each heating condition. The eutectic mixtures was prepared by forming a solid dispersion by heat on an IKA heated stir plate with a digital thermometer. The vials were set to heat from ambient conditions to 68 ˚C while mixing at 400 rpm. All of the mixtures melted into clear viscous solutions in < 5 minutes. The samples were immediately placed into an ice bath and left to cool completely for 2 – 3 hours. When completely cooled, the mixture hardened into a white solid mass. This heating and cooling process was repeated three times. The mixtures were broken up by a spatula and analyzed by XRPD.

The solubilities of **NAP** and 0.11 MF **NAP:VAN** mixture were determined from slurries in DI water or PBS (pH 6.8) at 37 °C or room temperature. DI Water (15 mL) or PBS (15 mL) were pipetted into the designated sample vial and a stir bar was added (400 rpms). This created saturated slurries of **NAP** in DI Water (0.5 mg/mL) and PBS (2.2 mg/mL). After 48 hours, the pH

of the suspensions were measured. Photomicrographs (200 x magnification) were recorded and compared. The samples were aliquotted in triplicate, by syringe, and filtered through 0.45 um PTFE 13 mm Acros filters. The first 5-7 drops of the filtrate were discarded to avoid any effect of filter binding. Concentrations were determined by HPLC-UV. Finally, remaining solids were isolated by filtration and characterized by PXRD.

Freeze-Thaw Stability. Stability during freeze-thaw cycling was evaluated for 0.11 and 0.8 MF **NAP:VAN** mixtures. For the 0.11 MF **NAP:VAN** sample, 8.5 mg **NAP** and 45 mg of **VAN** along with a single steel bearing were added to each of three 1.5 mL Retsch ball jars. Similarly, a 0.8 MF **NAP:VAN** sample was prepared using 43 mg **NAP** and 7 mg **VAN**. The ball jars were loaded into the mill and agitated for 2 minutes at 15 Hz. The contents of each ball jar were separated from the bearings and transferred to 4 mL screw toped vials along with Teflon coated stir bars. The vials were placed on a heated stir plate and heated to 68 °C and 150 °C for the 0.11 and 0.8 MF mixtures, respectively. All samples formed clear viscous liquids upon melting. The samples were placed in ice baths to freeze, and then the freezer overnight. One of the 0.11 and the only 0.8 MF **NAP:VAN** samples were analyzed by microscopy, DSC and HPLC-UV. The freeze-thaw cycling was repeated one and two more times for the remaining 0.11 MF **NAP:VAN** samples, after which the samples were characterized.

HPLC-UV samples were prepared by weighting 1.3 mg of each solid dispersion was weighed into a 20 mL scintillation vial. DMSO (20 mL) was pipetted directly into the vial. The vials were placed into a Branson sonic bath for 15 minutes to dissolve the samples, vortexed briefly, and the samples pipetted directly into HPLC vials.

Photomicroscopy. Polarized light microscopy (PLM) photomicrographs were taken using a Nikon LV100 polarized light microscope, equipped with a Nikon Digital Camera DS-Fi2,

operated by NIS Elements D software. Samples were placed on microscope slides, protected with a cover slip, and then analyzed at 200x magnification.

High Pressure Liquid Chromatography (HPLC-UV) Method. High pressure liquid chromatography-ultraviolet spectroscopy (HPLC-UV) was performed on an Agilent 1100 series HPLC (LC1027) equipped with a binary pump, DAD detector, auto sampler and a YMC pack Pro C18 4.6 x 50 mm ID, 12 nm pore size, 5 μm particle size column AS12S05-0546WT No. 040510798(W). Elution was achieved by a gradient method from 10 to 95 % of solvent B (98% acetonitrile, 2% water, 0.1% triflouroacetic acid) in solvent A (98% water, 2% acetonitrile, 0.1% triflouroacetic acid) at 0.5 mL/min for 15 min. Column and samples were maintained at 25 □C. NAP and VAN concentrations were determined using 275 nm and 230 nm wavelengths, respectively.

Thermal Analysis Methods

Differential scanning calorimetry (DSC). DSC analysis was conducted in hermetically sealed DSC pans on a TA Instruments Q100 calorimeter (New Castle, DE). The samples were equilibrated at 25 ˚C then heated at 10˚C/min to 275 ˚C. All DSC samples were weighed at 3.1 mg ± 0.2 mg.

DSC Heating/Cooling Cycling Experiments. The 0.11 MF and 0.80 MF **NAP:VAN** mixtures were heated and cooled in hermetically sealed DSC pans and analyzed by DSC. The mixtures were weighed (3.1 – 3.2 mg) directly into tared DSC pans. The samples were equilibrated at 25 ˚C then cycled between 150 °C and 10 °C at 10 °C/min two times.

Thermal gravimetric analysis (TGA) was performed on a Q500 analyzer at 10 °C/min from 25 °C to 275 °C in a platinum pan under dry nitrogen at 90 mL/min.

Results and Discussion

Naproxen Vanillin Organic Solubility Experiment

The solubilities of **NAP** and **VAN** in several organic solvents were determined by HPLC-UV (Table 2). Both compounds were soluble in all of the solvents screened except toluene and n-heptane. The organic solubility of **VAN** was lower in the solvents tested than **NAP**. The precipitates of the organic solubility screen were analyzed by XRPD and DSC and did not show any new forms in EtOAc, EtOH, and MeOH (Figure 1). Also, the DSC analysis of the original compounds matched the precipitates from the organic solubility screen, and no new forms or degradation was detected (Figure 2). The other solvents (toluene and n-heptane) were not analyzed by XRPD due to an insufficient amount of precipitate recovered after evaporation. The data supports future solvent evaporation experiments between **NAP** and **VAN** because of the neutrality of the compounds in the organic solvents and the mutual solubility in the solvents.

Phase Diagram

The presence of a eutectic was investigated in the mixtures prepared for the phase diagram of **NAP** and **VAN**. Before DSC analysis, the physical mixtures were analyzed by XRPD and showed that crystalline **VAN** and crystalline **NAP** were detectable in all of the **NAP:VAN** solid mixtures, confirming immiscibility in the solid state (Figure 3) [23 – 38]. The melting temperatures of **NAP** and **VAN** were determined by DSC analysis and then compared to the other mixtures (Figure 4).

The **NAP:VAN** mixtures prepared for the phase diagram shows the formation of a eutectic mixture at 0.11 MF and melt at 75.2 ˚C. The vertical line moving down the figure begins at the onset melt of **VAN** (top trace, Figure 4), and then follows the melt depression of **VAN** due to the presence of **NAP** in the mixtures to the 0.11 **NAP:VAN** mixture. The eutectic melt is measured

			Slurry Concentration (mg/mL)		Actual Concentration (mg/mL)	
Organic Solvent	**Naproxen** (mg)	**Vanillin** (mg)	**Naproxen**	**Vanillin**	**Naproxen**	**Vanillin**
NMP	1.7	3.1	6.8	12.4	> 7	4.2
DMSO	1.8	1.8	7.2	7.2	> 7	2.6
EtOH	2.1	2.1	8.4	8.4	> 8	2.6
MeCN	2.1	2.3	8.4	9.2	> 8	4.2
EtOAc	1.4	2.4	5.6	9.6	> 5	2.8
MeOH	2.1	2.8	8.4	11.2	> 8	3.7
Toluene	1.2	2.1	4.8	8.4	n/a	n/a
n-Heptane	1.5	1.4	6	5.6	n/a	n/a

Table 2. Organic solubility of **NAP** and **VAN** as determined by HPLC-UV. The solubilities of **NAP** and **VAN** in toluene and heptane were undetermined.

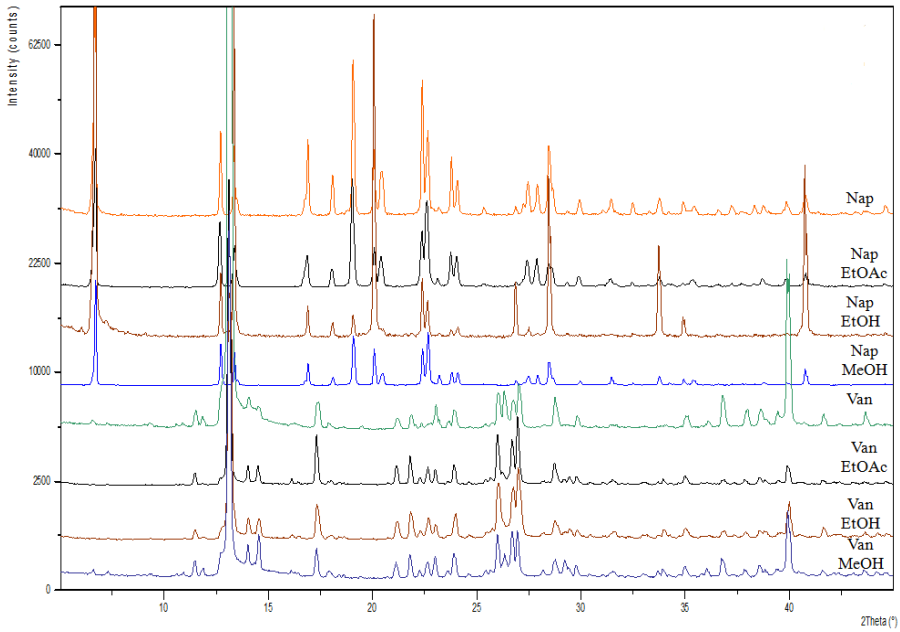

Figure 1. The PXRD diffraction patterns of **NAP** (top) and **VAN** (fourth trace from bottom) were compared to precipitates from the organic solvent screen as labeled in the figure. No new forms were detected.

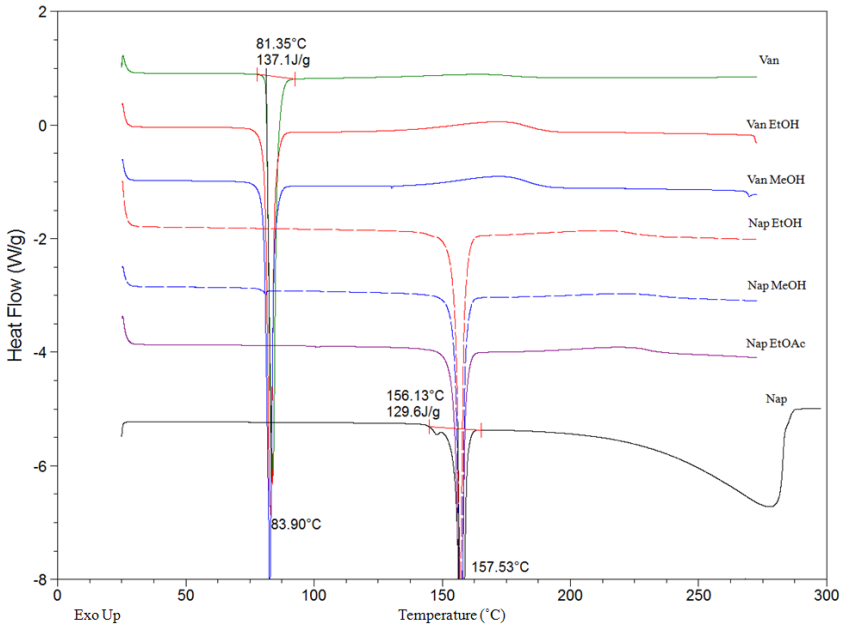

Figure 2. The precipitates of **NAP** and **VAN** from the slurries in organic solvents are compared to the onset melt of the original compounds **NAP** (bottom trace) and **VAN** (top trace). The precipitates of **VAN** in **EtOH** (second from top) and **MeOH** (third from top) do not show degradation (exothermic rise) until after the melt. The precipitates of **NAP** in **MeOH** (third from bottom) and **EtOA**c (second from bottom) also do not show degradation until after the melt.

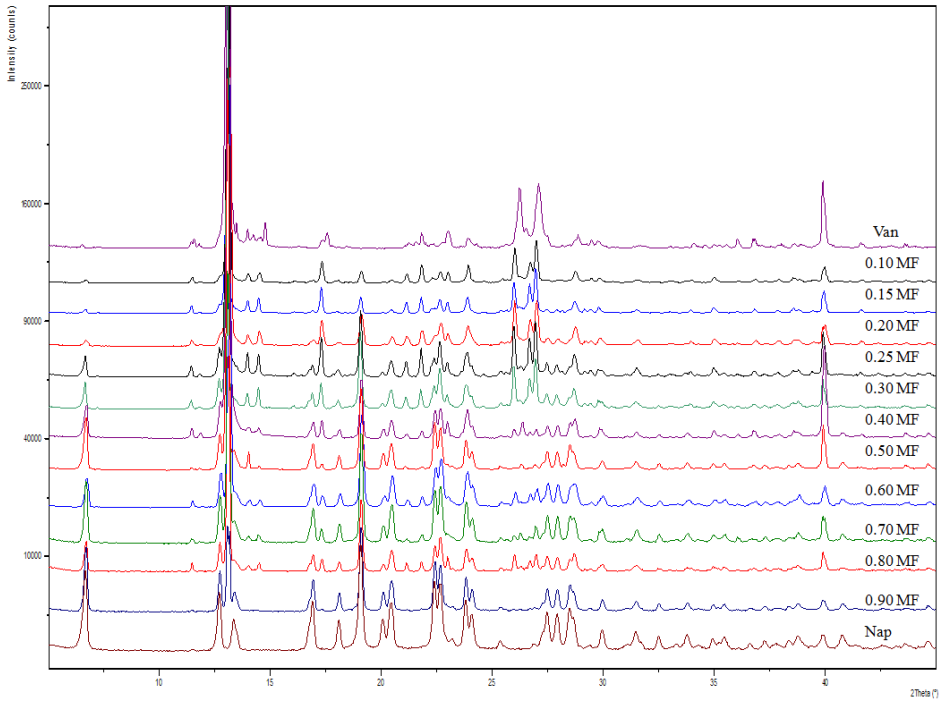

Figure 3. XRPD overlay of ball milled samples of **NAP** and **VAN** prepared for the phase diagram. The mixtures are organized with **VAN** at the top of the figure and then increasing **NAP** in the mixtures moving down the figure. No other forms besides **NAP** and **VAN** were detected.

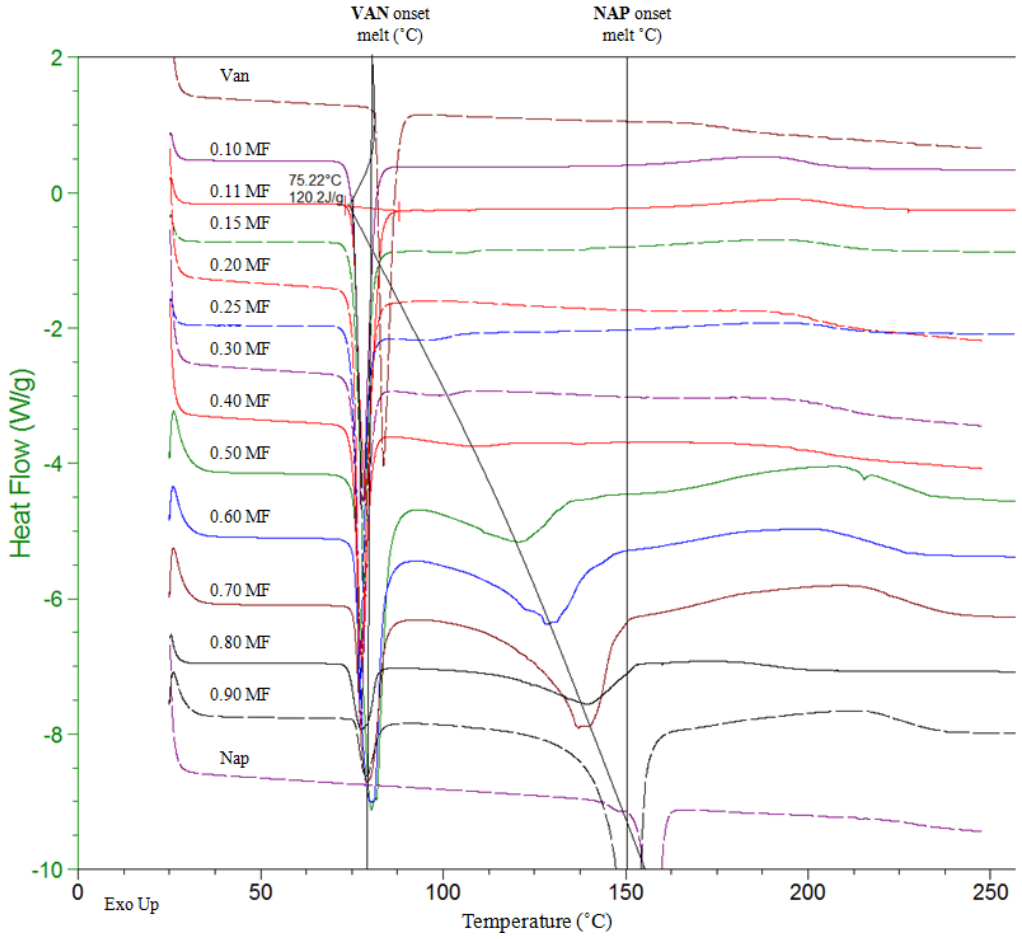

Figure 4. Thermogram of DSC overlay of **NAP VAN** physical mixtures as analyzed in hermetically sealed DSC pans at 10 °C/min. The eutectic mixture is at 0.11 MF and melts at 75.2 ˚C (third trace from top).

by the onset melt, and the liquidus melt is measured by the maximum peak temperature of the resulting melting endotherm as many studies have previously performed by most researchers [25 – 27]. One endothermic melt occurs between the 0.1 – 0.4 MF **NAP:VAN** mixtures, which reflect a solid solution is formed between **NAP** and **VAN** [20, 23]. After the initial melt of these mixtures, the resulting melting endotherm returns to baseline at slightly higher temperatures.

The resulting maximum temperature of the endotherm correlates to the melting of **NAP** in the mixture. The difference between the peak maximum temperature in the resulting melting endotherm between the 0.1 and 0.2 MF mixture are slight. At the 0.25 MF **NAP:VAN** mixture, the maximum peak temperature of the endotherm is more noticeable at around 100 ˚C (fifth DSC trace from top, Figure 4). When the drug content was decreased in the mixtures, the resulting melting endotherm gradually shifted to a lower temperature and the resulting melting endotherm broadened, losing its sharp, distinct appearance. As the **NAP**:**VAN** ratio further decreased, as in the 0.1 – 0.4 **NAP:VAN** mixtures, the DSC curves showed only one endothermic peak, corresponding to the melting of **VAN**. The melting temperatures of the 0.5 – 0.9 MF **NAP:VAN** mixtures correspond to an initial eutectic melt, followed by a broadening of the resulting melting endotherm due to excess temperature of the **NAP** melting at higher temperatures until the onset melt of pure **NAP** (bottom trace, Figure 4).

The **NAP:VAN** mixtures display the melting behavior of a monotectic system. A monotectic system contains mixtures where the lower melting compound is only slightly affected by the presence of the higher melting poorly soluble API is present [2]. This causes a lowering in the melt depression of the API as the amounts of the lower melting compound is increased and the corresponding amounts of API is decreased in the mixtures. This phenomenon can be seen in the

phase diagram in Figure 5. The ability of **VAN** to depress the melt of **NA**P is due to the solubility and miscibility of **NAP** and **VAN**.

The resulting melting endotherm of **NAP** is not detected by DSC analysis in mixtures that contain less than 11% **NAP.** Only the **VAN** melt is detected, which is significant because a solid solution may be formed. The melt of **NAP** is most depressed at the eutectic mixture of 0.11 MF. As the amounts of **NAP** is increased above the eutectic mixture, the solubility and miscibility of the two compounds is exceeded, at the melt of **NAP** shifts back to its original melting temperature. At this point, the endotherm of **NAP** is depressed less as more **NAP** is added to the mixture, and the vertical line in the figure reflects the maximum

The **NAP:VAN** system contains a eutectic melt at 0.11 MF **NAP:VAN** and the eutectic temperature, by DSC analysis, is 75.2 ˚C (**E**, Figure 5). There are two mixed phases on the left and right of the eutectic mixture, above the solidus line and under the liquidus line. The mixed phases are mirror images of **VAN** and **NAP** and are separated by the eutectic point **E** on the figure. Also, after the eutectic mixture, the lowest melting endotherm changes only slightly to a depressed temperature (~ 0.2 ˚C) as the amount of **NAP** increases in the mixtures. The rising liquidus curve corresponds to the drug solubility in the liquid **VAN**.

The purpose of the DSC/TGA analysis of the **NAP:VAN** mixtures is to determine if **VAN** is melting and degrading at the melting temperatures of **NAP** (Figure 6). The 0.10 MF **NAP:VAN** mixture was analyzed and the resulting melting depression of **VAN** occurs at 3 °C (76 ˚C) below the original onset melt of **VAN** (81 °C). The melt of **NAP** in the 0.10 physical mixture is not indicated due to the solubility of the compound in **VAN** at 70 ˚C. The DSC/TGA data also indicates simultaneous melting and weight loss of both compounds when heated after the initial melt of **VAN**. The 0.10 MF **NAP:VAN** mixture has an exothermic event at 200 ºC that may

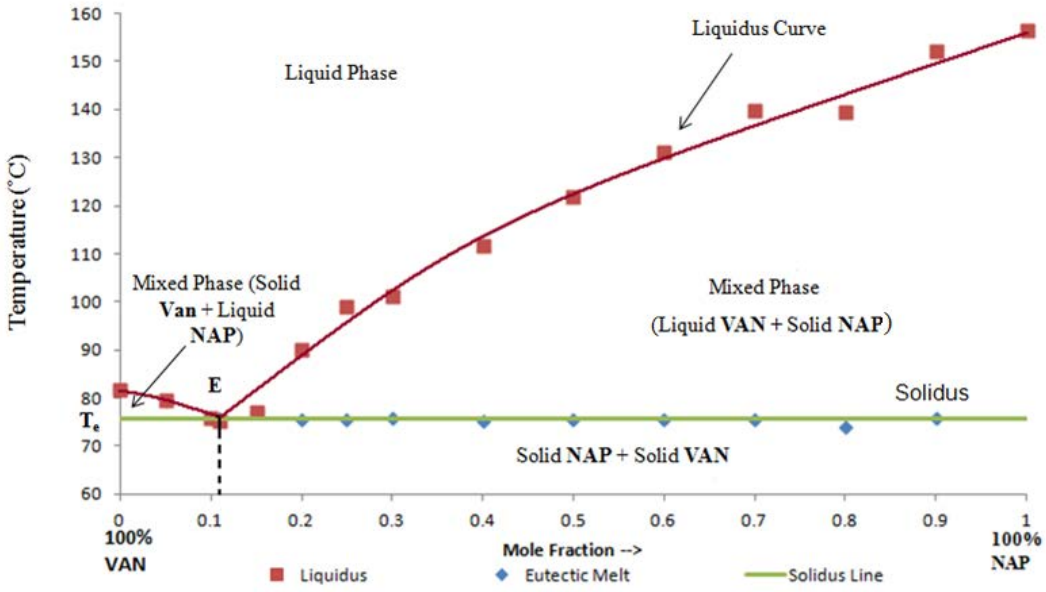

Figure 5. Phase diagram of **NAP:VAN** mixtures that shows the depression of vanillin from the onset melt of **VAN** to the eutectic mixture (**E**) at 0.11 MF at the eutectic temperature at 75.2 ˚C (**T_e**). When more NAP is added to the mixture after **E**, the liquidus curve reflects the solubility of **NAP** in **VAN** at higher temperatures. When more **VAN** is added to mixture, on the left side of **E**, the melt of **VAN** is depressed as more **NAP** is added to the mixtures.

correlate to a solid-solid transition due to the presence of a new form or degradation. A DSC heating/cooling experiment was designed to see if the mixtures were able to reform after melting and weight loss.

DSC Heating/Cooling Experiment

The physical mixtures prepared for the phase diagram demonstrated the melting behavior of **NAP** and **VAN** as soluble and miscible in proportions that contain less **NAP** below the eutectic mixtures (11% NAP/ 89% VAN) in the liquid state by DSC analysis. This is apparent because as the % of **NAP** increases above 11% mixtures prepared for the phase diagram, the **NAP** endotherm increases in the onset melting temperature and the resulting melting endotherm separates from the **VAN** resulting melting endotherm. XRPD analysis of the mixtures also confirmed that **NAP** and **VAN** are not soluble and immiscible in the solid state. To further determine if the **NAP:VAN** mixtures would be able to reform to the original compounds after melting, a DSC heating/cooling experiment was designed.

The 0.11 MF eutectic mixture (Figure 7) and the 0.8 MF **NAP:VAN** mixture (Figure 8) were heated and cooled to determine if the mixtures were able to reform to the original compounds after melting. The eutectic mixture melted at very similar temperatures during each heating cycle (75.2 ± 2 ˚C) but did not reform until the heating stage after the initial melt and cooling of the mixture. Two solid-solid state transitions (at 28.6 °C and 45.3 ˚C) indicate that recrystallizations or polymorphism may be occurring during this heating step. This was also shown in Chapter 2 of this work, where the DSC heating/cycling experiment on the 0.442 MF **U:BA** eutectic mixture reformed to the original compounds during the cooling process after the initial melt. The thermal behavior of the 0.8 MF **NAP:VAN** mixture was similar to the 0.11 MF **NAP:VAN** mixture, and also reformed during the heating cycle after the initial melt and cooling processes. The 0.8 MF

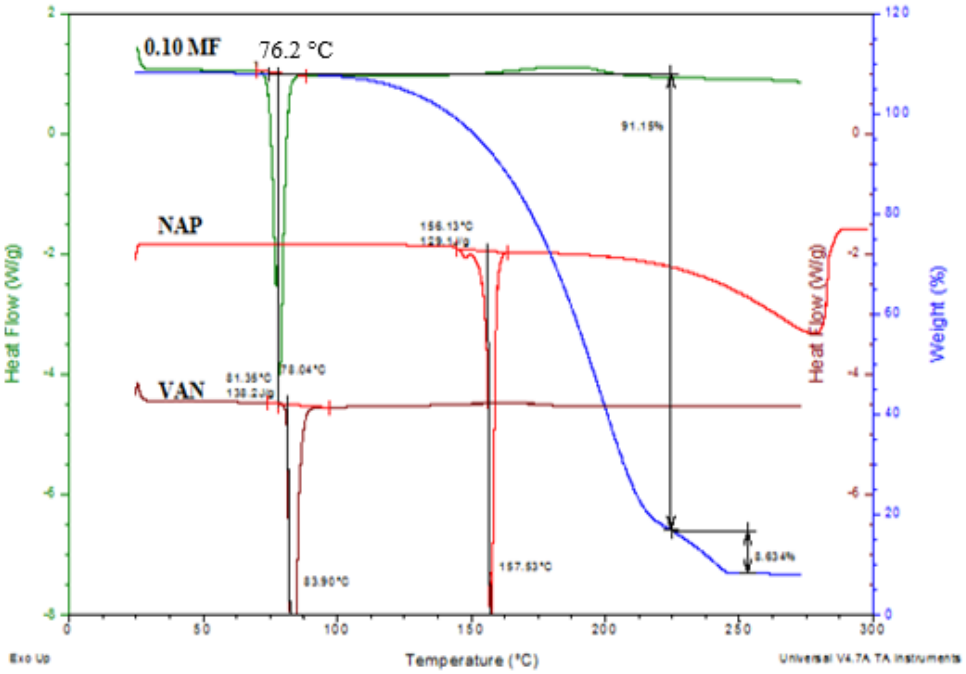

Figure 6. The DSC/TGA overlay of 0.10 MF physical mixture (DSC/TGA top traces) was compared to the DSC traces of **NAP** (middle trace) and **VAN** (bottom trace). All DSC samples were analyzed in hermetically sealed pans.

mixture melted between 76 – 77 ˚C and reformed during heating in multiple exothermic events from 41 – 56 ˚C. These events may be multiple solid – solid state transitions. However, the **NAP:VAN** mixtures consistently reformed to the original compounds after at least two cycles of heating and cooling.

0.11 MF Eutectic Mixture Solid State Characterization

The 0.11 MF **NAP:VAN** eutectic mixture was prepared by the fusion method and analyzed by DSC, XRPD, and HPLC-UV to determine degradation. The eutectic mixture was also compared to the 0.11 MF **NAP:VAN** physical mixture, with the main difference between the samples is that the physical mixture was ball milled and not melted before analysis. The DSC analysis of the 0.11 MF **NAP:VAN** physical mixture and the 0.11 MF **NAP:VAN** eutectic mixture are very similar (Figure 9). Both mixtures contain a slight melt depression of **VAN** (6 ˚C) and the melt of **NAP** is not detected. The DSC trace rises slightly from baseline after 150 ˚C that is present in both mixtures and is most likely due to the compounds degrading after melting. The 0.11 MF **NAP:VAN** physical mixture and the eutectic mixture both melt and degrade identically. The eutectic mixture contained less crystallinity after melting when compared to the physical mixture. However, the XRPD diffraction patterns of the eutectic mixture and the physical mixture did not show any new forms or an increase in amorphous content. **VAN** (top trace) and **NAP** (bottom trace) are present during all of the successive melts of the 0.11 MF **NAP:VAN** mixture (traces second – fourth from top, Figure 10).

The XRPD data of the 0.11 MF **NAP:VAN** physical mixture was compared to the 0.11 MF **NAP:VAN** eutectic mixture formed after melted and cooled three times and the 0.8 MF mixture melted and cooled once. These samples were also compared to the original compounds (**NAP**, **VAN** top and bottom DSC trace, Figure 10). None of the mixtures, despite melting and cooling

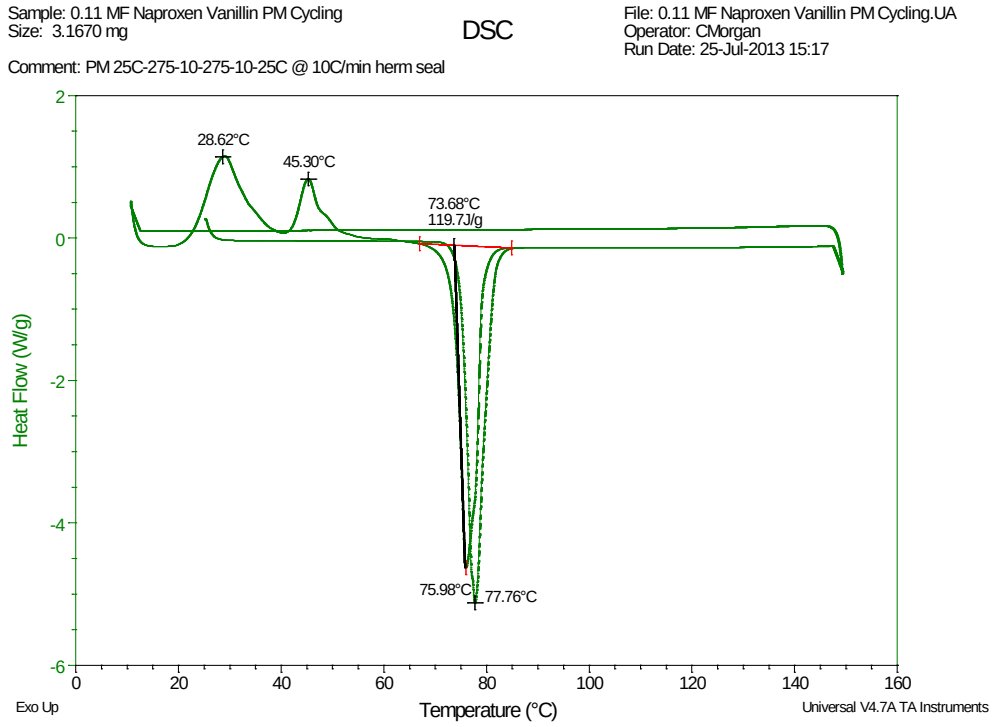

Figure 7. The 0.11 MF eutectic mixture does not degrade when heated between 10 – 150 ˚C. The mixture melts and the resulting endotherm at 76 - 78 ˚C is reproducible. The original components reform in two exothermic events at 28 and 45 ˚C.

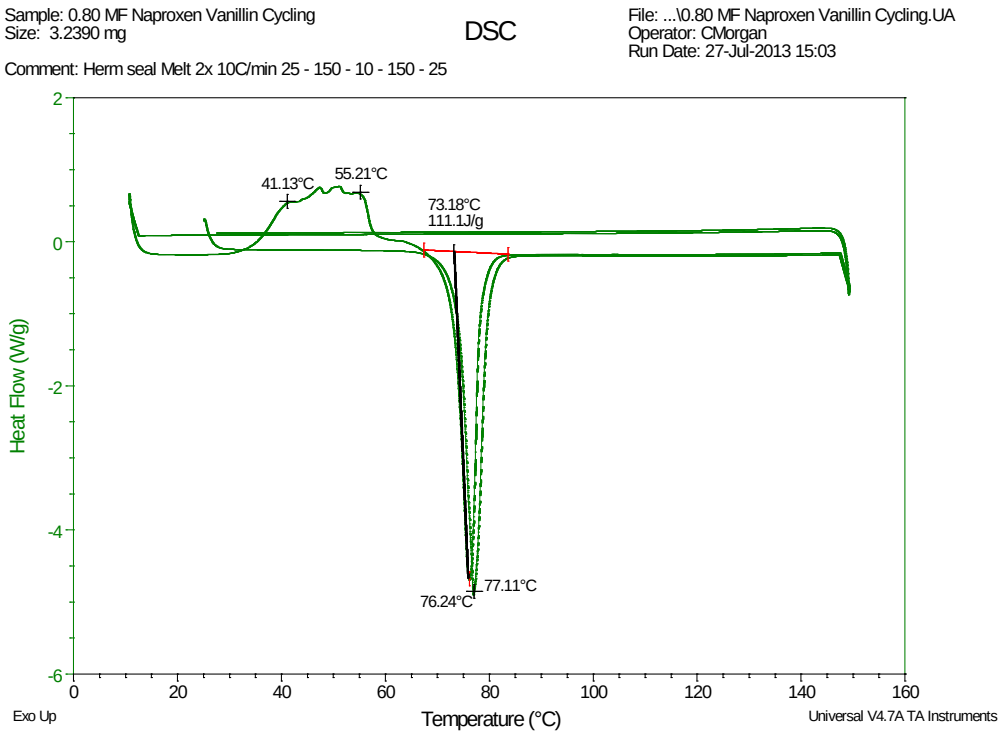

Figure 8. When the 0.8 MF **NAP:VAN** mixture is heated to 150 ˚C then cooled to 10 ˚C, the melt is reproducible and does not show degradation. After melting, the original compounds are reformed when heated from 40 – 55 ˚C.

in succession, did not produce any new forms or degradation. The 0.8 MF **NAP:VAN** mixture also contained **NAP** and **VAN**, but the peaks from the **NAP** diffractogram pattern were much more prevalent in this mixture, as would be expected in mixtures that contained increasing amounts of **NAP** and decreasing amounts of **VAN** (trace second from bottom, Figure 11). No degradation was present in this mixture as well.

The 0.8 MF **NAP:VAN** mixture, after melting and cooling, is a physical mixture that contains **NAP** and **VAN**. The 0.8 MF **NAP:VAN** mixture was also analyzed by DSC and TGA before (red, bottom DSC/TGA trace) and after melting (blue, top DSC/TGA trace, Figure 11). The 0.8 **NAP:VAN** physical mixture (red trace, bottom) and the 0.8 MF **NAP:VAN** melted mixture (blue trace, top) show similar melting behaviors which would be consistent with a reversible melting reaction. One difference between the two samples would be the melted mixture has a depressed melt around 5 ˚C below the melt of the physical mixture. Also, the resulting weight loss of the melted mixture is decreased by 5% as well. Overall, it seems that the melting behavior of the **NAP:VAN** mixtures are similar regardless of the amount of **NAP** or **VAN** present in the mixtures and before and after melting.

Solid dispersions, prepared by the fusion method, showed the same thermal behavior as the physical mixtures of the same compositions at similar temperatures. The similarities between the DSC data for the 0.11 MF **NAP:VAN** solid dispersions, even when melted multiple times, and the corresponding physical mixtures (Figure 12) are similar and indicate the absence of a well-defined chemical interaction between **NAP** and **VAN**. There is a noticeable pattern in the depression of the endotherm that is depressed from the melt of the physical mixture (Figure 12, trace second from top) and the melt of the mixture after the solid dispersion was formed by

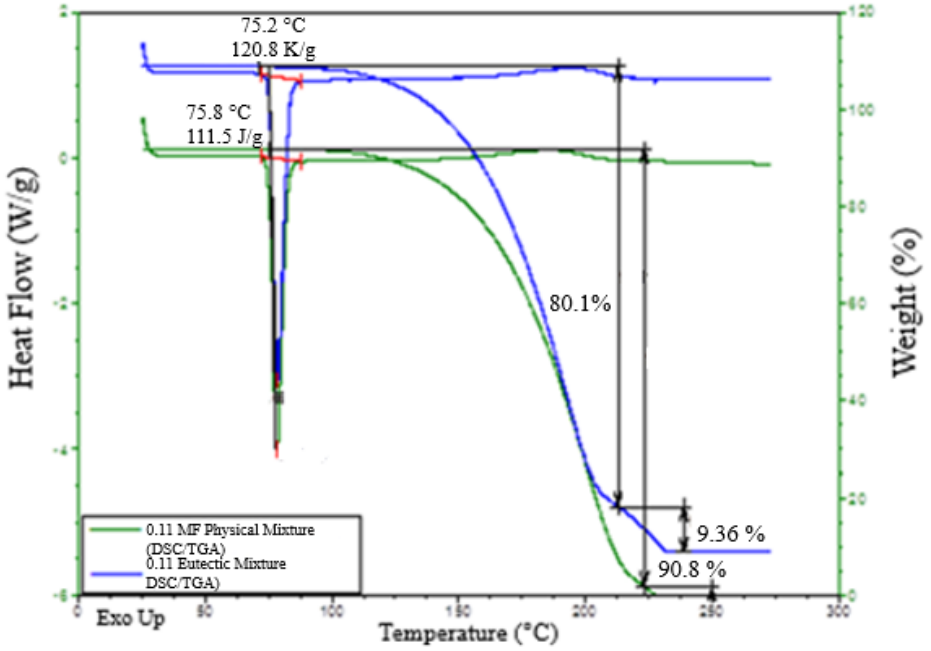

Figure 9. The DSC and TGA of the 0.11 MF physical mixture (top) and the eutectic mixture (below) are compared.

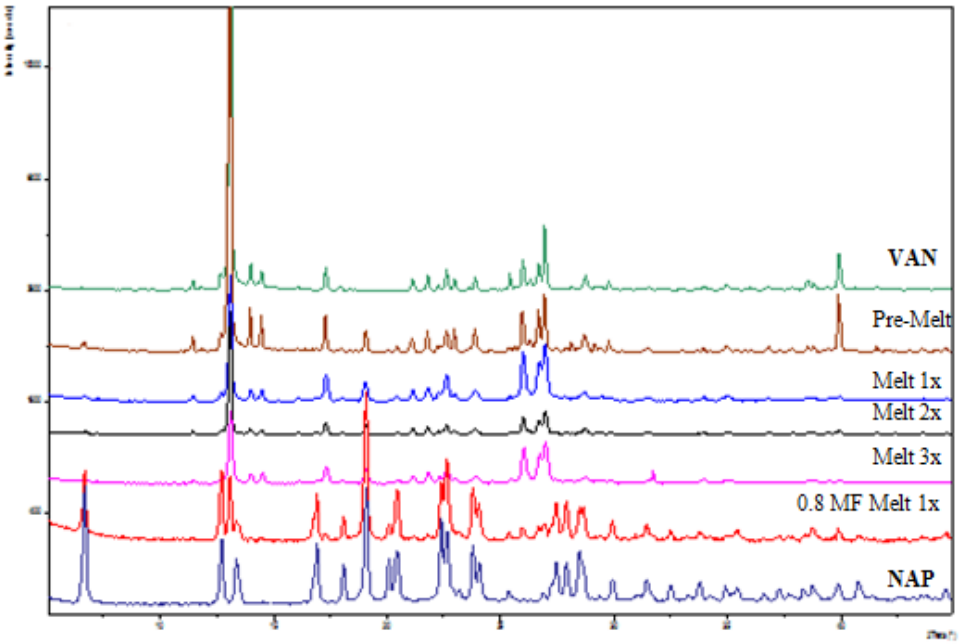

Figure 10. XRPD overlay of 0.11 MF physical mixture (Pre-Melt) compared to the mixture melted once (Melt 1x), twice (Melt 2x), three times (Melt 3x), and the original compounds **VAN (**top trace) and **NAP** (bottom trace). The 0.8 MF mixture also (second from bottom), after melted once and cooled, does not have any form changes.

heating and cooling in three cycles (Melt 3x, DSC trace second from bottom.) The resulting melting endotherm of the physical mixture has an onset eutectic melt at 75.8 ˚C (second trace from top, Figure 12). The onset melt of the 0.11 MF **NAP:VAN** solid dispersion, that was melted and cooled three times, is 72.9 ˚C (second to bottom trace, Figure 12). The significance of the change in temperature of almost 3 ˚C may be that the eutectic mixture is the solubility of **NAP** in **VAN** is thermodynamically favored, but such a small difference melt depression temperature would likely have no effect on solubility or dissolution rate.

The solid dispersion of the 0.11 MF **NAP:VAN** eutectic mixture was analyzed by **PLM** HPLC-UV (Figures 13 and 14). The **PLM** shows crystallinity resulting from the formation of a solid dispersion at 68 ˚C. This temperature was determined visually (sample was completely melted) and the temperature was indicated by the digital thermometer on the IKA heated stirrer. This mixture melts at 7 °C below the measured 75.2 ˚C eutectic temperature by DSC analysis of the physical mixture (Figure 5). **PLM** shows the three phases of the solid dispersion at 68 ˚C (Figure 13): the liquid phase (circle at bottom), the mixed phase (bottom right corner), and the solid phase (white mass middle and top). After 24 hours, the solid dispersion is completely cooled and is a hardened to a crystalline solid dispersion (Figure 14). The white mass consists of **VAN** crystals and the blue particles is **NAP**. **NAP** may be inserted into the crystal lattice of **VAN** interstitially or by substitution.

HPLC-UV analysis was utilized to detect changes in the chemical composition of the 0.11 MF eutectic mixture and the 0.8 MF mixture. The mixtures were prepared as solid dispersions by melting and cooling. A weighed portion of the 0.8 MF mixture solid dispersion (melted and cooled in once cycle) was analyzed in triplicate and no degradation was detected. The solubility of **NAP** analyzed by HPLC-UV in the experiment was also less than expected in the mixture (Table 3).

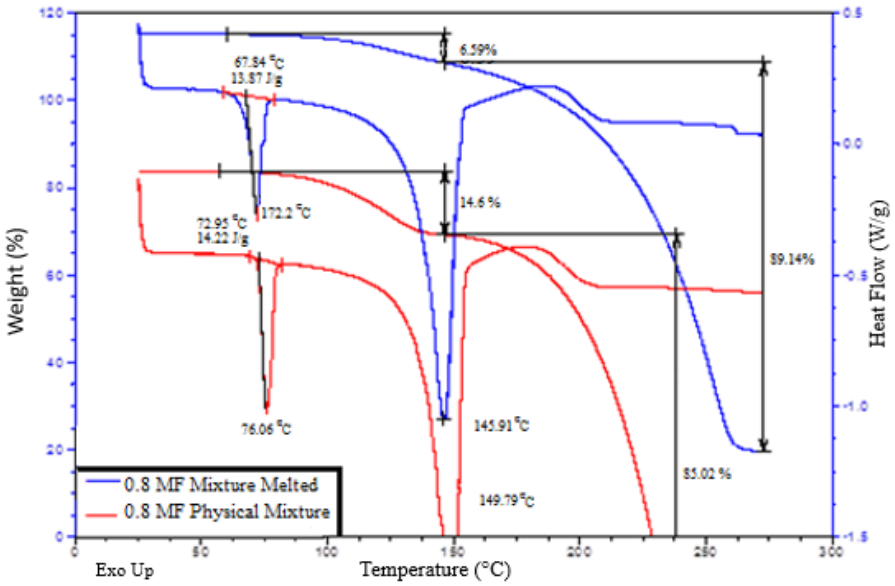

Figure 11. The 0.8 MF mixture was analyzed was by DSC and TGA before and after melting. The DSC and TGA show similar melting behavior and weight loss and no degradation occurring.

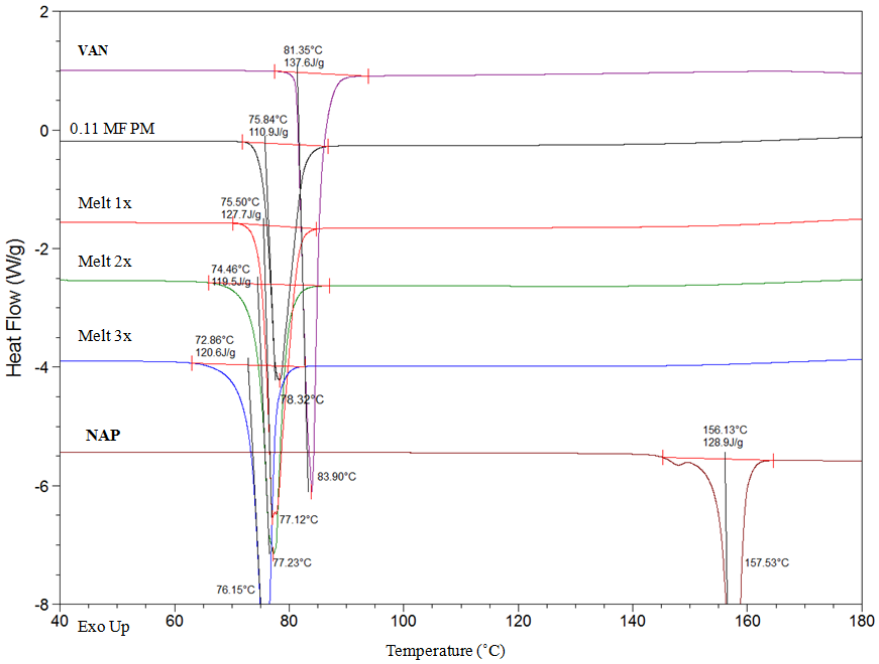

Figure 12. The 0.11 MF **NAP:VAN** physical mixture (second trace from top) was analyzed by DSC and compared after melting once (third trace from top), melting twice (third from bottom), melting three times (blue, second from bottom), and the original compounds (**VAN** at top, **NAP** at bottom.) The onset melts of the mixtures are depressed slightly after each melting cycle and no degradation is detected.

This discrepancy may be due to the majority of **NAP** was not dispersed homogeneously in the portion of the 0.8 MF solid dispersion dissolved for analysis. Insufficient mixing may also be an issue because the viscosity of **VAN** is greater than **NAP** even at small percentages present in the mixtures. The 0.11 MF mixture was also analyzed by HPLC-UV analysis (Figure 17), and four samples were compared: the physical mixture (**P1**), the solid dispersion prepared by one melting/cooling cycle (**E1**), the solid dispersion prepared by two cycles (**E2**), and then a final sample prepared in three cycles (**E3**). The retention times of the peaks of the standards of **NAP** (**N**) and **VAN** (**V**) were compared to the samples to detect changes in retention times of the, the areas under the curve (**AUC**), and if new degradant peaks were present (Figure 17). The peaks of the standards matched all of the sample peaks in the mixture and did not show evidence of degradation. Also, the peaks of the samples do not show a shift in retention times and there was no presence of new degradant peaks. These findings were also consistent in the 0.8 MF mixture that was prepared in one heating/cooling cycle. The full recovery of **NAP** in the 0.8 MF **NAP:VAN** mixture signifies that all of the **NAP:VAN** melts in the phase diagram are reversible and not limited to the 0.11 MF **NAP:VAN** eutectic mixture.

Solubility experiment of NAP and 0.11 MF mixture in DI Water and PBS

The solubility of **NAP** was compared to the solid dispersions of the 0.11 MF **NAP:VAN** eutectic mixture in DI Water and PBS at room temperature and 37 ˚C conditions. The GSE, as mentioned previously, estimated the aqueous molar solubility of the compound at room temperature. Therefore, the solubility of **NAP** at room temperature and at 37 ˚C was measured. The solubility in PBS was determined because PBS is often used for formulations that may be dosed intravenously. The condition of 37 ˚C was also chosen for DI Water and PBS, because of the association between intrinsic dissolution testing and correlated human *in vivo* testing. Therefore,

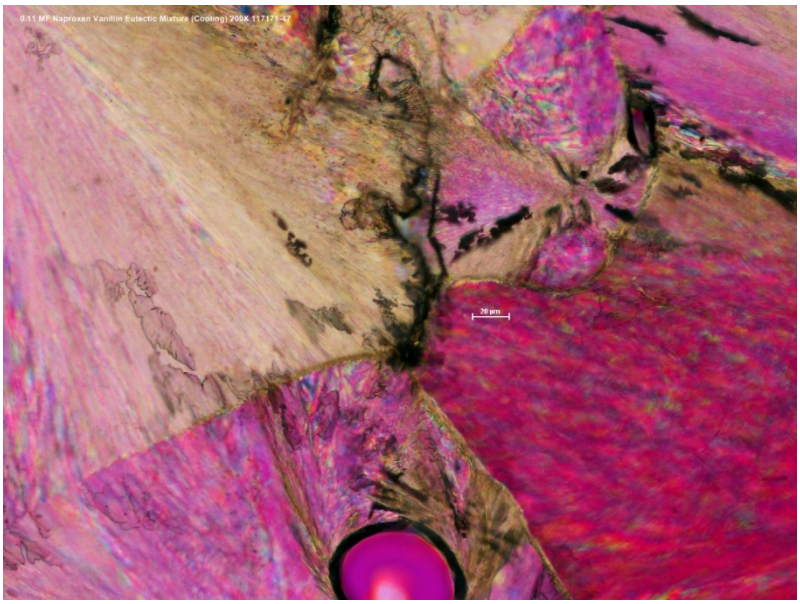

Figure 13. The 0.11 MF **NAP:VAN** mixture was analyzed by microscopy immediately after melting into a clear solid solution. The photomicrograph contains white **VAN** crystals and **NAP** blue crystals that form a crystalline solid dispersion. There is also some liquid present (circle at bottom) and a mixed phase of solid and liquid (bottom right hand corner). The middle white line is 20 μm for scale.

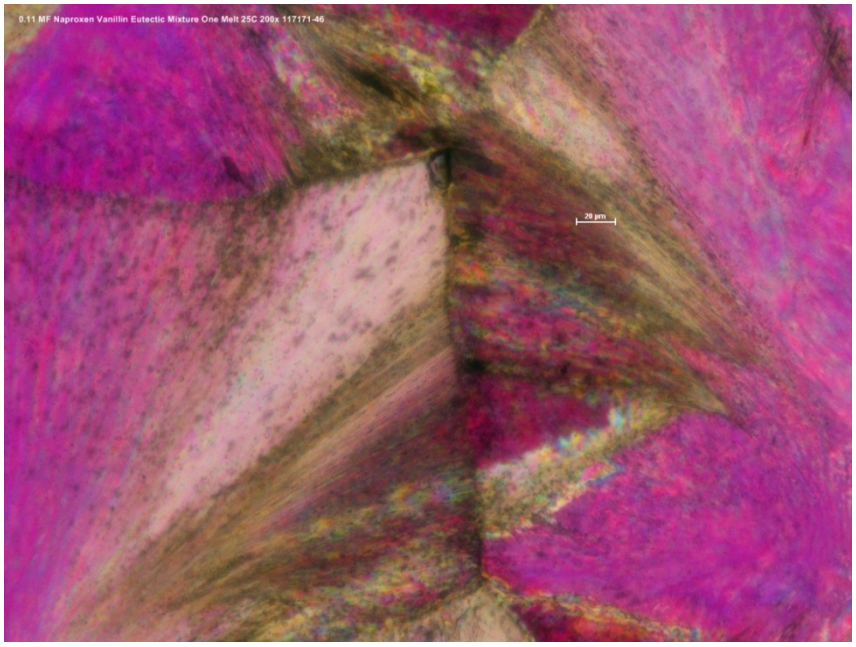

Figure 14. The 0.11 MF **NAP:VAN** mixture was analyzed 24 hours after sampled at the 68 ˚C eutectic temperature. The sample is completely cooled is a crystalline solid dispersion of **NAP** and **VAN**. The middle white line in the figure is 20 μm for scale.

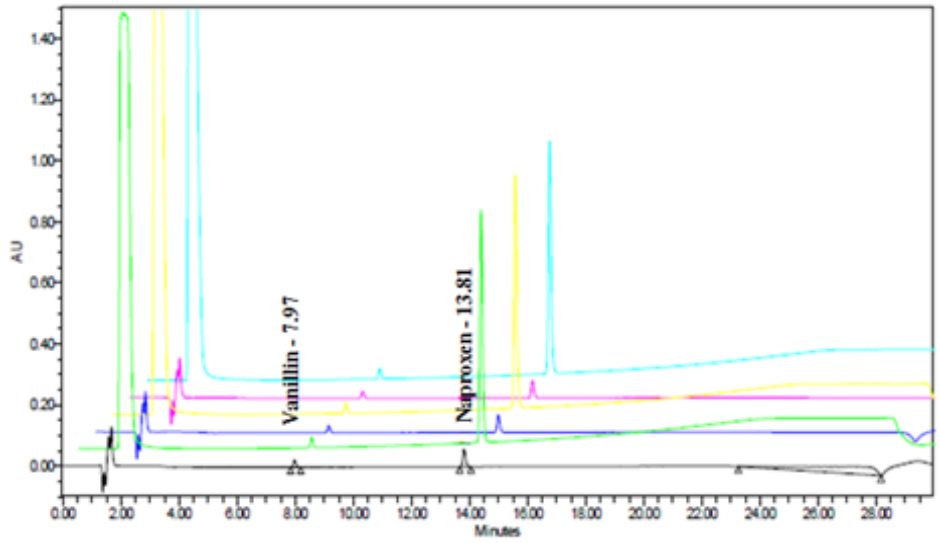

Sample Name	Inj Vol (µl)	Peak Name	RT (min)	Area (µV*sec)	Dilution	Conc (mg/mL)	Target Con (mg/mL)	% Target Conc
80 **NAP:VAN** Melt 1x A	5	**VAN**	7.976	210754	1	0.0069	0.009	76.66
80 **NAP:VAN** Melt 1x A	5	**NAP**	13.811	378500	1	0.0548	0.0559	98.03
80 **NAP:VA**N Melt 1x B	5	**VAN**	7.974	210059	1	0.0068	0.009	75.55
80 **NAP:VAN** Melt 1x B	5	**NAP**	13.813	382558	1	0.0554	0.0559	99.1
80 **NAP:VAN** Melt 1x C	5	**VAN**	7.97	379034	1	0.0068	0.009	75.55
80 **NAP:VAN** Melt 1x C	5	**NAP**	13.814	207449	1	0.0549	0.0559	98.21
VAN Conc Average						0.0068		
Standard Deviation						5.77E-05		
NAP Conc Average						0.0550		
Standard Deviation						0.0003		

Figure 15 and Table 3. The 0.8 MF **NAP:VAN** mixture (melted and cooled in one cycle) was solubilized in DMSO and analyzed in triplicate (Samples A, B, and C in Table 3) by HPLC-UV. The concentration of **NAP** and **VAN** in a small portion (1.3 mg) of the solid dispersion). No degradation was detected.

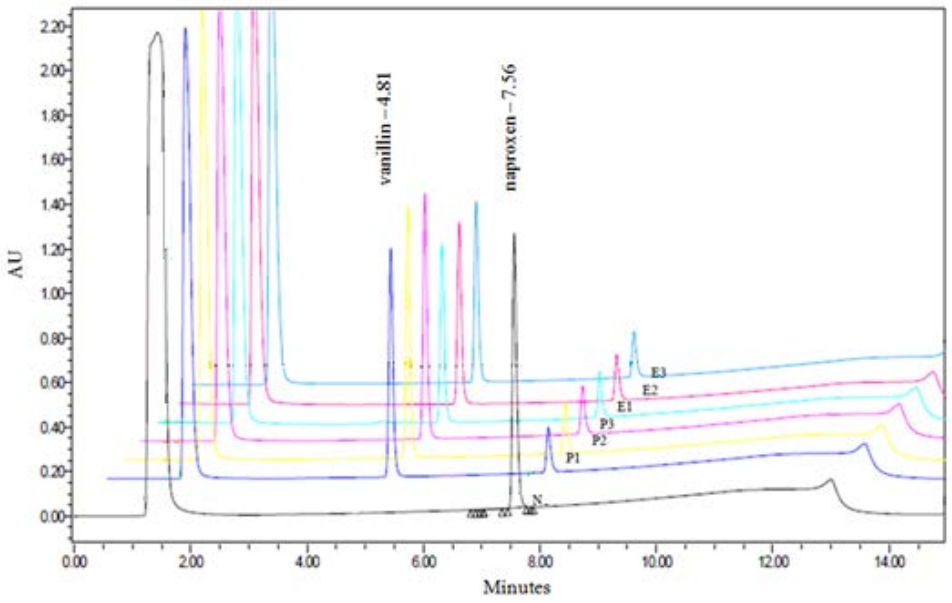

Figure 16. The HPLC-UV analysis of the 0.11 MF eutectic mixtures analyzed in triplicate (E1 – 3) contain **NAP** (ret time 7.56 min) and **VAN** (ret time 4.81 min). The **NAP** standard peaks are at 7.56 retention time (N, bottom). The 0.11 MF physical mixture (pre-melt) contain peaks that match the retention times of **VAN** and **NAP** (P1 – 3). The eutectic mixture does not contain any peaks that do not match **VAN** or **NAP** (E1 -3) and does not contain any degradation after melting.

PBS may be chosen for further dissolution testing, if necessary. The measured **NAP** solubility in DI Water at room temperature was 0.05 mg/mL at pH 4.4 (Table 4). The solubility of **NAP** increases slightly to 0.07 mg/mL when slurried at 37 ˚C in DI Water, but the pH remained at 4.4. The measured **NAP** solubility in PBS at room temperature was measured at 0.9 mg/mL at pH 6.0, but increased slightly to 1.3 mg/mL at pH 5.88 when heated to 37 ˚C. The solubility of **NAP** increased slightly with increased temperatures above ambient conditions. The solubility of **NAP** was higher in buffered conditions near pH 6, as would be expected of a compound with a pKa of 4.2. Higher aqueous solubility is usually correlated with values above the pKa when more of the compound is ionized. The XRPD analysis of the filtrate of **NAP** for all conditions and concentrations confirm that **NAP** did not change form during the experiment. Therefore, when the eutectic mixture of **NAP** and **VAN** was tested for solubility, the benchmarks for **NAP** has been established.

The 0.11 MF eutectic mixture was prepared at two **NAP** concentrations at 0.5 mg/mL and 2.3 mg/mL to ensure that the slurries were saturated by **NAP** in DI Water and PBS, respectively. The eutectic mixtures in both conditions did not have higher solubility than **NAP** alone. The solubility of **NAP** was slightly lower in the eutectic mixture in DI Water in both conditions and in PBS at 37 ˚C. The solubility of **NAP** and the eutectic mixture was highest in PBS at 37 ˚C. However, the solubility of **NA**P at 37 ˚C was slightly higher (1.3 mg/mL) than the eutectic mixture (1.14 mg/mL) in the same conditions.

The particle size of **NAP** was recorded, by **PLM,** after 48 hours of slurry in both media, and was measured between 1 – 5 μm. This particle size was compared to the slurries of the eutectic mixture in both conditions and between the solid dispersion and the native drug. However, the solubility of **NAP** and the eutectic mixture was measured to be highest in PBS at 37 ºC than DI

Naproxen Solubility	Average Conc Naproxen (mg/mL)	St Dev	% Recovery (Avg)	Max Conc (mg/mL)	pH final
DI Water at RT	0.05	4.16E-04	6.84	0.5	4.47
DI Water at 37 ˚C	0.068	4.36E-04	14.98	1	4.78
PBS at RT	0.93	2.36E-02	57.89	2	5.88
PBS at 37 ˚C	1.3	7.67E-02	64.21	2	6.2

Table 4. **NAP** solubility was measured in DI Water and PBS at room temperature and at 37 ˚C. The solubility of **NAP** increased with higher temperatures and at pH values (column far right) above the pKa at 4.2. This is reflected in the % recovery (third column from right) that lists the % of NAP dissolved in the media at the conditions listed.

0.11 MF Eutectic Mixture of **NAP VAN**	Ave Conc **NAP** (mg/mL)	St Dev	% Recovery (Avg)	**NAP** (Solubility mg)	Average Conc **VAN** (mg/mL)	St Dev (±)	% Recovery (Avg)	**VAN** Solubility (mg)	Solubility MF (Recovered)	pH final
DI Water (RT)	0.035	0.001	6.30	0.525	2.550	0.018	88.25	38.250	0.090	4.37
DI Water (37 ˚C)	0.061	0.004	11.00	0.060	2.648	0.134	84.98	39.750	0.100	4.22
PBS (RT)	0.94	0.01	41.59	14.1	8.815	0.093	73.460	132.225	0.066	5.8
PBS (37 ˚C)	1.135	0.041	49.36	17.025	10.797	0.095	89.98	161.95	0.065	5.51

Table 5. Solubility of the 0.11 MF **NAP:VAN** eutectic mixture in DI water and PBS at 37 ˚C and at ambient temperatures was determined by HPLC-UV analysis. The solubility of **NAP** in the eutectic mixture was similar as **NAP** in that increasing temperature and higher pH produced higher solubility. The **NAP** and **VAN** solubility could be calculated to determine the mole fraction that was solubilized in the media. The PBS mixture, although higher in overall solubility of **NAP** and **VAN**, had less amounts of **NAP** and **VAN** (~ 0.065 MF **NAP** in sample) dissolve in solution than the original 0.11 MF **NAP:VAN** mixture.

Water, most likely due to the higher pH (~ pH 6) and temperature. However, the 0.11 MF **NAP:VAN** mixture did not show an increase in solubility over **NAP** alone. This may be due to some of the crystalline **VAN** did not release the drug into the aqueous slurry due to the solubility of **VAN** was also exceeded. If the **VAN** crystal lattice does not dissolve, then the drug will remain in the solid and never be released.

Conclusions

The purpose of investigating a eutectic mixture in **NAP** and **VAN** is due to the significance of the role of solubility to the melting point and the partition coefficient as described by the General Solubility Equation (GSE) (Equation 1):

$$\text{Log } S_w = -0.01 \text{ (mp } -25) - \log K_{ow} + 0.5 \qquad \textbf{Equation 1}.$$

The GSE can be utilized to predict the log of the aqueous molar solubility (log S_w), which is the amount of moles dissolved in 1 L of DI Water, of a non-electrolyte organic compound by the melting temperature (mp ˚C) and the partition coefficient (K_{ow}). It is apparent by the relationships in Equation 1, that the melting point does not have as much of an impact on the molar solubility as the partition coefficient. However, the melting temperature of **NAP** can be depressed by **VAN**, as shown in the phase diagram (Figure 5). The eutectic mixture was successfully found at 0.11 MF (11% **NAP**/ 89% **VAN**) and visually observed to melt at 68 ˚C. Therefore, by utilizing the GSE with the eutectic melt, the new calculated aqueous solubility is expected to be near 0.30 mg/mL, which is a 6x higher from the original experimental aqueous solubility of 0.05 mg/mL (Table 6). When the eutectic mixture was tested at ambient and at 37 ˚C, the resulting solubility did not show such an increase in solubility. This discrepancy might be due to the nature of the

	MW (g/mol)	(mp ˚C)	log K_{ow}	Calculated Log Sw	Calculated Aqueous Solubility (mg/mL)	melt depression (˚C)	New Calculated Log Sw	New Calculated Aqueous Solubility (mg/mL)	Change in Solubility
Naproxen	230.3	154	2.88	-3.67	0.05	-79	-2.99	0.30	4.9x

Table 6. The GSE for **NAP** with eutectic melt of the 0.11 MF mixture at 75˚C. The new calculated aqueous solubility of **NAP** is 4.9x higher than the original solubility of **NAP.**

crystal dispersion, which may decrease the dissolution rate by retaining the drug in the crystal lattice for a longer interval than the drug alone.

The solid dispersions of **NAP** and **VAN** were found not to be effective in improving **NAP** solubility in DI Water and **PBS** due partly because, unlike solid dispersions of **NAP** prepared using polyvinyl pyrrolidone (PVP) and cyclodextrins, dispersed systems prepared using **VAN** did not appear to contain any amorphous drug [6]. An amorphous drug is usually advantageous in dissolution by increasing the dissolution rate when compared to the crystalline form [2, 4, 5, 9]. However, a possible disadvantage of the amorphous form is a loss of stability over me. Therefore, although the **NAP**:**VAN** mixtures do not have higher solubility than **NAP** alone, the solid dispersion may increase the stability of the drug over time.

References

1. Sekiguchi, K.; Obi, N. Studies on Absorption of Eutectic Mixture. I. A Comparison of the Behavior of Euectic Mixture of sulfathiazole and that of Ordinary sulfathiazole in Man. *Chem. Pharm. Bul*. **1961**, *9*, pp 866-872.
2. Vippagunta, S.; Wayne, Z.; Hornung, S.; Krill, S. Factors Affecting the Formation of Eutectic Solid Dispersions and their Dissolution Behavior. *J. of Pharm. Sci.* **2007**, *96*(2), pp 294-304.
3. Chiou, W. L.; Riegelman, S. Pharmaceutical Applications of Solid Dispersion Systems. *J. Pharm. Sci.* **1971**, *60*, pp 1281-1302.
4. Jansenns, S.; Van den Mooter, G. Review: Physical Chemistry of Solid Dispersions. *J. Pharm. Pharmacol*. **2009**, *16*, pp 1571-1586.
5. Vasnthavada, M.; Tong, W.; Serajuddin, A. Chapter 18 Development of Solid Dispersion for Poorly Water-Soluble Drugs. In *Water-Insoluble Drug Formulation*. 2nd ed; Liu, R., Ed.; CRC Press: Boca Raton, Fl, 2008; pp 499-529.
6. Mura, P.; Faucci M. T.; Manerioli, A.; Bramanti, G.; Parrini, P. Thermal Behavior and Dissolution Properties of naproxen from Binary and Ternary solid dispersions." *Drug Dev. Ind. Pharm.* **1999**, *25*(3), pp 257-764.
7. Jain, N.; Yalkowsky, S. Prediction of Aqueous Solubility of Organic Compounds by the General Solubility Equation (GSE). *H. Chem. Inf. Comp. Sci.* **2001**, *41*, pp 1208-17.

8. Amidon, G.; Lennernas, H.; Shah, V.; Crimson, J. A Theoretical Basis for Biopharmaceutic Drug Classification: the Correlation of *in-vitro* Drug Product Dissolution and *in-vivo* Bioavailability. *Pharm. Res.* **1995,** *12*, pp 43-420
9. Tong, W-Q., Wen, H. Chapter 4 Preformulation Aspects of Insoluble Compounds. in *Water Insoluble Drug Formulation*. 2nd ed; Liu, R., Ed.; CRC Press: Boca Raton, Fl, 2008, pgs 61- 80.
10. Naproxen, MSDS, Sigma-Aldrich Company.
11. Vélaz, I.; Sánchez, M.; Martín, C.; Martínez-Ohárriz, M. C. Effect of PEG 4000 on the Dissolution Rate of naproxen. *Eur. J. Drug Metab. Pharmacokinetics* **1998**, *23*(2), pp 103-108.
12. Moreno, M.; Garidel, P.; Suwalsky, M.; Howe, J.; Blaudenburg, K. The Membrane-Activity of ibuprofen, diclofenac, and naproxen: A Physico-Chemical Study with Lecithin Phospholipids. *Biochim Biophys Acta* **2009** June; *1788*(6), pp 1296-1303.
13. McGettigan P.; Henry, D. Current Problems with Non-Specific COX Inhibitors. *Curr. Pharm. Des.* **2000**, *6*(17), pp 1693-724.
14. Naproxen, pKa and LogP, ACD Labs Software Suite 12.
15. Yalkowsky, S. *Solubility and Solubilization in Aqueous Media*. American Chemical Society: Washington D.C., pp 1-55.
16. Singh, N. B.; Das, S. S.; Gupta, P.; Dwivedi, M. K. Phase Equilibria and Solidification Behaviour in the vanillin-p-anisidine system. *J. Crys Grow* **2008**, *311*, pp 1118-1122.
17. US Food and Drug Administration (FDA) database of Everything Added to Food in the United States (EAFUS). Vanillin. http://www.accessdata.fda.gov/scripts/fcn/fcnDetailNavigation.cfm?rpt=eafusListing&id=2162
18. Vanillin, MSDS, Alfa-Aesar.
19. Vanillin, pKa and LogP, ACD Labs Software Suite 12.
20. Stott, P. W.; Williams, A. C.; Barry, B. W. Transdermal Delivery from Eutectic Systems: Enhanced Permeation of a Model Drug, ibuprofen. *J. Controlled* Release **1998**, *59*: pp 297-308.
21. Sangster, J. Phase Diagrams and Thermodynamic Properties of Binary Organic Systems Based on 1-,2-, 1,3-, 1,4-diaminobenzene or benzidine. *J. Phys. Chem.* **1994**, *23*, pp 295-338.
22. Pilling J. *Phase Diagrams and Microstructure: A Computer-Aided Learning Guide*. Institute of Materials: London, UK, 1992; pp 28-85.
23. Stott P. W.; Williams, A. C.; Barry, B. W. Mechanistic Study into the Enhanced Transdermal Permeation of a Model β-blocker, propranolol, by Fatty Acids: a Melting Point Depression Effect. *Intl. J. Pharm*. **2001**, *219*, pp 161-176.
24. Rai U S.; Pandey, P. Solidification Behaviour of Binary Organic Eutectics and Monotectics; 1,2,4,5-tetrachlorobenzene-*m*-aminophenol system. *Mat. Let*. **1999**, *39*, pp 166-172.
25. Marinescu, D-C.; Pincu, E.; Meltzer ,V. Thermodynamic Study of Binary Systems propafenone hydrochloride with metoprolol tartrate: Solid-Liquid Equilibrium and Compatibility with α-lactose monohydrate and corn starch. *Intl Journ Pharm* **2013**, *448*, pp 366-372.

26. Herman, C.; Haut, B.; Aerts, L.; Leyssens, T. Solid-Liquid Phase Diagrams for the Determination of the Solid State Nature of both Polymorphs of (RS)-2-(2-oxo-pyrrolidin-1-yl)-butyramide. *Intl. J. Pharm*. **2012**, *437*, pp 156-161.
27. Khimeche, K.; Dahmani, A. Measurement and Prediction of (Solid + Liquid) Equilibria of alkanediaminide + biphenyl) Mixtures. *J. Chem. Thermodyn*. **2006**, *38*, pp 1192-1198.
28. Wei D, Jin K 2009. (Solid + liquid) equilibria of (naphthalene + isomeric dichlorobenzenes). J Chem Thermodyn. 41:145-149

Chapter 6. Conclusions and Future Considerations

Eutectic mixtures have been utilized in the world of metallurgy and industrial settings for a long while, and the possibility of being able to use eutectic mixtures with the same utility in the pharmaceutical world remains unlikely. The nature of organic compounds remain fragile and thermally sensitive when compared to the metals forged in blends of steel alloys. Innovative technology developed to unravel the mystery of eutectic mixtures press on with computer models that present theoretical phase diagrams of organic systems. However, the tactile instruments of utilizing the models, and translating the theoretical to the practical, is the final chasm that has yet to be successfully negotiated.

In this work, three different small molecules: AMG 517, glipizide, and naproxen were all mixed with a second small molecule to determine the presence of a eutectic by constructing the binary phase diagrams. The investigation into the AMG 517 mixtures were difficult for the same reason as the search for eutectic mixtures in glipizide: the thermal degradation of the API or the second compound. If the mixtures include a compound that melts and degrades before mixing between the two compounds is achieved, then it is very difficult to find the eutectic mixture successfully. In the AMG 517 mixtures, although the API was thermally stable, the co-crystal formers were not and caused degradation to interfere with the identification of the eutectic mixture. However, the glipizide was thermally unstable at temperatures below the melting point, which presented an obstacle to determining the eutectic mixture in the system too difficult to overcome.

Finally, the eutectic mixture in the naproxen vanillin binary system was successfully identified at 0.11 MF (11% naproxen/ 89% vanillin). The system formed a monotectic system where naproxen and vanillin were miscible and soluble in all compositions in the liquid phase and immiscible and insoluble in the solid phase. Some reasons the eutectic mixture was successfully

identified were the mutual solubility and miscibility of the two compounds, the thermal stability of both compounds when melted and cooled, and the ability to mix the compounds successfully by melting. The 0.11 MF mixture, however, did not show an advantage in solubility when compared to naproxen alone in DI Water and PBS. The eutectic mixture formed a crystalline solid dispersion that does not always lead to higher solubility. In some cases, the crystal lattice retains the API for a period of time that retards the release of the drug into the media. However, an advantage of a crystalline solid dispersion may be an increase in stability. This may explain the lower solubility of the eutectic mixture, where the solubility of vanillin was exceeded in both media. Therefore, if the vanillin crystal lattice does not dissolve completely, naproxen may not be released into the aqueous media.

In conclusion, the search for eutectic mixtures is a worthwhile endeavor in which the current state of pharmaceutical development includes more and more API candidates that suffer from poor physicochemical characteristics. Future work will continue to search for other candidates of eutectic mixtures, expand the organic solvents tested for the API's tested for future mixing experiments, and test the eutectic mixture of naproxen and vanillin in intrinsic dissolution studies. The search for technologies to expand the strategies to change the poor physicochemical characteristics of API candidates in development continues to evolve and, hopefully, present new opportunities that would have otherwise been unknown.

Chapter 7. Appendix

Compilation of data obtained by XRPD, DSC, TGA, particle size, polarized light microscopy (PLM), and near Infrared (NIR) analytical techniques.

Urea Benzoic Acid Mixtures (**U:BA)**
Heating/Cooling DSC Experiments
0.2 MF **U:BA** heated and cooled three times.

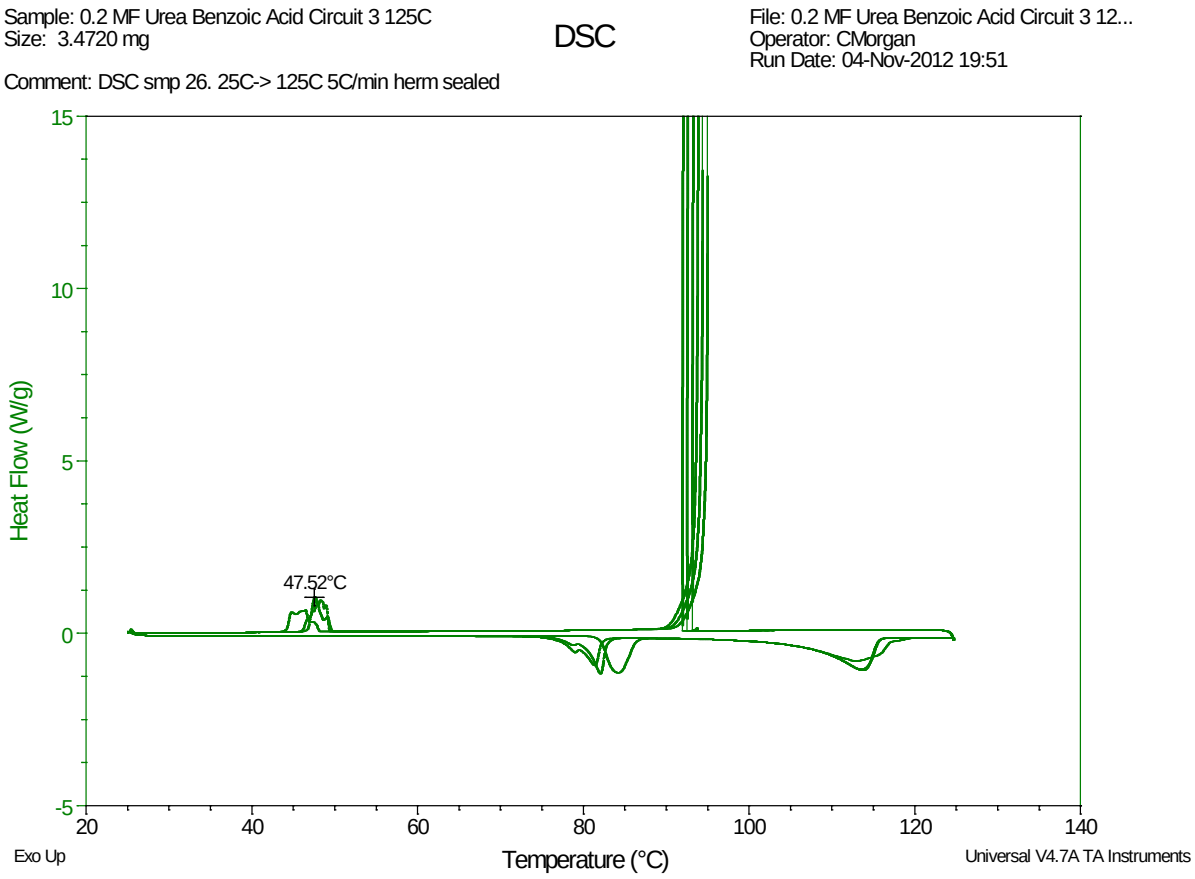

0.6 MF U:BA Mixture
Analyzed in DSC heating/cooling experiment cycled twice. Run once.

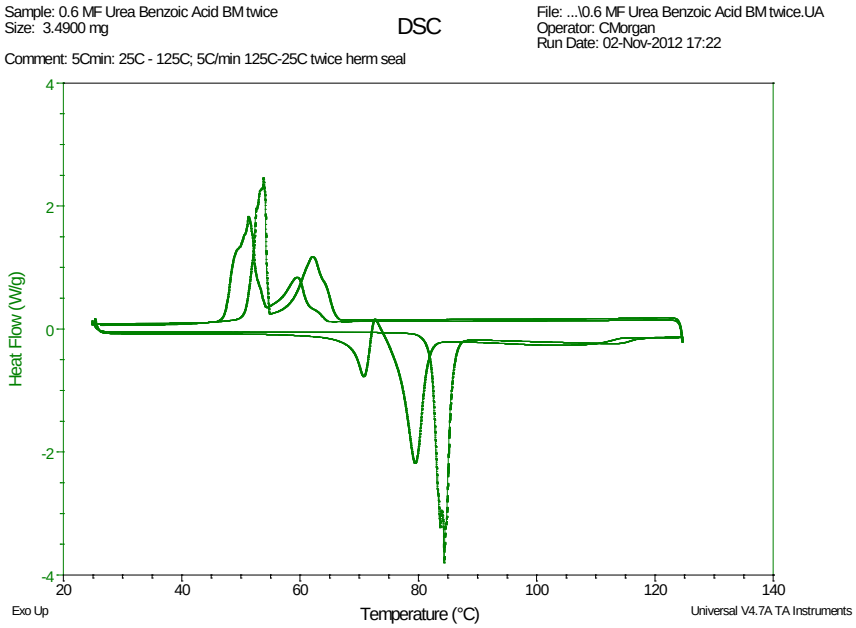

0.8 MF U:BA Mixture
Analyzed in DSC heating/cooling experiment cycled three times. Run once.

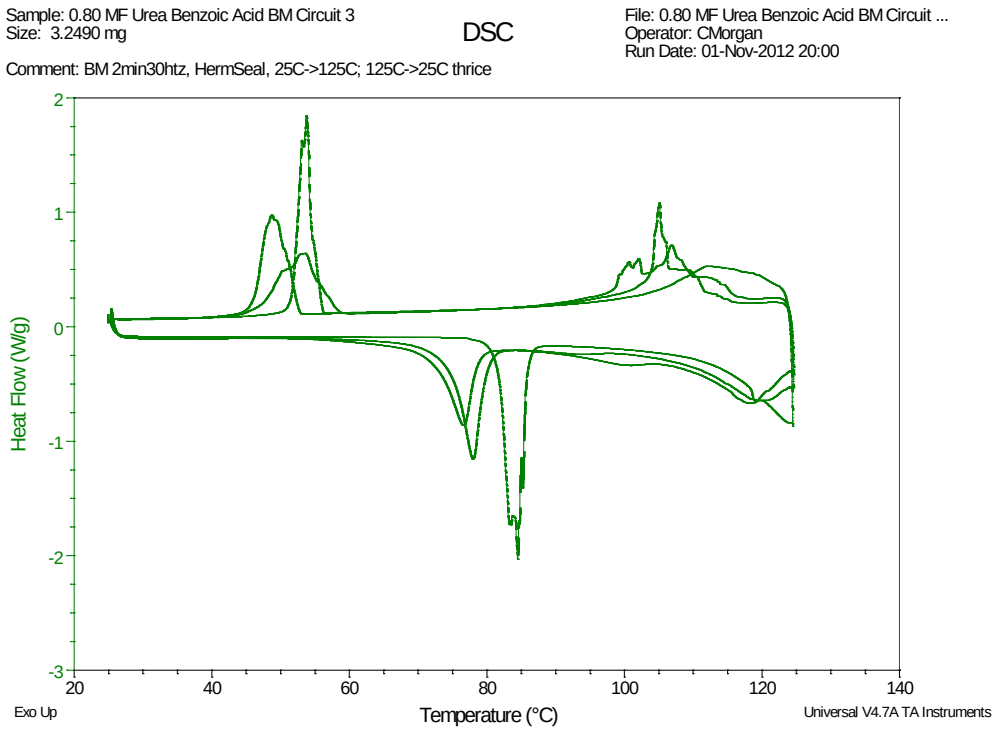

AMG 517 Anhydrous (AMG 517) in Solvent Screen

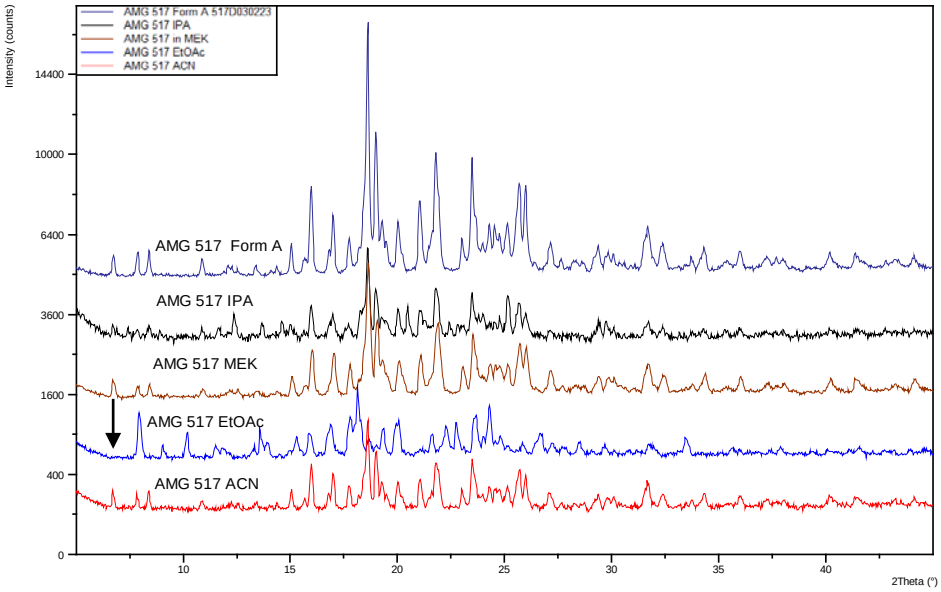

Some interaction of **AMG 517** and organic solvents. MEK chosen because no interaction seen with **AMG 517**.

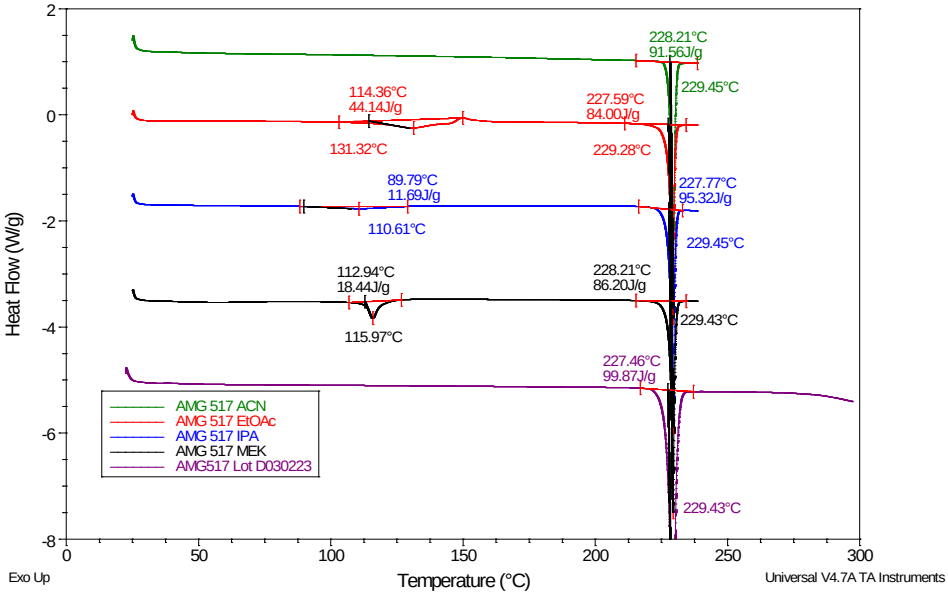

Onset melt of **AMG 517** in various organic solvents does not change significantly.

AMG 517:SA System

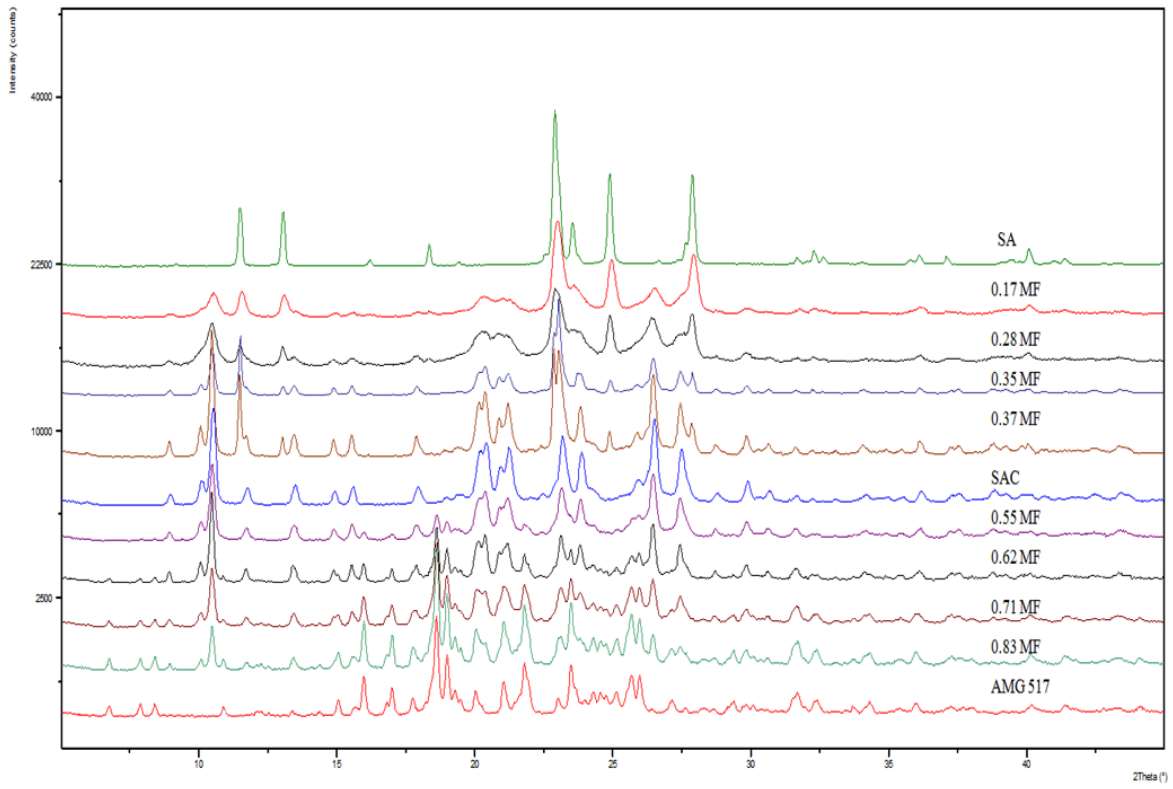

XRPD diffractogram this an overlay of the powder patterns of **AMG 517 /SA** (**SAC** in the figure) and added amounts of **SA** and **AMG 517.** The starting material is the middle trace (**SAC**) and added amounts of **SA** is the upper half of the diffractogram while added amounts of **AMG 517** was used to prepare the bottom half of the figure. No unknown forms was detected.

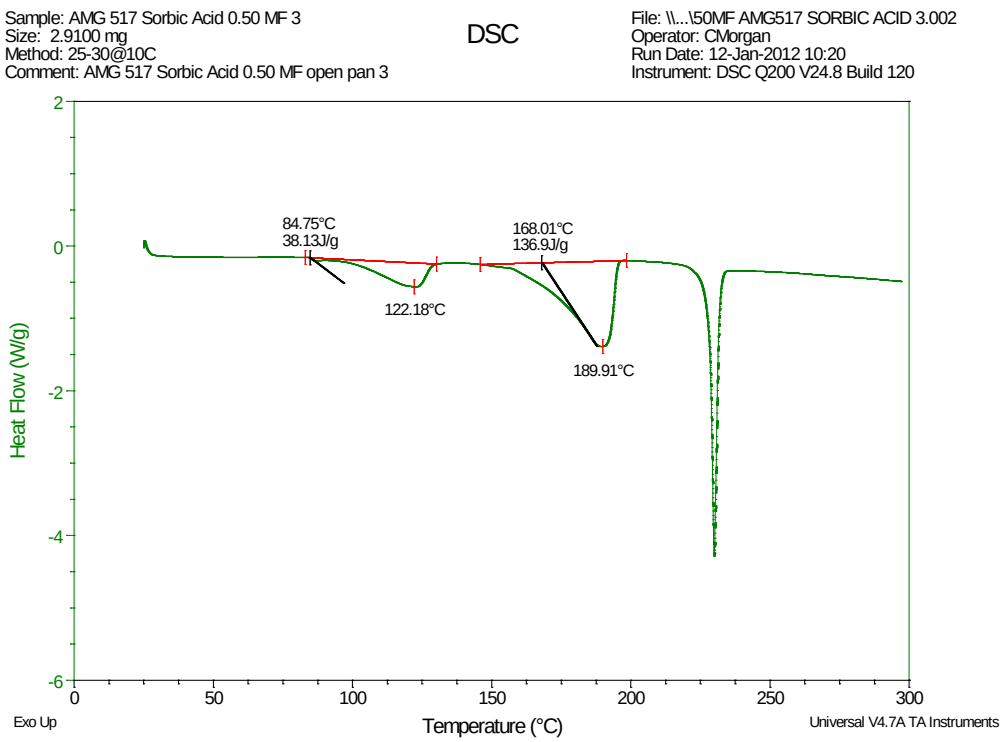

0.5 MF **AMG 517 SA** BM mixture did not form a co-crystal, which would be characterized by one endotherm with an onset melt of 159 °C and the AMG 517 endotherm at 222 – 228 °C.

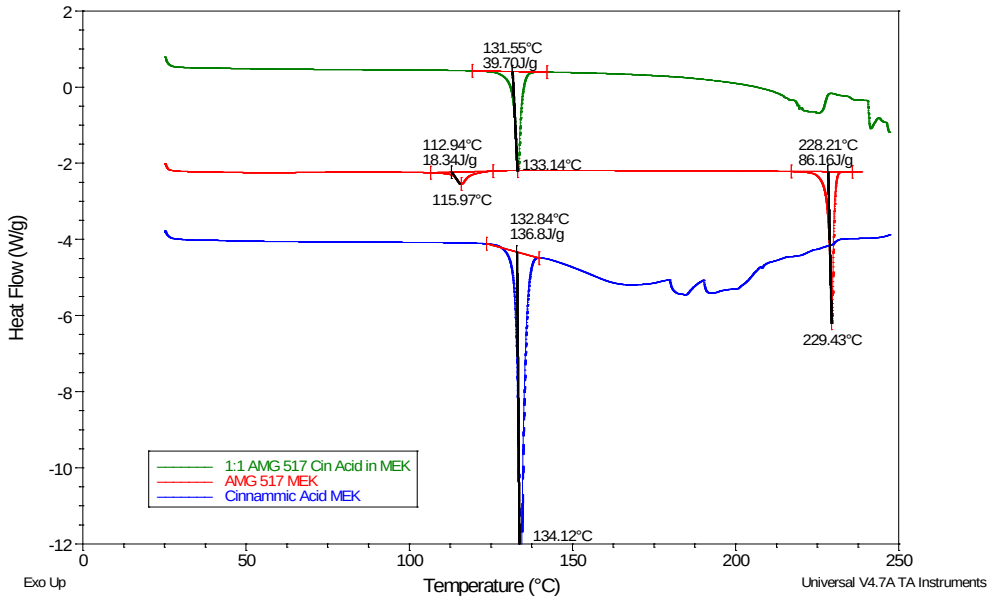

AMG 517 and **CA** did not form a co-crystal was slurried in MEK.

0.5 MF AMG 517:XYL in dioxane and water

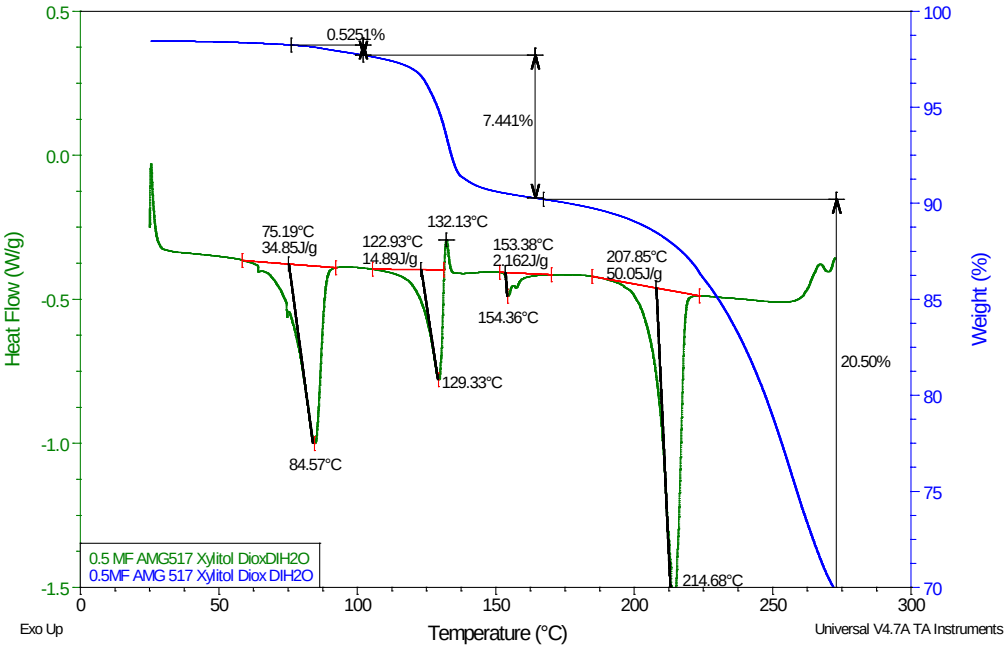

0.8 MF **AMG 517 XYL** in dioxane and water

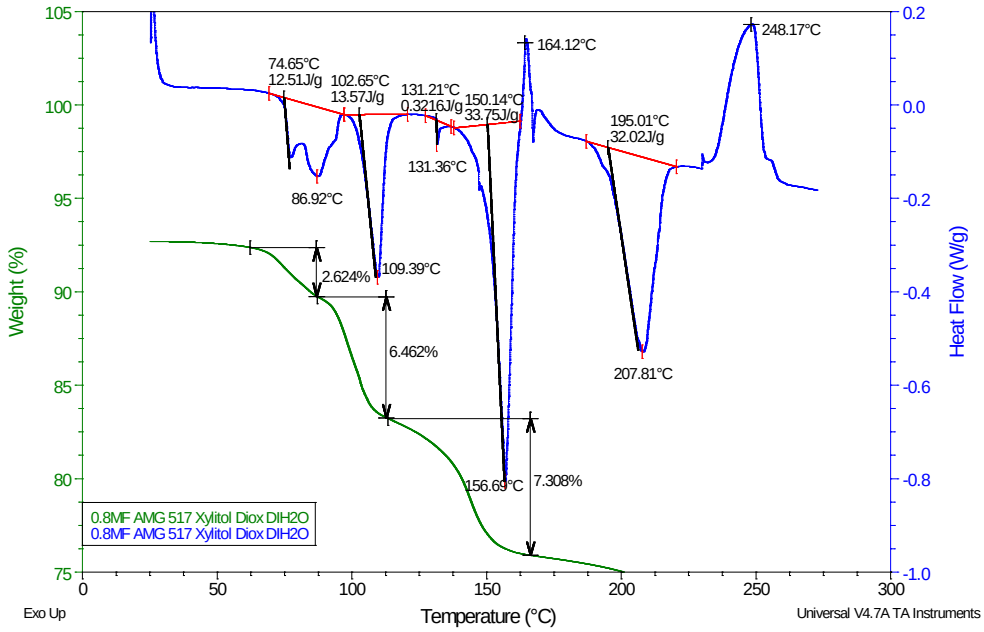

Naproxen and Vanillin Mixtures

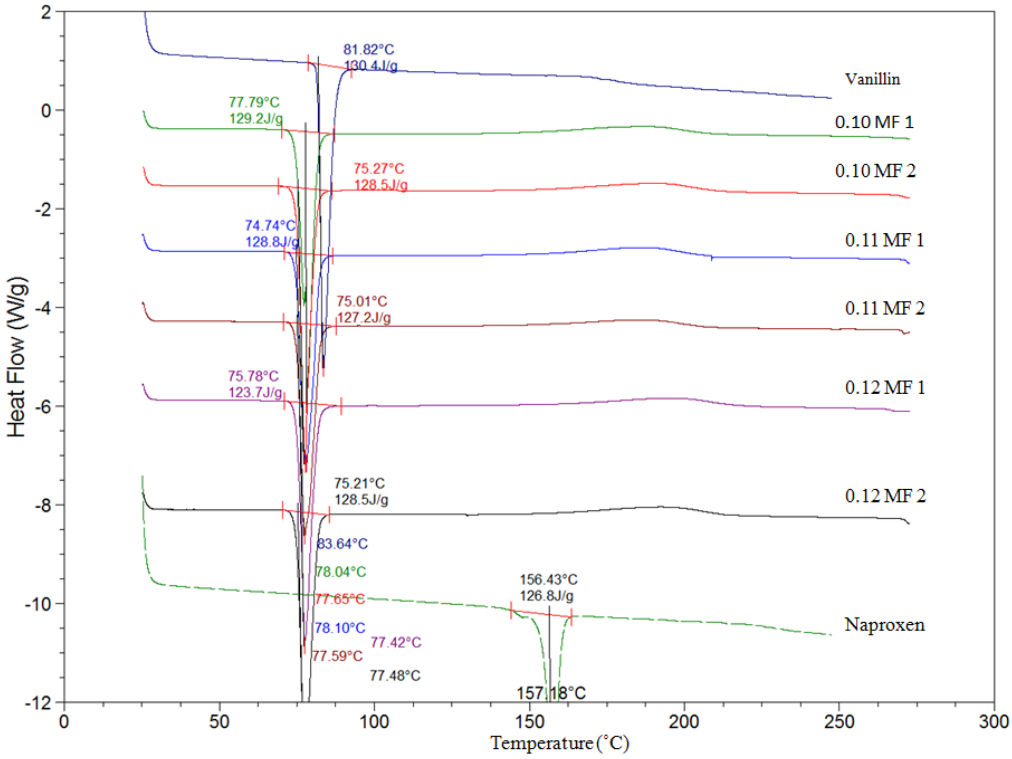

The mixtures between 0.10 – 0.12 MF **NAP:VAN** were analyzed in duplicate to further refine the eutectic mixtureswere The melt of the 0.11 MF mixture included the lowest melt (74.8 ˚ avg) of the other mixtures. All of the melts between 0.10 – 0.15 MF were very similar (± 0.5 ˚ C) and a slight rise at 150 ˚C in the baseline is most likely indicative of **NAP** melting and degrading.

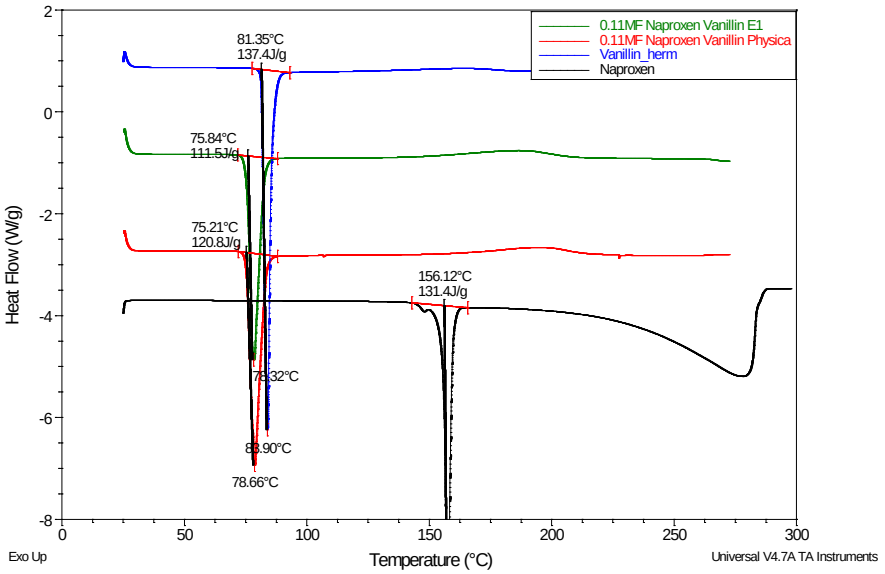

The melts, as obtained by DSC analysis, of **VAN** (top), the eutectic mixture (second from top), the 0.11 MF physical mixture (second from bottom), and **NAP** is compared.

0.5 MF NAP:VAN DSC/TGA Overlay

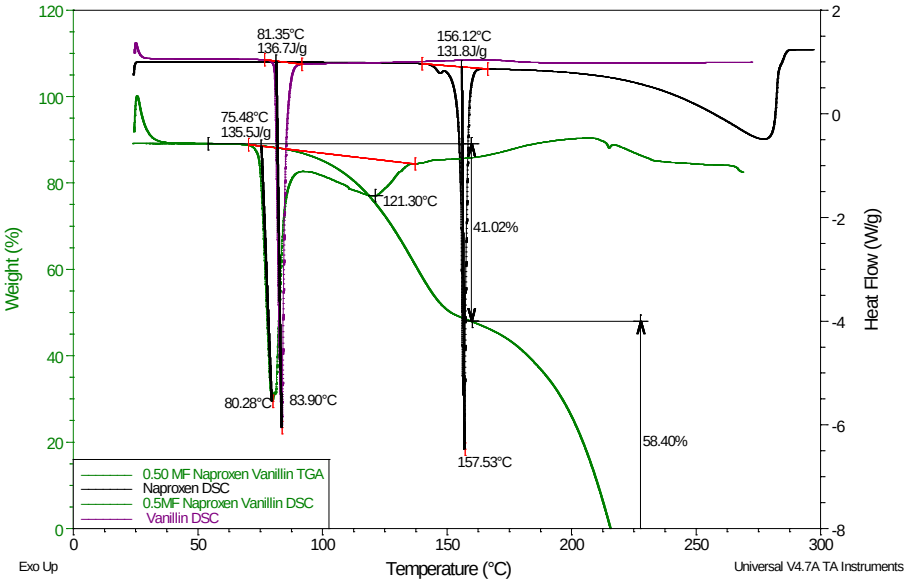

DSC/TGA overlay of 0.5 MF **NAP VAN** mixture.

0.6 MF NAP:VAN DSC/TGA Overlay

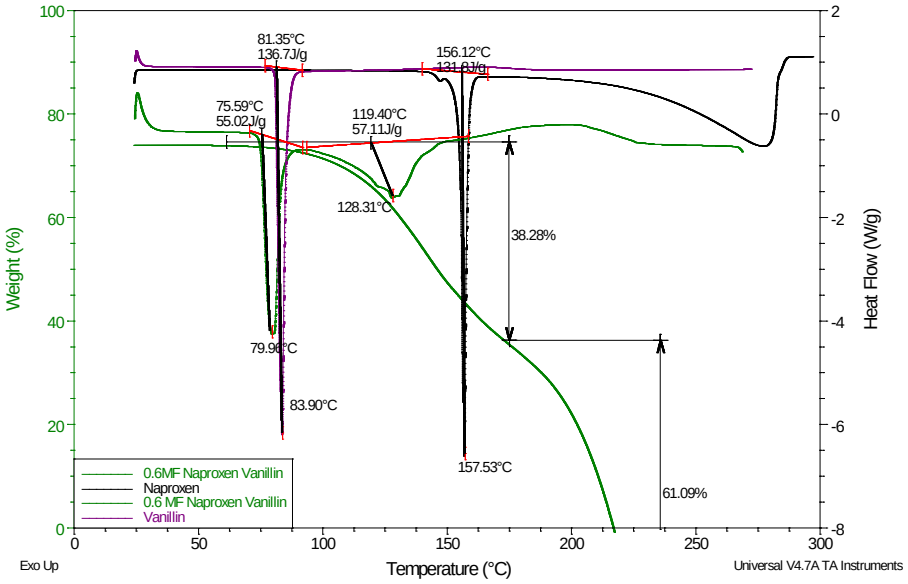

DSC hermetically sealed pans. A sharp melt at 75.6 ˚C followed by degradation. The TGA shows weight loss as expected for a mixture of 40% Vanillin/ 60% Naproxen. The DSC/TGA overlay shows that vanillin has a slightly depressed melt followed by degradation. The melt of naproxen is obscured by the previous degradation of vanillin.

0.7 MF NAP VAN DSC/TGA Overlay

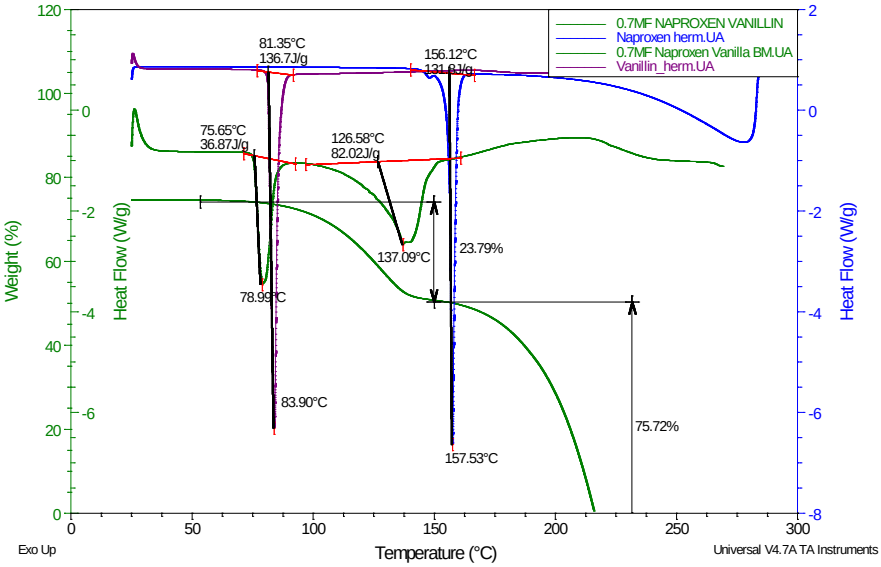

TGA/DSC (herm) overlay of 0.7 MF **NAP:VAN** mixture. Shows same behavior as 0.6 MF mixture.

0.9 MF NAP:VAN DSC/TGA

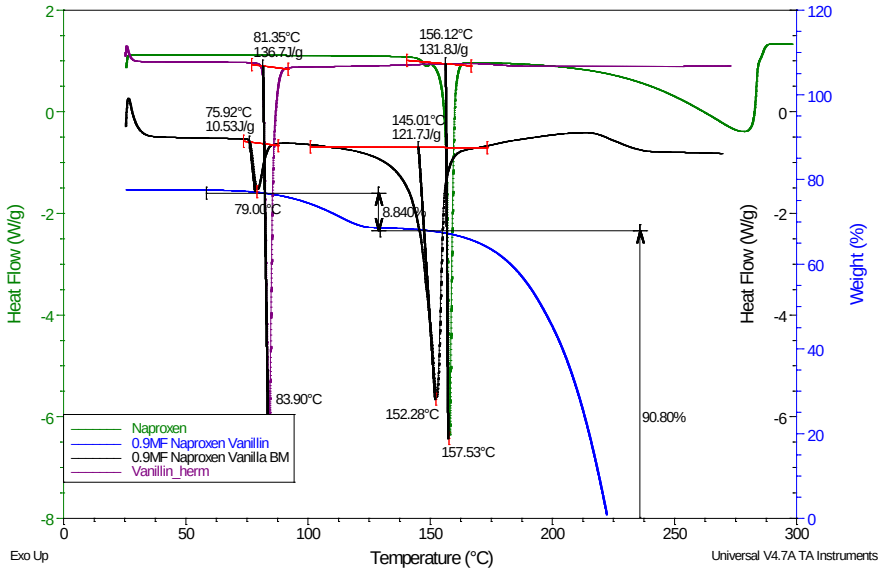

Hermetically sealed DSC Pans. **VAN** begins to melt and degrade upon heating from 50 ˚C onward. Mixture is thermally sensitive and not viable for a phase diagram.

Comparison of 0.8 MF NAP:VAN Physical Mixture and melted mixture.

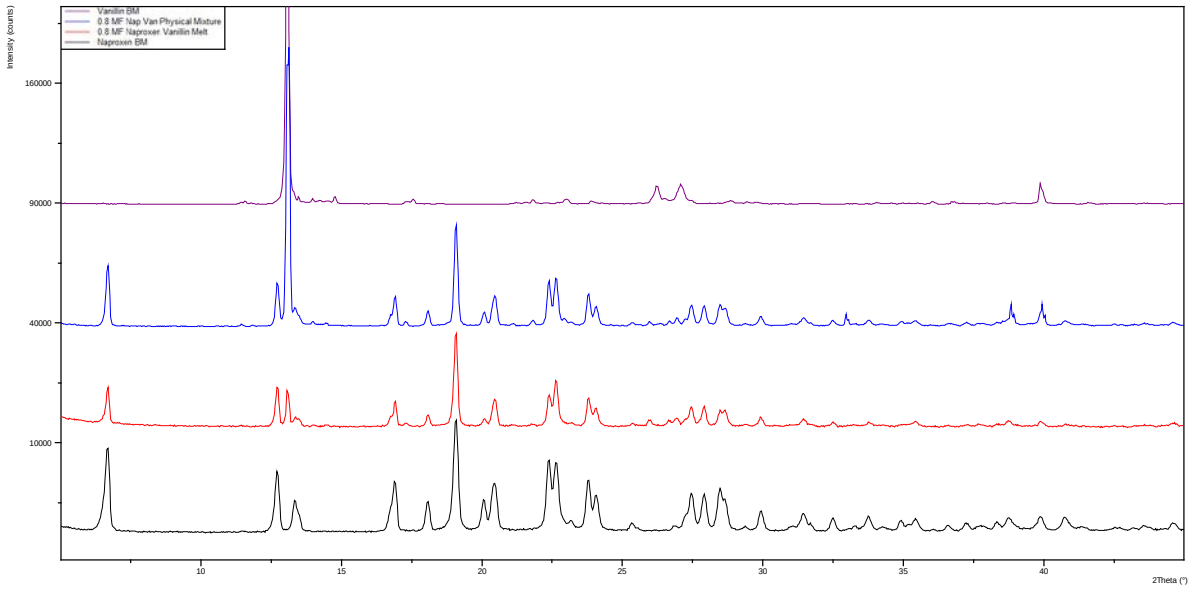

0.8 MF mixture melted once (second from bottom) then compared to the physical mixture (second from top) and compared to the original compounds **VAN** (top) and **NAP** (bot). The physical mixture and the melted mixture match and do not contain any degradation or new forms.

NAP 48 hour slurry in PBS vs. DI Water at Room Temperature (RT) and 37 ˚C

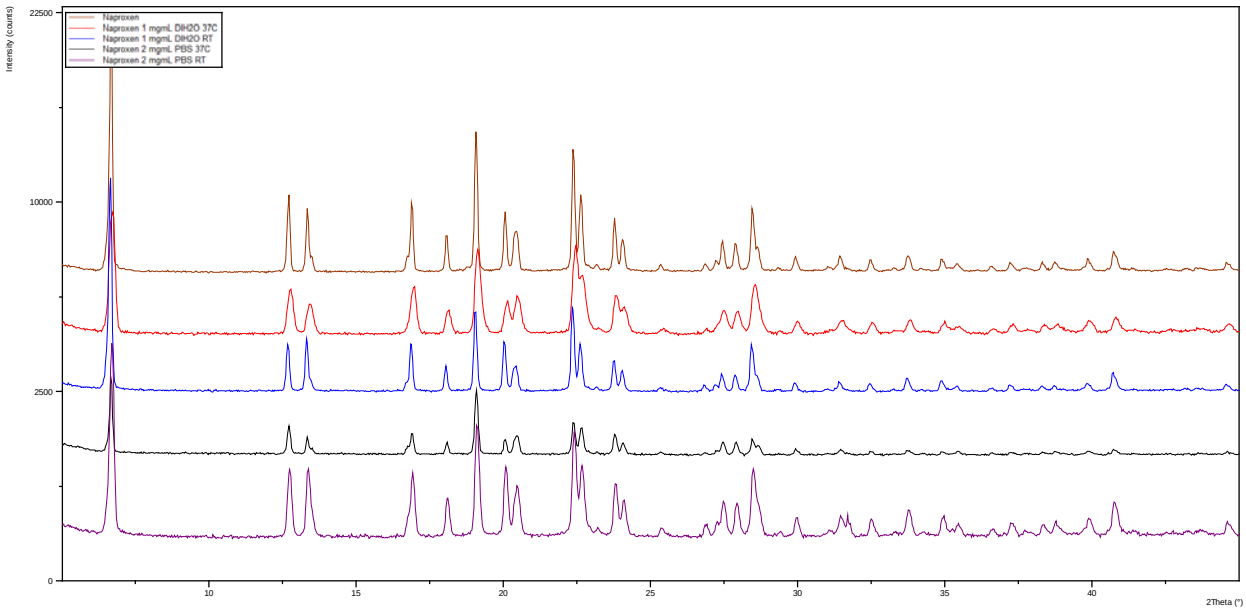

There was no form change by naproxen in PBS vs. DI Water at 37 ˚C at RT. **NAP** (top trace) is compared to the isolated solids after a 48 hour slurry at 1mg/mL in DI Water at 37 ˚C (second trace from top), at 1 mg/mL in DI Water at RT (third trace from top), 2 mg/mL in PBS at 37 ˚C (second trace from bottom), and at 2 mg/mL in PBS at room temperature (bottom trace).

Naproxen Slurries in PBS and DI Water at RT and 37C

PLM: 200x 48 hour slurry of **NAP** at 1 mg/mL at 37 ˚C. The **NAP** particles are smaller than 5 µm but has a tendency to conglomerate (20 – 50 µm in size).

Naproxen Slurries in PBS and DI Water at RT and 37C (cont.)

PLM: 200x of **NAP** slurry in DI Water for 48 hours at 1 mg/mL at RT.

PLM: 200x of **NAP** slurry in PBS for 48 hours at 2 mg/mL at 37 ˚C.

Naproxen Slurries in PBS and DI Water at RT and 37C

PLM: 200x of **NAP** slurry in PBS for 48 hours at 2 mg/mL at RT.